EMPIRICAL MODELS FOR QUANTIFYING SEAWATER PARAMETERS FOR OPEN DESALINATION INTAKE SYSTEM

By:
Samar Omar khuzundar

Supervisor
Dr. Khaldoun S. Abualhin
Assistant Professor
Al-Azhar University of Gaza

Thesis Submitted to the Institute of Water and Environment (IWE), in Partial Fulfillment of the Requirements for the Degree of Master in Water and Environment

MEDRC Water Research
Muscat
Sultanate of Oman
2019

Al-Azhar University-Gaza

Deanship of Postgraduate Studies

Institute of Water And Environment

Master of Water and Environment

Empirical Models for Quantifying Seawater Parameter for Desalination Open Intake System

By
Samar Omar Khuzundar

Supervisor
Dr. Khaldoun S. Abualhin
Assistant Professor
Al-Azhar University – Gaza

Thesis Submitted to the Institute of Water and Environment (IWE), in Partial Fulfillment of the Requirements for the Degree of Master in Water and Environment

2019

Al-Azhar University-Gaza
Deanship of Postgraduate Studies
Institute of Water And Environment
Master of Water and Environment

Empirical Models for Quantifying Seawater Parameter for Desalination Open Intake System

A Thesis Submitted In Partial Fulfillment of the Requirements for the Degree of Master in Water and Environment

By

Samar Omar Khuzundar

This thesis was defended successfully on 29/07/2019.

Committee of Evaluation

Dr. Khaldoun S. Abualhin ....

Main supervisor

Dr. Mazen R. Abuamro ....

Internal Examiner

Dr. Mazen T. Abualtatyef ....

External Examiner

2019

DEDICATION

My father, who aspired me to deliver my very best each and every day, whose good examples have taught me to work hard for what I believe. He have always loved me unconditionally and always provides me with best opportunities in life. Thanks for his supporting and guidance.

My Mother, who has been a constant source of patience and strength during my life. Her prayers and her confidence in me made me realize that I could not have done it without her. I will be forever grateful for her loving support.

My brothers, *Baker and Mohammed*, my heroes, have always been an inspiration whom I am truly grateful for having in my life.

My Supervisor, *Dr. Khaldoun Alhin*, who taught me a lot and do me so many favors, I will never be able to pay him back. Thanks for his support, patience and immense knowledge.

My best friends, *Israa and Nadeen*, who have always been unwavering source of support, encouragement and understanding during the challenges of my whole college life. This thesis is as much hers as mine.

Loving memory of my friend, *Reem*, who I am sure that she would have been happy for me. May her soul rest in peace. I could not have imagined that he would leave us so early.

For everyone, who has been there for me, I cannot list all the names here, but you are always on my mind. Thanks for always being there for me. This thesis is only a beginning of my journey.

DECLARATION

I, the undersigned hereby, declare that the thesis titled:

<u>Empirical Models for Quantifying Seawater Parameter for Desalination Open Intake System</u>

Is my own research work and the work provided in this thesis, unless otherwise referenced, is researcher's own work, and has never been submitted elsewhere for any other degree qualifications nor for any other degree qualifications nor for any academic titles, nor for any other academic or publishing institutions.

I, hereto, affirm that I will be completely responsible in academic and legal terms if this work proves the opposite.

Student's name: Samar Omar Khuzundar

Signature:

Date: 29/07/2019

ACKNOWLEDGEMENT

First, Praise be to *Almighty Allah*, the most compassionate and magnificent, who grant me the strength of thinking and working.

I am most grateful to my supervisor, *Dr.Khaldoun Alhin*, for his timely supervision guidance during all research stages.

I would like to express my thanks and gratitude to all the staff member of institute of water and science. I appreciate highly the full support provided to me.

Many thanks are also extended to my family, siblings and friends for their steadfast understanding and patience. My wholeheartedly special thanks go to my mother and my father for all their and prayers for me during studies. Thanks also maintained to my uncle, *Dr. Marawan elkhazendar*, for supporting me spiritually throughout my life.

Kind thanks are also to staff members of Discussion and Judgment Committee members,
Dr. Mazen Abualtatyef, "Associate Professor in Civil/Environment Engineering", and *Dr. Mazen Abuamro*, "Associate Professor of Mechatronics Engineering", who accepted to examine and judge this thesis.

Special thanks are extended to the *(Middle East Desalination Research Center (MEDRC)),* for their financial support. I am very grateful for funding and covering all the research's costs.

Finally, I am very grateful to all people*, the unknown warriors,* who helped me throughout the succeeding stages of my study.

ABSTRACT

Coastal zones are considered as one of the most vital areas in the world as they are exposed to continuous natural and anthropogenic interferences. Regular and updated monitoring of the coastal changing conditions are necessary to ensure the proper planning and management of the marine resources. This study was implemented in the highly polluted coastal zone of Gaza strip as result of sewage discharge and unmanaged human activates. However, the Gaza coastal zone is projected to be promising spots for development projects in the near future e.g. central desalination plant. Thus, frequent monitoring programs are highly prerequisite in terms of seawater quality and bathymetrical changes. Remote sensing has proved its efficiency as a monitoring and prediction tool in different areas compared with conventional methods.

This study focused on the potential of using the Landsat8 satellite imagery, as one of the most available and free of charge satellite imagery, to develop empirical predictive models of seawater quality (SDD, P) and bathymetry, in order to evaluate the coastal water clarity and to assess the compatibility of using open intakes system in the Gaza strip coastal area.

The Field campaign was conducted and synchronized with the overpass of Landsat 8 satellite in an effort to develop accurate empirical relationships that link in-situ measurement with reflectance values of Landsat 8 image using band-ratio and single-band models. Based on the obtained in-situ data that includes depth measurements, biological, chemical and physical parameters collected at different depths, the study can be divided into main parts; seawater quality and bathymetry. The accuracy of derived data was assessed by comparing the retrieved values with in-situ measurements using statistical indictors; coefficient of determination and root mean square errors that were calculated for all model options.

The final results demonstrates that, with high stand of the large polluted coastal water, the Landsat 8 can be effectively used to retrieve Secchi Depth Disc values and phosphorus concentration in the study area with high $R^2 > 0.5$. Regarding bathymetry, significant relations are found between water depth values and Landsat8 reflectance using different model types, single-band, and band ratio and combined model, over various depth ranges; shallow (0m-8m), deep (8m-20m) and entire measured depth range (0m-20m). For instance, band-ratio model of B2/B3 achieved the highest accuracy R^2 accuaracy = 0.78 and acceptable RMSE =2.81m, in retrieving depth over the entire measured depth range (0m-20m). A combined model of single-band and band ratio (B3, B2/B3) demonstrated a reasonable improve in depth retrieval accuracy. The final results of the combined model have led to the highest accuracy (R^2 accuaracy =0.84, RMSE=2.55m) and used to retrieve depth over the study area.

V

ملخص الدراسة

تعتبر المناطق الساحلية واحدة من أكثر المناطق حيوية في العالم وذلك لما تتعرض له من لتغيرات طبيعية وتدخلات بشرية. لذلك يعد نظام المراقبة الدوري والمحدث للظروف الساحلية المتغيرة ضرورة لضمان التخطيط والإدارة السليمين للموارد البحرية. تم تنفيذ هذه الدراسة في المنطقة الساحلية لقطاع غزة والتي تعتبر شديدة التلوث نتيجة للتصريف المباشر لمياه الصرف الصحي الغير معالج إليها، إضافةً إلى النشاطات البشرية العشوائية. مع ذلك، فإنه من المتوقع أن تكون منطقة الدراسة من المناطق الواعدة لإنشاء مشاريع تنموية في المستقبل القريب، على سبيل المثال المحطة المركزية لتحلية مياه البحر. وبالتالي تعتبر برامج المراقبة الدورية وبالتحديد في مجال جودة مياه البحر، وقياس تغيرات الاعماق متطلب أساسي.

أثبت الاستشعار عن بعد فعاليته كأداة للمراقبة والتنبؤ في مجالات مختلفة مقارنة بالطرق التقليدية. تناولت هذه الدراسة إمكانية استخدام صور القمر الصناعي Landsat 8 في تطوير model يستخدم لقياس جودة مياه البحر والتنبؤ بها (الفسفور، SDD) بالإضافة الى قياس اعماق البحار، من أجل الاستدلال حول درجة نقاء مياه البحر وتقييم مدى ملاءمة استخدام نظام السحب المباشر لمياه البحر open intake system في محطات تحلية مياه البحر في المنطقة الساحلية لقطاع غزة.

تم القيام بالرحلة الميدانية بالتزامن مع مرور القمر الصناعي في محاولة لتطوير علاقات تجريبية empirical دقيقة تربط بين القياسات في الموقع وقيم الانعكاس reflectance لصورة landsat8 باستخدام نوعين من النماذج: (band-ratio model وsingle-band model). تركز الدراسة على جزئين رئيسين بناءً على القياسات التي تم جمعها في الموقع وهما: قياس جودة مياه البحر وقياس الأعماق. تم تقييم دقة النماذج المطورة من خلال مقارنة القيم المشتقة مع القياسات في الموقع باستخدام مؤشرات إحصائية وهي؛ معامل التحديد ومعامل الخطأ. اظهرت النتائج النهائية انه يمكن استخدام القمر الصناعي landsat8 لاستخلاص قيم اعماق SDD وتراكيز الفسفور في منطقة الدراسة بمعاملات تحديد أكبر من 0.5 لكل منهما.

فيما يتعلق بقياس الأعماق بينت النتائج علاقات ملحوظة بين اعماق مياه البحر وقيم الانعكاس reflectance للقمر الصناعي في منطقة الدراسة باستخدام أنواع مختلفة من النماذج، على مدى نطاقات عمق مختلفة؛ ضحل (من 0 متر إلى 8 متر) وعميق (من 8 إلى 20 مترًا) والعمق الكلي المقاس (من 0 إلى 20 مترًا). على سبيل المثال، حقق (B2/B3) أعلى دقة من ناحية معامل التحديد بمقدار 0.78 وقيمة معامل خطأ بمقدار 2.81م، في استخلاص الاعماق على كامل نطاق العمق المقاس (0م -20م). كذلك اظهرت نتائج ال combined model المكونة من ال B3 وB2/B3 تحسنًا معقولا في دقة استخلاص الاعماق (قيم الخطأ= 2.55 م) بحيث تم اعتماده لاستخلاص الاعماق في منطقة الدراسة.

TABLE OF CONTENTS

VIII

LIST OF FIGURES

LIST OF TABLES

LIST OF ABBREVIATIONS

AOPS   Apparent Optical Properties

COD   Chemical Oxygen Demand

DN   Digital Number

ETM+   Enhanced Thematic Mapper Plus

FC   Fecal Coliform

CFU   Colony Forming Unit

GCDP   Gaza Central Desalination Plant

GIS   Geographic Information System

GPS   Global Positioning System

IOPS   Inherent Optical Properties

Lidar   Light Detection and Ranging

MSS   Multispectral Scanner System

NIR   Near infrared

NOAA The National Oceanic and Atmospheric Administration

OLI   Operational Land Imager

P   Phosphorus

R^2 R-Squared

Rrs(Λ) Reflectance Values

RS   Remote Sensing

SDB   Satellite Derived Bathymetry

SDD   Secchi Disc Depth

SWIR   Shortwave Infrared

TM   Thematic Mapper

TOA   Top of Atmosphere

TSS   Total Suspended Solids

USGS   United States Geological Survey

UTM   Universal Transverse Mercator

WGS84 World Geodetic System 19

Chapter (1)

Introduction

1.1 Background

Constant changes of the coastal conditions are mainly caused by long-term natural processes and intense anthropogenic activities. The resulting changes and consequences are at varying degrees, ranging from microscopic (grains of sand) to global (changes in sea level) depending on regional and local characteristics of coasts. Monitoring and assessing these changes are necessary to ensure the proper planning and management of coastal resources.

The coastal city of Gaza strip, located in the southern part of Palestine, spans along the Mediterranean coast with 40 km long. Due to natural and anthropogenic activities, the coastal zone has been undergoing various changes.

Geologically occurring changes of the Gaza Strip coastal zone are mainly caused by being a part of the wider Nile littoral cell, which extends from the Nile Delta in Egypt. This cell consists of quartz, sand, silt and clay sediments derived from the Nile Delta by long-shore drift, which transports sand by waves and currents north and eastward along the Sinai coast towards the Gaza Strip. Therefore, the movement of significant quantities of sediment to inshore and offshore areas subjects local sea bed areas to changes depending on prevailing current, volume of sediment, waves, and thus it is a dynamic environment (Hastie, 1983). Additionally, due to the human activities, the Gaza coastal environment have constantly been changing. Generally, economic investment along the beach, which include all aspects of life such as tourism, port construction, roads, fishing and others, have a major impact on the marine geomorphology and their living species. Furthermore, the sewage discharge of about 110,000 m3/day has caused a degradation of seawater quality (Isaac et al., 2015).

Despite all these natural and anthropogenic challenges along Gaza coastline, seawater is anticipated to be one of the additional water resources as the population suffer lack of access to fresh water due to excessive consumption of groundwater. Desalination projects including the planned Gaza Central Desalination Plant (GCDP) is expected to serve the community in the future by 55 MCM capacity of desalinated water. Seawater intake system is a fundamental part of a desalination plant and have to be designed and installed with due care to grant the performance requested and protect equipment and the intake system itself (Lattemann et al., 2008).

Therefore, database as well as continuous monitoring and assessment of the coastal zone changes are necessary for short-term and long-term planning process to ensure the optimal projects design and to avoid all problems associated with continuous growth and urban expansion. Generally, this information is important for the decision makers; both governmental and non-governmental agencies/users. Some of these probable data users are municipalities, country planners, environmental specialists, statisticians, non-governmental agencies, land owners etc.

The field of remote sensing plays an important role in collecting wide range of data and monitoring all changes that occur on the earth's surface features, infrastructures, managing natural resources, in addition to environmental changes. Developed tools of Remote Sensing (RS) and Geographic Information System (GIS) rapidly spread in recent years in order to monitor changes along sea shores.

The purpose of the study is to assess the compatibility of using open intakes system in the Gaza strip coastal area in terms of seawater quality and turbidity. The study will be based on remote sensing and in situ measurements by investigating seabed characteristics taken into account a site-specific seawater quality, and conducting bathymetric surveys.

1.2 Problem Statement

Recently, the Gaza coast has witnessed extensive urban expansion, population growth and developmental activities such as buildings, road construction, and many other human activities. These manmade interventions in addition to seawater water pollution due to sewage discharge have resulted in enormous changes over time without any detailed monitoring to evaluate the status. The large scale central desalination plant project (GCDP), is expected to be constructed in the study area, therefore, a detailed baseline about the seawater quality and bathymetry is in demand for optimal design of the project components. Moreover, the problem of using an open intakes system and considering the best location and depth of installing the intake pipe is one of the main issues that should be investigated deeply especially for the dynamic of the seabed morphology and the volume of sediment being transported in the shallow coastal zone. In general, there is a dearth of studies concerning the investigation of coastal baseline data and the ongoing changes, particularly in terms of net sediment transport in the shallow coastal area,

bathymetric maps, and seawater quality of Gaza coastal area, and therefore there is a necessity for updating the data. Even there are some related studies, but none of these studies includes actual measurements using field survey, that maximizes the contact between the researcher and the coast and provides the most reliable technique for studying small processes in small areas. In addition to field survey, remote sensing methods will be used to study the coastal zone. The expected data could be used in further investigations or by concerned stakeholders and authorities to protect the marine life and the beach.

1.3 Justification of the Study

In recent years, the Gaza beach has been experiencing increasing changes in terms of seawater quality and morphological change, mainly by human activities and sewage discharge. Due to the lack of planning and monitoring programs, this has led to complex serious problems such as: deterioration of seawater quality, beach erosion, health problem affecting both human and marine organism (Post et al., 1996).

Monitoring and detection of such changes and assessment of their trends as well as their environmental consequences are necessary for future development. So, this study has been carried out to provide update information and to provide empirical prediction models of bathymetry and seawater quality of Gaza coastal area. Remote sensing as a powerful, credible and fast tool is used for studying coastal changes in the study area to effectively map and monitor their impacts.

1.4 Aim and Objectives

The aim of this research is to assess the compatibility of using open intakes system in the Gaza strip coastal area in terms of water quality and bathymetry.
- Developing empirical prediction model for water quality (SDD, TSS and COD).
- Developing Bathymetric model for deriving Bathymetric map.
- Estimation the sediment and seabed profile changes in Gaza coastal area.
- Offering recommendations for the planners to reduce probable negative impacts on both anticipated projects and seawater in the Gaza City.

4

1.5 Organization of the Thesis

This thesis consists of eight chapters. Chapter (1) presents the background to the study, problem statement, justification for the study, the aim and objective of the study area and the structure of the research methodology. Chapter (2) examines existing literature and techniques of seawater quality and bathymetry monitoring using remote sensing; a summary of these techniques and application areas is provided in this chapter. Chapter (3) describes the study area, and illustrates the methodology used to achieve the objectives of the study. The results and analyses as well as discussion of those results are present in Chapter (4), (5), (6) and (7). Chapter (8) concludes the study and highlights some limitations and recommendations.

Chapter (2)

Literature Review of Remote Sensing for Coastal Studies

2.1 Remote Sensing and Coastal Water Monitoring

Coastal zones are always under continuous stress due to industrial, commercial and touristic development in addition to human population growth and migration patterns. Thus, there is an urgent need to conserve the coastal ecosystems and aquatic organisms. In order to ensure sustainable coastal development and proper management, it is necessary to develop accurate, up-to-date and comprehensive scientific databases on all coastal factors including habitats, protected areas, seawater quality, bathymetry and environmental indicators as well as to carry out periodic assessment of the system.

As opposed to in-situ measurements that are time-consuming and labor-intensive, remote sensing has proved its potential in in coastal monitoring as a tool of obtaining information about the area under investigation with no physical direct contact and providing reliable, continuous as well as synoptic database on different aquatic life aspects. Some of these aspects addressed by remote sensing are:

1. Prediction of potential fishery zones by providing information on phytoplankton and sea surface temperature (SST)
2. Protection of Shoreline by studying Suspended sediment dynamics (erosion or disposition)
3. Prediction of Coastal water quality through identifying non-point and point pollution and Phytoplankton blooms.
4. Development of coastal zone by monitoring the changes in seabed topography, land cover and land use.

2.2 Using Landsat Satellite for Coastal Studies

Over the past 30 years, many satellite and airborne sensors have been developed to gather information on the biological activities occurring within water body. (Canh, 2016). The Landsat series (30 m) is commonly used in surface water quality studies due to its longest time series and the free data accessibility. In particular, because of the 30 m spatial resolution of the Landsat data, it is ideal for synoptic observations of different water bodies (Rodrigues et al, 2017).

Landsat satellites were firstly equipped with Multispectral Scanners (MSS), with four bands that cover the green to near infrared (NIR) portion of the spectrum (500 nm - 1000 nm) at 80 m resolution. Later, Landsat satellites have been launched with improved resolution (spatial resolution of 30 m) onboard and more spectral bands; Thematic Mapper (TM) and Enhanced TM (ETM) sensor (Vrieling, 2006).

After the retirement of Landsat 5, the failure of Landsat 6, and limitations with Landsat 7, the Landsat 8 satellite was launched on February 11, 2013, and operations began on May 30 of the same year. The OLI instrument on Landsat 8 is a nine-band push broom scanner with a swath width of 185 km, eight bands at 30-m spatial resolution, and one panchromatic band at 15-m spatial resolution. (NASA, 2016; USGS, 2016).

Compared with previous Landsat missions, Landsat 8 also offers higher signal-to-noise ratios. This is primarily the result of longer integration times associated with the push broom scanner as well as improved quantization (NASA, 2016; USGS, 2016). Because of inclusion of the Operational Land Imager (OLI), Landsat 8 has the potential to become the first Landsat sensor with the radiometric resolution necessary for retrieval of chlorophyll and suspended material constituents in oceans and lakes (Gerace et al., 2013).

2.3 Remote Sensing Models

Model is essential part for quantifying water parameter using remote sensing approach. Based on radiation transfer theory, the satellite sensing data can be divided in two types: Apparent Optical Properties (AOPs), Inherent Optical Properties (IOPs). The First type depends on the medium and the geometric structure of the source fields such as the radiance, reflectance coefficients, and diffuse attenuation. The later parameter depends only on the substances comprising the water mass but not the geometric structure of the various light fields, such as the absorption and the scattering coefficient (Mobley, 1994).

In general, depending on what type of optical properties is used, there are three distinguished remote sensing models for estimating both bathymetry and concentration of water quality parameters; empirical, semi-empirical, and analytical approach (Ma et al, 2005). Empirical approaches seek statistical relationships between spectral bands or band combinations and the measured water parameters, without including knowledge of spectral characteristics of the

constituents or any physical explanation of the relationship. Semi-empirical methods utilize the physical and spectral information (e.g. absorption features) to develop the algorithms, which are then correlated to the measured constituents. The statistical coefficients are typically bound to the specific region and time of calibration. Analytical approaches determine the constituents' concentration by modeling the reflectance of surface water and utilizing the inherent and apparent optical characteristics (Morel et al, 1980).

In the present study, empirical approach has been employed to investigate the relationship between different water characteristic and Landsat8/OLI reflectance values. Different examples of using empirical models in coastal water monitoring will be mentioned in the following sections.

The biggest advantages of using empirical approaches that they are easy to implement and require less mathematical skills and computation time. Such simplicity and rapidity in data processing are convenient for processing large data sets such as satellite images. They give better accuracy if the in-situ measurement is at the same time as the acquisition date of remotely sensed imagery. However, due to the nature of regression, it is generally only applicable to waters with characteristics similar to those used in the model development. The empirical characteristics of these relationships limit their applications to the condition for which the data were collected (Canh, 2016).

2.4 Water Quality

Water quality monitoring can be defined as process of determining the chemical, physical and biological characteristics of water bodies and identifying the possible contamination sources that degrade the quality of water (Usali, 2010).

Quality degradation of water resources may result from point and non-point sources including massive input of industrial, agricultural and sewage effluents which trigger toxic algal blooms affecting biodiversity, fisheries, tourism, recreation and other activities. The understanding of these changes in coastal water quality is critical for the management of marine system and developing baselines of data upon which future impacts can be judged. (Gholizadeh, 2016).

2.4.1 Water Quality Monitoring and Remote Sensing

Satellite remote sensing is already internationally used for water quality estimation. However, because of the optical complexity of waters, the creation of a widely used algorithm is difficult and an ongoing research is necessary (Bukata et al., 1985; Carder et al., 1989; Theologou et al., 2016).

In terms of remote sensing, the common qualitative water parameters can be divided in two types optically active and optically inactive constituents based on their interaction or influence on the spectral distribution of the solar light back-scattered by the water body. Determining the concentrations of optically active water constituents are of paramount importance for monitoring changes in the marine ecosystem. These water constituents interacts with light and change the energy spectrum of reflected solar radiation from water bodies. The induced changes in the spectral signature are quantified using remote sensing techniques and then these measured changes are related by empirical or analytical models to a water quality parameter. The optimal wavelength used to measure a water quality parameter is dependent on the substance being measured, its concentration, and the sensor characteristics (Gholizadeh, 2016).

The other type parameters (optically inactive) have no changes on the spectral properties of reflected light and have no directly-detectable signals, e.g. acidity, chemicals, and pathogens, however, they might be interpretable and inferable from those detectable water quality parameters with which strong correlations can be found. (Ritchie et al., 2003; Kallio, 2000).
To achieve the purpose of the study, some of water quality parameters has been examined in this research including TSS, Secchi Disk Depth, P and COD.

2.4.2 Secchi Disc Depth and Remote Sensing

SDD is one of the parameters measured to indict water transparency and to evaluate the turbidity level in the water body using simple optical tool (Secchi disc).

Due to its easy measuring procedures, SDD results have been widely used and applied to develop theories and to manage aquatic ecosystems (Padial et al, 2008). For instance, it can be used to assess the eutrophic characteristics of a water body with other variables using a trophic state index proposed by (Carlson, 1977).

Also, it can be used in quantifying light attenuation through varying water depths that is dictated by water molecules, phytoplankton productivity and dissolved matter distribution (Kirk, 1975; Mobley, 1994).

In several studied literature, remote sensing technology has been successfully employed in determination of SDD using empirical models. The best band/band-ratio differs from study to study depending on band ratio and atmospheric conditions (Brezonik et al., 2005). Previous studies have also shown that water clarity and Landsat data have an established relationship (Kloiber et al., 2002). Some of SDD-related studies are listed below:

- Kabiri, (2017) examined Landsat-8 OLI imagery, visible bands, for SDD estimation along near-shore coastal waters of Chabahar Bay in the southern part of Iran. Final outcomes demonstrated that combination of linear terms including B1, B2 and B3 bands and band-ratio terms of B4/B3, B3/B1, and B2/B1 has yielded the highest accuracy (R^2=0.866 and RMSE=0.919) with the model form of SDD= 0.077exp (1.209RB1-1.739RB2+0.412RB3-5.198RB3/RB1+10.408RB2/RB1).

- Alameddine et al., (2014) utilized statistical approach to develop Landsat based model to monitor lakes and reservoirs water quality by correlating some water quality parameter including SDD with optical properties of the water in the visible and near infrared (NIR) regions of the electromagnetic spectrum. Landsat 8 showed a low skill in accurately predicting SDD in the reservoir. On the other hand, the Landsat 7 based model showed more promising predictive capabilities with an R^2 of 0.82.

- Kabbara et al., (2008) implemented a study in the Tripoli coastal area to build predictive algorithms derived from matching in situ measurements and Landsat 7 ETM+ data achieving a correlation coefficient (R) of 0.54 using regression analysis based on B1 and B2.

- Powell et al., (2008) successfully used a regression equation to model the distribution of in-situ SDD data in lakes via Landsat imagery using a linear regression model.

- Alparslan et al., (2007) achieved a R^2 of 0.996 using correlation analysis to predict the relationship between SDD and reflectance values of Landsat TM image in Ömerli Dam in Istanbul.

- Hellweger et al., (2004) conducted a study in the New York Harbor to study the relationship between SDD and spectral bands of Landsat satellite. It was found that blue and green bands had lower correlation with SDD compared to red band. They pointed out that wavelengths within the red band are less affected from atmospheric conditions.
- Zhang et al., (2003) developed a model in order to predict SDD values via Landsat TM satellite in the Gulf of Finland and the Archipelago Sea using regression analysis and neural network modeling. In both studies, better results were obtained from neural network models compared to regression analysis. In regression models, calculated coefficient of determination (R2) values were in the range of 0.74– 0.77. For neural network models, the range was 0.91 – 0.95.
- Kloiber et al., (2002) tested many combinations of Landsat 5 bands and then narrowed down the band combinations to a ratio of bands 1 and 3 that were a reliable predictor of SDD. The produced regression model, (In (SDT) = a (TM1/TM3) + bTM1 + c), was applied to all lakes within the study area.

2.4.3 Chemical Oxygen Demand (COD) and Remote Sensing

Chemical oxygen demand (COD) is a measure of the total amount of oxygen required to oxidize all organic material into carbon dioxide and water using chemical method. Biological oxygen demand BOD can be estimated using COD values, always less than COD values, yet measuring the latter take only a few hours while measuring BOD takes five days (Gholizadeh et al., 2016).

Any wastewater effluent with high BOD levels flowing into water bodies spontaneously accelerates bacterial growth, which in turn consumes its oxygen content and thus reduces its levels of the water. One pertinent implication is that the oxygen might diminish to levels that are lethal for most fish and many aquatic species (Gholizadeh et al., 2016).

In general, COD has a weak optical characteristic making it difficult to estimate COD levels by remote sensing technology (Gholizadeh et al., 2016). Several water quality models were developed to investigate the relationship between laboratory-measured COD and remote sensing reflectance, by establishing linear, exponential, and logarithmic regressions. However, interpretation of the satellite or airborne images and making authentic relationships between

spectral characteristics of images and in situ measurements of DO, BOD, and COD in the aquatic ecosystems are still poorly understood. Some of these related studies are listed below:

- Phuong et al., (2017) applied the Artificial Neuron Network (ANN) approach to measure and map spatial changes of the COD concentration using Landsat8 imagery in river reaches of the Binh Dai district, a downstream river network of the Vietnamese Mekong Delta. The results show that ANN approach could provide a better performance compared with linear approach producing a significant correlation R of 0.89.

- He et al., (2008) examined the potential of using Landsat 5 Thematic Mapper (TM) data to predict eight common water quality variables including COD in Guanting Reservoir. The results show no effective retrieval model for COD was found.

- Miao-fen et al., (2007) successfully proved that Landsat TM model provides an effective means to obtain rapidly and low-cost review of COD concentration at Huanjiang River, Rouyuan River and Malian river in Qingyang city, Gansu province of China. The accuracy reaches 83% with the validation of the rest 10% samples.

- Wang et al., (2004) obtained a relatively good correlation through utilizing linear regression approach between reflectance value retrieved from the Landsat TM images and in-situ data of COD reported in reservoirs of Shenzen, Guangdong Province, China.

2.4.4 Total Suspended Solids (TSS) and Remote Sensing

Total suspended solid (TSS) concentration is the amount of solid material suspended in water-sediment mixture, which refers to the weight of all the matter with a particle size of smaller than 150 mm and larger than 0.45 mm. It usually be characterized by its "dry weight expressed in milligrams per liter (mg/l). All natural water bodies contain a suspended matter component that comprises organic and inorganic material. High TSS concentration strongly affects aquatic ecosystems and their productivity (Canh, 2016).

Total suspended solids (TSS) concentration is an important indicator to evaluate estuarine and coastal water quality conditions, which directly affects the light attenuation and thereafter the ocean primary production of plankton, and benthic algae, sea grass and coral reefs (Chen et al,2004). The level of turbidity or murkiness is entirely dependent on the amount of suspended particles in a sample of water. The more suspended particles, the more difficult for light to travel

through the water and therefore, the higher the water's turbidity. Suspended sediments are responsible for most of light scattering (Myint et al., 2002).

The interaction between TSS and the reflected solar and/or emitted thermal radiation from surface waters induces changes in spectral signals that are inferable by remote sensing techniques from many platforms.

Various visible and NIR band combinations have been proposed as TSS indicators on coastal, estuarine, lagoon, lake and reservoir environments. The present study mainly focused on discovering and demonstrating the existence of relationships between suspended solid and Landsat 8 spectral reflectance based on empirical methods. Reviewing the literature demonstrated that the Landsat/TM was used much more than other sensors. Some of these studies are listed below:

- Manoppo et al., (2017) suggested that Landsat 8 OLI can be used effectively to derive TSS concentrations of Lombok coastal waters utilizing empirical and analytical approach. The statistical analyses showed a consistent pattern between Landsat 8 OLI and in-situ measurements with R^2 and RMSE 0.79 and 0.23 respectively.

- Fauzi et al., (2016) found that Landsat 8 band-ratio model of red and green bands produced the best correlation with the TSS (R = 0.533) to model the spatial distribution of the TSS in Wadaslintang Reservoir with standard error of 10.8 mg/l.

- Jaelani et al., (2016) evaluated the accuracy of the atmospherically corrected product of USGS as well as the developed algorithms for estimating TSS concentration using Landsat 8-OLI data over Poteran's waters and over Gili Iyang's waters. The outcomes indicts that low correlation between actual and extracted TSS concentrations was caused not only by the performance of developed TSS estimation retrieval algorithms but also the accuracy of atmospherically corrected reflectance of Landsat product.

- Lim et al.,(2015) found that suspended solids was correlated with Bands 2–5 of Landsat-8/OLI, and constructed 3 multiple regression models through single bands of OLI.

- Sudheer et al., (2006) suggested that a combination of TM1, TM2, TM3 and TM4 was significant to retrieve suspended sediments information from remote sensing data.

2.4.5 Phosphorus (P) and Remote Sensing

Phosphorus are important plant nutrients and essential micronutrients for algae that stimulates their growth very quickly. It is also needed for DNA, RNA, and energy transfer, and required to support aquatic plant growth as well considered as key limiting nutrients in most aquatic and terrestrial ecosystems (Domagalski et al., 2016).

The presence of Phosphorus is either naturally occurring or anthropologically produced. The main unnatural sources of high phosphorus in water bodies comes from organic and inorganic fertilizer-rich agricultural runoffs as well effluents from municipal and industrial wastewater treatment plants that threaten many worldwide ecosystems (Cavalli et al., 2009). The overabundance of phosphorus stimulate the over-production of algae, and lead to undesirable states of eutrophication in lakes and reservoirs (Hadjimitsis et al., 2010). Therefore it was important to monitor the P concentration on a large scale. However, because of the lack of suitable well-established methods, a spatial overview of Phosphorus concentration has been rarely measured on a large scale (Domagalski et al., 2016).

Remote sensing approaches to predict the P levels in plants has been widely used, however, there is still little literature with regard to estimate and P levels in water bodies from remote sensing.

There are direct and indirect methods to retrieve P levels in water bodies. Based on the high correlation between P and optically active constituents, several studies have used indirect retrieval methods to estimate TP concentrations using other water quality parameters, such as TSS, chlorophyll-*a*, or CDOM. Such feasible approach was delineated by (Cavalli et al., 2009; Hadjimitsis et al., 2010) and (Volpe et al., 2011) through using spectral measurements from satellite sensors such as Landsat Thematic Mapper (Landsat/TM) to estimate Chl-a, SSC and CDOM concentration, which would provide possible to infer Phosphorus Concentrations from remote sensing.

Some other studies have achieved good retrieval accuracy by directly exploring the relationship between P concentrations, and satellite image data by establishing empirical models (Volpe et al., 2011; Chebud et al., 2012; Torbick et al., 2013).

Results from reviewed literature indicate that there is a potential to estimate Phosphorus concentration at different scales using airborne and satellite images, in particular, Landsat MS.

- Saputra et al., (2017) has investigated the potential of Landsat 8 OLI image for observing, mapping and monitoring water quality of Riam Kanan Lake. The result of correlation test shows that band 2 of the image as coefficient of phosphate.

- Lim et al., (2015) used bands 2, 3, 4, and 5 of Landsat-8/OLI, and constructed 3 multiple P regression models by selecting both single bands and band ratios, and obtained significant correlation coefficients.

- Song et al., (2011) studied the correlation between TP and TM1, TM2, TM3, and TM4 from the Landsat 5, and found that each band had a correlation with TP of 0.62, 0.59, 0.55, and 0.51, respectively.

- Alparslan et al., (2009) used the first four bands of Landsat 7-ETM satellite data to map total phosphate in Ömerli Dam, Turkey.

- Limin et al., (2008) evaluated the benefits of the use of Landsat/TM imagery data for improving point prediction of N (Nitrogen) and P (Phosphorus Concentration) in Taihu Lake, China. Both two algorithms produced well performance in estimating NC and PC in Taihu Lake, but the PC retrieval model had a superior performance to NC retrieval model. The RE (Relative Error) of the PC and NC retrieval models were 11.7% and 35.6%, respectively. According to no more than 30% accuracy requirements of water quality estimation for remote-sensing technology, the accuracy of PC retrieval model is more acceptable than the NC retrieval model.

2.5 Bathymetry

Bathymetry is a branch of the oceanography dealing with the study of the beds or floors of water bodies, including the ocean, rivers, streams, and lakes. It includes the shapes and depths of the underwater terrain. Bathymetric maps illustrate the land that lies underwater (NOAA, 2016).

Generally, bathymetry is obtained by measuring the distance between average ocean surface and bottom of the sea. Both shallow bathymetry and deep bathymetry are significantly important aspects for planning and management activities of coastal zones, seabed morphology studies, and environmental researches. Bathymetry Measurement can be performed either conventionally or using modern methods depending on time, budget and targeted area.

2.5.1 Bathymetry Mapping and Remote Sensing

Ever since the 1970s, satellite remote sensing technology has been gradually adopted as an alternative to minimize field work for clear water bathymetry mapping. Due to extensive coverage, easy access, and dynamic nature, remote sensing technology can be regarded as one of the most promising alternative tool and considerably cost-effective solution for effective and efficient bathymetry mapping, especially in dynamic areas where level of depth changes quickly. Furthermore, the remote sensing technique can be used to produce bathymetric map of politically inaccessible areas as well shallow and wavy waters as in a reef area that is difficult and expensive even sometimes very dangerous.

The total amount of light observed and reflected from the water body provides a physical basis for modeling water depth from remote sensing spectral data. Depending on spectral variation per depth, remote sensing system (visible light) is capable to detect bottom waters objects and measure bathymetry (IOCCG, 2000, in Siregar and Slamet, 2010). Multispectral sensor, especially green and blue band, can penetrate up to 20 meters below the sea surface in a clear water condition (Sutanto, 1992). To derive the bathymetry using satellite imagery, environmental conditions such as water clarity, cloud cover, a sun glint are needed to be considered.

Remote sensing technique is primarily adopted to infer the depth of clear and shallow water region due to limited penetration of electromagnetic wave energy is turbid waters (Zheng et al.,

2014). Successful launches of several remote sensing satellites such as Ikonos, QuickBird, and Worldview-2 offer imageries with both high spatial land spectral resolution.

Satellite images have been successfully used for bathymetry measuring. Previous researches have showed that the seawater profile can be surveyed by retrieving the corresponding spectral reflectance data of the water body in case of high correlation. The visible range of 400 to 850 nm is often chosen for research aimed at estimating bathymetry within the water column from remote sensing data. The maximum depth that can be detected by satellite imagery is a function of wavelength and brightness waters. On clear water condition, the mapping of bathymetry in the clear ocean water is successfully mapped up to the depth of 25–30m by utilizing 490 nm spectral channel (Eugenio et al., 2015; Lyzenga et al., 2006; Mishra et al., 2007). For the same water condition, channels with a spectrum of 430 to 580 nm and 400 to 610 are capable to detect up to 20 m and 10 m depth respectively.

Jupp,1988 mentions that Landsat8 imagery can be used to determine the depth of water; for Band 1 has the ability to penetrate 25 meters deep, Band 2 to penetrate 15 meters, Band 3 to penetrate 5 meters, and Band 4 to penetrate 0.5 meters.

Stumpf et al. (2003) developed a reflectance ratio model for bathymetry mapping based on the variable radiant absorptivity among spectral bands. The algorithm establishes the linear relationship between the ratio of radiance in two bands (green and blue) and water depth (Stumpf et al., 2003).Using Stumph model has an advantage of reducing the number of parameters to infer bathymetry by making use of two bands only, and the calibration of the model only requires a few water depth points from nautical charts. The algorithm is capable of retrieving depths greater than 25-30m in clear water coastal environments and it is also can determine the depth of the turbid coastal environment efficiently.

2.5.2 Empirical Model and Bathymetry Mapping

Some of the important literatures for estimating the bathymetry of ocean using remote sensing technology (empirical model) are discussed below:

- Alhin and Niemeyer (2018) applied depth-invariant index to derive and map underwater seabed morphology via QuikBird imagery. The method enables mapping and delineates the major underwater sand bars along the entire coastal zone of the Gaza Strip.

- Wee Tang and Razali Mahmud, (2018) utilized two different band ratio empirical models including stumph to map bathymetry in shallow and highly turbid waters in Strait of Johor, Malaysia. The findings shows that Stumpf model could be used to derive SBD achieving a Correlation coefficient value of 0.76 and a RMSE of 0.885 meters.

- Poppenga et al., (2018) used passive multispectral satellite imagery; Landsat 8 and WorldView-3 (WV-3), to estimate near-shore bathymetry in low-lying atolls in the coastal waters surrounding the Majuro Atoll, Republic of the Marshall Islands, by applying the band ratio technique .The results showed that L8 SDB using blue/green band ratio exhibited a water attenuation extinction depth of 6 m with an R2=0.9324.

- Pushparaj and Hegde, (2017) used ratio transform algorithm for estimating the bathymetry of near-shore region along the Mangaluru coast of Karnataka, India, using Landsat-8 imagery. The results of satellite image show a good correlation of $R2 =0.8503$ with the hydrographic chart data for the depth up to 5m.

- Also, Alhin and Niemeyer (2016) examined the accuracy of two different bathymetric derivation algorithms: liner and band-ratio in the highly polluted coastal zone of the Gaza Strip. The results revealed that liner has outperformed the band-ratio transformation and more suitable in the case of the coastal shallow waters.

- Jagalingam et al, (2015) carried out a study aiming at determining the bathymetry of the southwest coast of India using the ratio transform algorithm on the blue and green bands of Landsat 8 satellite imagery. The results of satellite image show a good correlation of R2 =0.8503 with the hydrographic chart data for the depth up to 5m

- Abualtayef et al. (2013) studied the spatiotemporal changes of Gaza shoreline between 1972 and 2010 using ERDAS and GIS tools. The outcomes revealed that erosion was a dominant process in the area studied particularly on northern side of the harbor at an annual rate of 14,000 m2.

- Alhin and Niemeyer (2009) utilized remote sensing/GIS techniques to monitor and analyze the coastline dynamics during the last two decades in the Gaza Strip using

different modern techniques such as the Tasseled Cap Transformation, Band Ratio and Normalized Difference Vegetation Index (NDVI).

Chapter (3)
Study Area Description & Methodology

This chapter consists of two main parts: study area description and model extraction steps.

3.1 Study Area

The study area is part of coastal zone of the Gaza strip which is extended along the seashore of the eastern Mediterranean Sea. The coastal area is about 42 km long, and about 6 to 12 km wide, bordered by Egypt from the south. The sedimentation of the Nile River has shaped the coastline of the Gaza strip. Sand dunes are the dominant feature along the coastal zones (south and north) in addition to the coastal cliffs (exposed Kurkar ridges) in the middle to north (Ali, 2002).

The study area, illustrated in Fig (3.1), includes the surroundings of Gaza fishing harbor, covering about 7 km along the shore and about 3 km offshore. The research focuses on the study area that covers the busiest beach in Gaza city and was previously a sediment-active zone due to anthropogenic activities.

As study area that is naturally dynamic and full of anthropogenic activates, the bio-physical seawater parameters have been adversely affected. In addition, the presence of irregular distributed sewage outfalls of raw and partially treated wastewater have heavily polluted the Gaza coastline and caused degradation of seawater quality. Currently, 110,000 m^3/day is discharged along the coastal line of the Gaza Strip from multiple outfall (Isaac et al., 2015). There are 6 sewage outfalls spotted in operation in the study area, three of them located in the south and two sewage outfalls in the north in addition to outfall (6) that is located in the Gaza harbor basin.

The northern outfalls of the Gaza harbor along the study area are Al-Shata'a Pump station outfall (5) which disposes sewage directly to the sea when the power is cut and outfall (4), which dispose both storm water and sewage whereas the southern outfalls are outfall(1 ,2, 3),outfall (2) is owned by fish farm which discharge nutrient-rich sewage. These sewage outfalls are unequally distributed in distance, distance between is different to, therefore their effluents are varying in quantity per time and per site.

The irregular flow from each sewage outlets, containing significant amounts of pollutants and nutrients, and the constant variation of sediments influx coming from Nile River discharged into the region make Gaza Sea one of the highly turbid and eutrophic waters. Based on the varying

volume of effluent coming from each sewage outfalls, the seawater quality of the Gaza Sea varies temporally and spatially. Therefore, in this area, the flow of wastewater from the sewage outlets play significant role in determining the conditions in Gaza Sea.
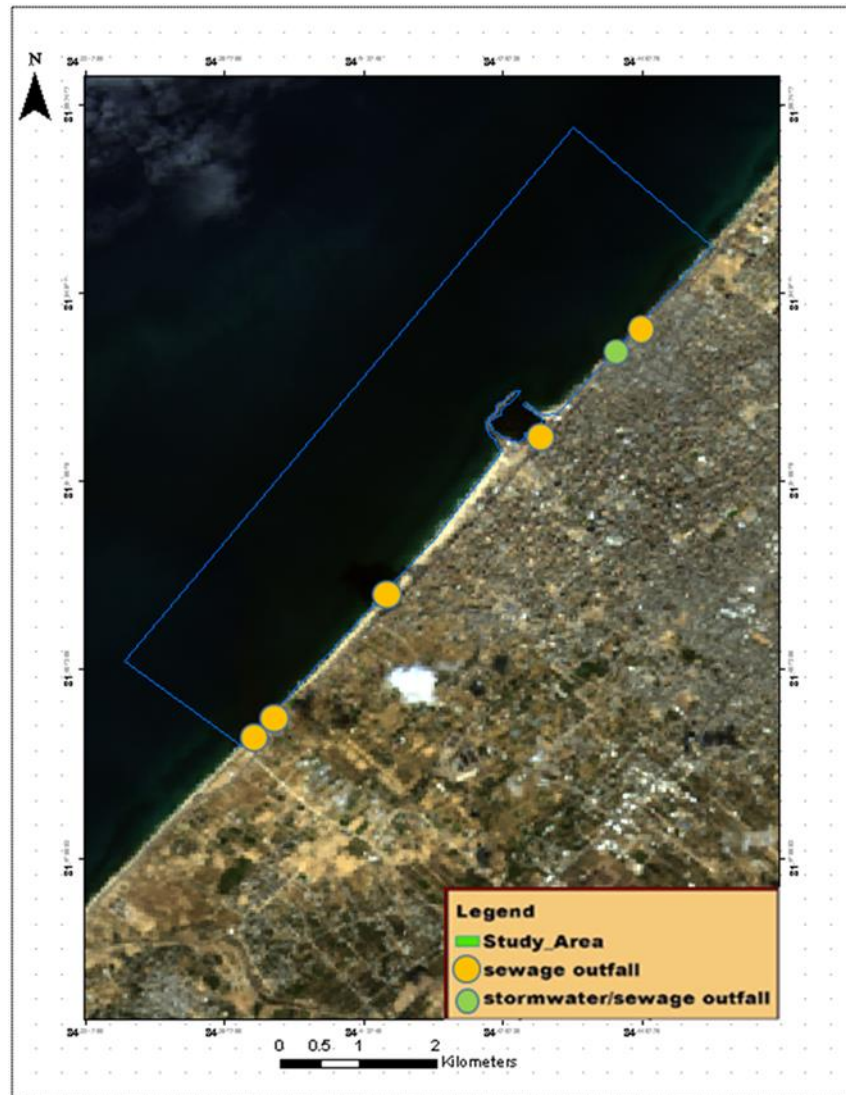
Fig (3.1): Map of sewage outfall spotted along the study area

.

3.2 Model Extraction Steps

The steps to perform model extraction in this research are illustrated in flowchart, Fig (3.2). The followed steps were explained in details:
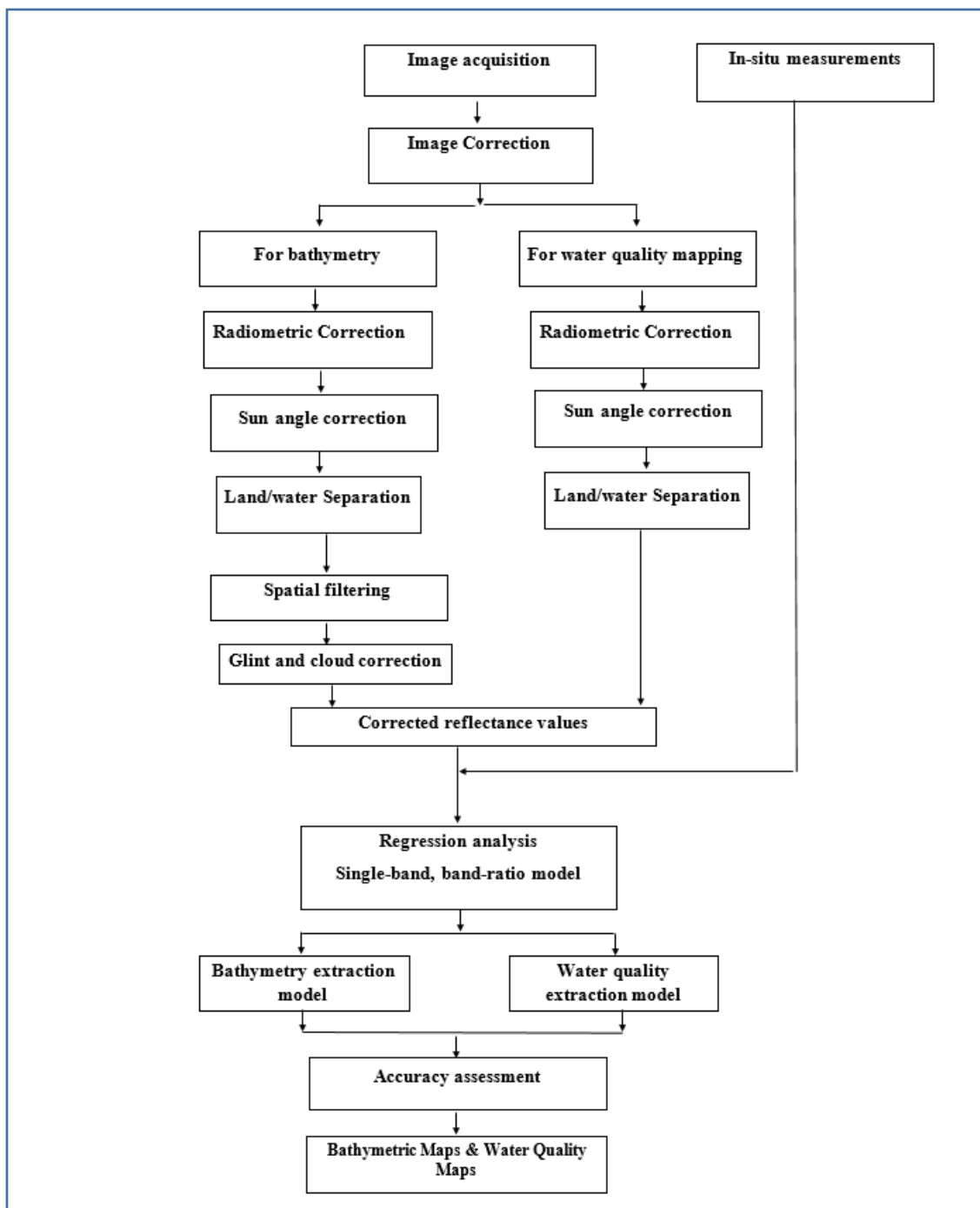
Fig (3.2): Bathymetry and water quality model extraction flowchart

3.2.1 Data Collection and Acquisition

Landsat8/OLI satellite images data were downloaded from USGS Website obtained by specific path and row. Gaza Strip is covered by two paths and two rows namely, path/row 174/38 and path /row 175/38. The spectral and spatial characteristic of used Landsat OLI optical bands are illustrated in Table (3.1). Seven satellite imageries of good-quality were obtained based on definite criteria including suitable atmospheric and metrological conditions, covering the period between 2014 and 2018. Table (3.2) shows the details of the selected images.

Table (3.1): Spectral bands characteristics of Landsat OLI (USGS, 2016)

Band	Wavelength (µm)	Resolution (m)
Band 1 -Coastal	0.435 – 0.451	30
Band 2 - Blue	0.452 – 0.512	30
Band 3 - Green	0.533 – 0.590	30
Band 4 - Red	0.636 – 0.673	30
Band 5 - NIR	0.851 – 0.879	30
Band 6 – SWIR-1	1.566 – 1.651	30
Band 7 – SWIR-2	2.107 – 2.294	30
Band 8 - Pan	0.503 – 0.676	15
Band 9 - Cirrus	1.363 – 1.384	30
Band 10 – TIR-1	10.60 – 11.19	100
Band 11 – TIR-2	11.50 – 12.51	100

Table (3.2): Satellite images characteristics and source

Satellite	Path/raw	Acquisition Date	Resolution [m × m]	Pixel Depth	Image Source
Landsat 8	174/38	10/27/2014	30×30	16 Bit	USGS
Landsat 8	174/38	9/1/2017	30×30	16 Bit	USGS
Landsat 8	175/38	10/27/2017	30×30	16 Bit	USGS
Landsat 8	174/38	11/4/2017	30×30	16 Bit	USGS
Landsat 8	175/38	11/11/2017	30×30	16 Bit	USGS
Landsat 8	175/38	11/27/2017	30×30	16 Bit	USGS
Landsat 8	175/38	11/30/2018	30×30	16 Bit	USGS

3.2.2 Seawater Sampling

The sampling trip was conducted on 4, November, 2017 which coincides with the passage of the Landsat 8 satellite over Gaza strip, covering path 174, row 38. The metrological conditions were suitable to collect samples.

Different activities were involved in the sampling trip including recording the coordination of each point using GPS, measuring depth using depth electronic sounder, measuring turbidity using Secchi disk, and collecting samples at different depths (surface, 2m, 3m) using 1000 ml bottle for physio-chemical analysis (TSS, COD) and 50 ml bottles for sterile container for biological analysis.

The trip track started from Point 1 (p1) to Point 41 (p41) forming grid as illustrated in Fig (3.3). The selection of sampling points was random and representative of the study area. A total of 106 seawater samples were collected from different near-shore and offshore points at different depths except 10 points (18, 19, 24, 34, 35, 36, 37, 38, 39, and 40).

Initially, the longitude and latitude of each sampling points were determined, recorded and noted. Afterward, the bottom depths of 41 points were measured, the deepest point found to be 20 m and the shallowest was 0.54 m.

Subsequently, the seawater turbidity for each point, except points (18, 19, and 24), was measured through the employment of hand-made Secchi disk of 15 cm diameter with alternating black and white quadrants following the steps below:

1. Slowly lower the Secchi disc into the water on the shady side of the boat until it is no longer visible. Record this depth.
2. Slowly raise the disc until it just becomes visible once again. Record this depth.
3. Average the depths from steps 1 and 2 to get the Secchi depth.
4. This may be repeated for a measurement of precision

The 106 samples could be divided in two set:

1. Microbiological samples: The first set includes 33 samples representing 31 points out of 41 were collected from surface water using sterile containers. Every sample was directly labeled after collection by M_X where x is the number of the point, then kept at $10\,^{\circ}C$ in ice box and transferred to the lab in order to be processed within 24 hr.

Thereafter, concentrations of fecal coliform were measured for every sample. Samples M_9 and M_{32} were duplicated due to the high turbidity of the samples.

2. Chemical and physical samples: The Second set of samples were utilized for chemical and physical analysis of COD, TSS, and P.

During sample collection, about 2 to 3 samples for each sampling point were gathered using 1000 ml bottle and labeled according to its depth:

- C_1 surface sample
- C_2 sample at 2 m depth
- C_3 sample at 3 m depth

The number of samples collected at each point depends on their depth and its level of turbidity; 3 samples were collected for shallow points or points of turbid surrounding, while 2 samples were collected for the deeper and less turbid surrounding.

According to the criteria above. The 74 samples can be divided to 3 groups excluding the aforementioned ten points:

1. 3 sample for every points between sample 1 to sample No.12 except No.2, No.5, and No.3.
2. 5 samples for sample No.3
3. 2 sample for every point between samples (No.13 to No. 17, No.20 to No.23 , No.25 to No.35 and No.41)
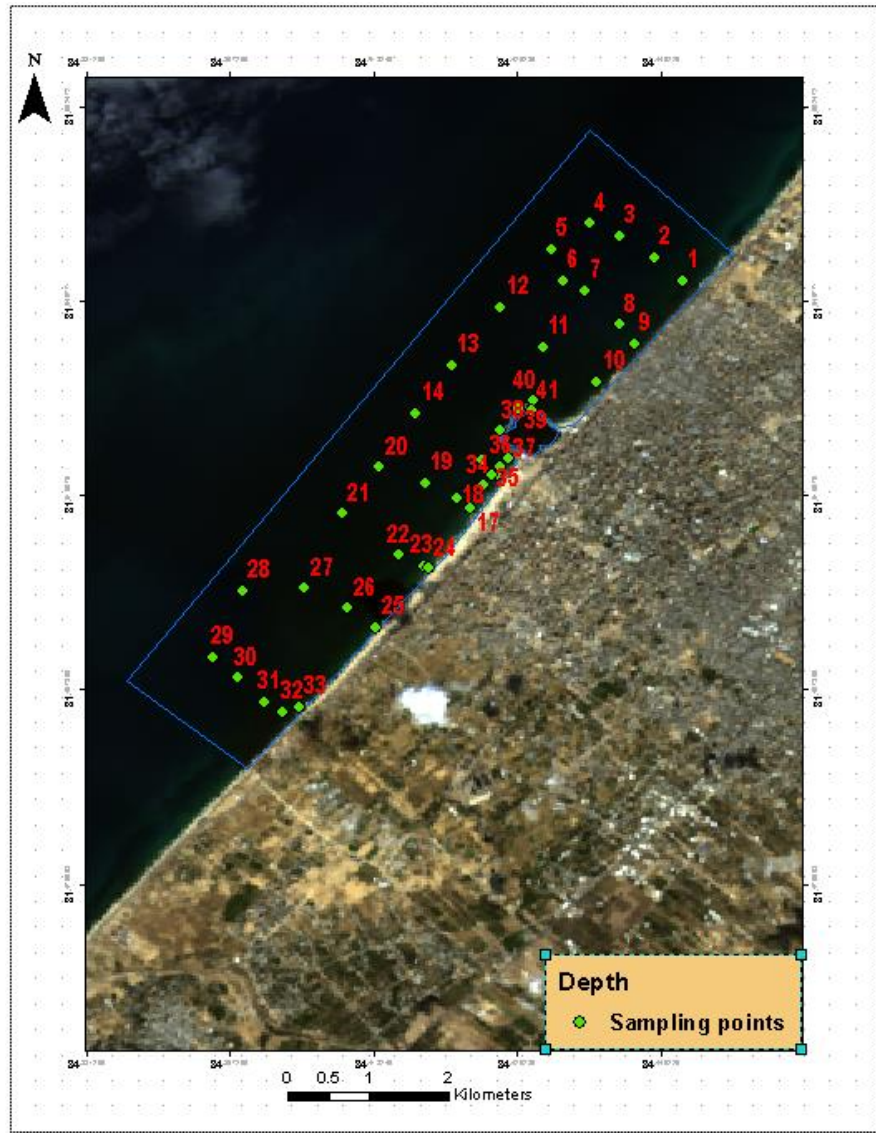
Fig (3.3): Study area and sampling locations

Fig (3. 4): Some of devices used in field survey A) Hand-made Secchi disc, B) Sampler
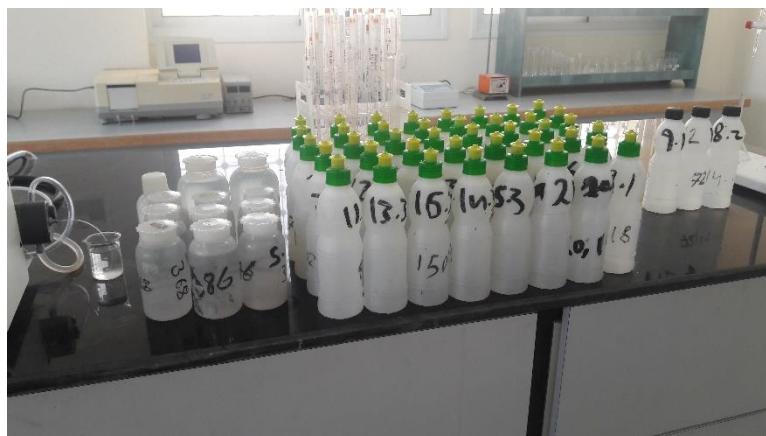
Fig (3.5): Collected samples during field survey

3.2.3 Laboratory Analyses

- **Fecal Coliform Analysis**

At first, concentrations of fecal coliform were measured using Membrane Filter Technique recommended by the APHA Standard Methods (APHA 1995). The Samples passed through Gellman Millipore filter under negative pressure (vacuum). These membranes were transferred by a forceps and placed on the surface of the media by passing them carefully to avoid any air bubbles. The plates used for isolation of fecal coliform were incubated at 44°C for 24 to 48 hours. The colonies appeared on the surface of the membrane were counted and identified by the Gram stain, Biochemical tests and specific antisera. All the concentrations reported are in CFU.
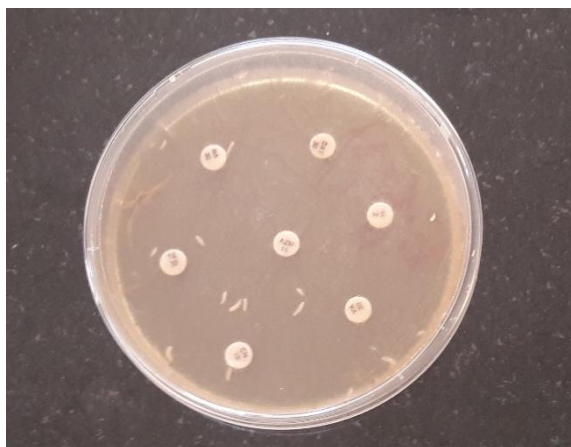
Fig (3.6): Fecal Coliform plates prepared for laboratory analysis

- **COD**

A composite sample was formed by taking 10 ml from every sample using pipette. A sample volume of 2.5 ml was transferred to culture (digestion tube), then a 0.2 mercuric sulfate has been added to inhibit the Cl interferences in seawater in addition to 1.5 ml digestion solution. Following that, 3.5 ml of sulfuric acid reagent was poured down inside the tube so an acid layer is formed under the sample. The sample tubes were completely mixed and placed in block digester (COD incubator) at 150 ^{o} C for two hours. The tubes were cooled down to room temperature. The content of culture tube was transferred to a larger container for titration. About 0.05 to 0.1 ml (1 to 2 drops) of Ferroin indictor was added and stirred rapidly on magnetic stirrer. The end point, a sharp color change from blue-green to reddish brown, can be achieved by titrating with 0.10 M FAS. In the same manner, blank, containing the reagent and a volume of distilled water equal to that of the sample, was refluxed and titrated.

The cod can be calculated as

$$COD\ (mg/l) = \frac{(A-B)*M*8000}{ML\ SAMLE} \qquad (3.1)$$

Where A=Ml FAS Used For Blank

B=Ml FAS Used For Sample

M=Normality of FAS

Fig (3. 7): COD reactor for Laboratory analysis

- **Phosphorus Analysis**

Measurement of phosphorus was done using HI96706 portable photometer. The HI96706 uses an adaptation of the Standard Method for the Examination of Water and Wastewater. When the reagent (HI93706-0 ready-made) is added to samples containing phosphorus, the sample will turn a blue hue; the greater the concentration, the darker the color. The associated color change is then colorimetrically analyzed according to the Beer-Lambert Law. For phosphorus determination, a narrow band interference filter at 525 nm (blue-green) allows only blue-green light to be detected by the silicon photo detector and omits all other visible light emitted from the tungsten lamp.

- **Total Suspended Solids Analysis**

TSS were estimated using a conventional methods due to the lack of fiber glass filter in Gaza. The utilized method was Based on the fact that the difference between total solids (TS) and total dissolved solids (TDS) is a measurement of TSS. Thus, the concentrations of total solids (TS) and total dissolved solids (TDS) were measured. Primarily, the total solid (TS) concentration was measured, starting by taking 2 clean porcelain dishes for every sample which has been washed and dried in hot air oven at 180 for one hour. Secondly, the number of samples were noted down on the empty dishes. The weight of empty evaporating dishes gauged by analytical balance was denoted using W_{p1}, W_{p2}. Then, each sample was mixed very well and 25ml was grabbed using graduated cylinder and pour into dish. The step was duplicated for the second dish to ensure accuracy. Afterwards, the sample to be dried placed into the oven and allowed to reach 105 $^{\circ}$C heat for long duration usually 1 to 2 hours to get constant mass. Finally, the dishes were left to cool down in the desiccator to provide an environment of standard dryness. As soon as they were cooled , the dishes were weighted to avoid absorption of moisture noting the weight of the residue as W_{p3}, W_{p4}. The Total solids is calculated by subtracting W_{p1}/W_{p2}, and W_{p3}/W_{p4} respectively and the results was then averaged.

The next step involved measuring TDS. Similarly, another two clean porcelain dishes for every sample have been washed and dried in hot air oven at 180 $^{\circ}$C for one hour. The steps of noting down numbers of samples on the empty dishes, weighing the empty evaporating dishes in analytical balance and denoting the weigh measured using different name WB_1 ,WB_2 as well mixing the sample very well were repeated. Subsequently, the step of taking and measuring

25ml using a graduated cylinder was duplicated. Afterward, Samples were filtrated using filtration apparatus. The filtrated water was added to the dishes, then placed into the oven at 105° C to be heated for about 2 hrs. After being cooled down, the weight of the residual was noted as WB_3, WB_4. The dissolved solids is calculated by subtracting WB_1/WB_2, and WB_3, WB_4 respectively and the results was then averaged. Finally, the TSS was estimated by subtracting TS and TDS.

3.2.4 Image Pre-Processing Steps

After the acquisition of the Landsat 8 image, bands of interest (B1 to B7) were stacked in order to be processed. Secondly, the stacked image was resized to help focusing on the study area. The image preprocessing for water quality model and bathymetry model are almost the same except two bathymetry related step: Glint and cloud correction and spatial filtering.

- **Radiometric correction**

Radiometric correction is necessary at the pre-processing steps to help handling and interpretation digital satellite image. Initially, the multispectral satellite image downloaded in the form of digital number. The Digital Number (DN) is the pixel value of grayness of an image that has not yet been calibrated into physically meaningful units. The conversion of DN to TOA is done using reflectance rescaling coefficients provided in the product metadata file (MTL file). This calibration steps are prerequisite for analyzing remote sensing imagery. The following equation is used to convert DN values to TOA reflectance for OLI data as follows:

$$Rrs(λ)' = MρQcal + Aρ \qquad (3.2)$$

Where:

$Rrs(λ)'$= TOA planetary reflectance, without correction for solar angle.

$Mρ$ = Band-specific multiplicative rescaling factor from the metadata.

$Aρ$= Band-specific additive rescaling factor from the metadata

$Qcal$ = Quantized and calibrated standard product pixel values (DN)

- **Sun angle correction**

Using band math function, TOA planetary reflectance of each band was corrected by entering the equation 3.3. The average sun elevation angle is available in the MTL files provided with the image. Using the average Sun elevation angle, the solar zenith angle ($θ_s$) can be calculated using following Equation $θ_{SZ} = 90 − θ_{SE}$.

$$Rrs(\lambda)=\frac{Rrs(\lambda)\prime}{cos(\theta SZ)}=\frac{Rrs(\lambda)\prime}{sin\,((\theta SZ)} \qquad \text{(3.3)}$$

Where:

Rrs(λ)   = TOA planetary reflectance

θSE   = Local sun elevation angle. The scene center sun elevation angle in degrees is provided in the metadata (SUN_ELEVATION).

θSZ   = Local solar zenith angle; $\theta SZ = 90° - \theta SE$

- **Water/ land separation**

Separating water area from other non-water portion (land/cloud) is required for easily distinguishing water body from the rest of the image and visualizing analysis results more conveniently. Separation step was done using threshold value of B5 wherein the NIR band reflects water and appears dark and it also reflects the land area and appears bright.

- **Glint and cloud correction**

This step is intended to correct the radiometric contribution from sun glint and low clouds; the method proposed by Hedley et al. (2005) is performed to rectify the radiometric correction on the bands of interest. The linear relationship between the NIR and visible bands (i.e. green and blue) is established using the linear regression, based on a selected sample area of the image pixels. Following the recommendation of Hochberg et al. (2003), sample region of image is selected where sun glint is evident, but the spectral brightness of the selected region is expected to be more or less homogenous. The equation for removing the sun glint and low clouds is shown below

$$R_i{\prime} = R_i - bi\,(IR_{NIR} - Min_{NIR}) \qquad \text{(3.4)}$$

Where Ri is the pixel value in visible bands (i.e. green and blue), bi is the regression slope, ($IR_{NIR} - Min_{NIR}$) is the difference between the pixel NIR value of IR_{NIR} and the ambient NIR level Min_{NIR} which gives the $Ri\prime$ sun glint–corrected pixel brightness in blue and green bands. The value of Min_{NIR} indicates the pixel brightness of NIR with no sun glint, and can be assessed by the minimum NIR value, which is found in the regression sample. Generally, the minimum NIR pixel is less prone to problematic outliers than the maximum NIR pixel. The following steps are implemented to remove the radiometric correction on blue and green bands (Hedley et al., 2005).

- **Spatial Smooth filtering**

Before performing spatial filtering, technique float is performed to convert each pixel of satellite image into a floating point representation. Later, a spatial filtering technique called occurrence filter (kernel size of 3× 3) is applied on visible bands and NIR bands of Landsat-8 imagery to remove the speckle noise.

- **Data extraction**

To obtain the empirical model of water quality parameters using remote sensing image, the pixel value of each sample location was extracted using ArcGIS.

3.2.5 Model Development and Accuracy Assessment

- **Correlation Analysis**

Correlation analysis was conducted to look at the relation as well as the direction of the relation of two or more variables. This was done in order to find spectral bands with significant relationship with depth values/water quality parameters, which is necessary to perform regression analysis. Only spectral bands with significant correlation coefficient (R) that can be used as input in the regression analysis. The input pixel values for the empirical model are the value of a single-band or band-ratio.

- **Regression Analysis**

Regression analysis was used to build the prediction model for the parameter of interest (SDD, TSS, P …etc.) using Landsat OLI image reflectance values. The Independent Variables are reflectance value and the dependent variables are in-situ values. Scatterplot was applied to represent linear equation model of the regression analysis. The regressions that used in this study were simple and multiple regressions as explained below:

- Simple Regression: Linear regression model, in its simplest (bivariate) form, shows the relationship between one independent variable (x) and a dependent variable (Y).The formula for the resultant regression function is as follow:

$$Y=A+BX \qquad (3.5)$$

Where: **Y** is dependent variable (In-situ data), **A, B** are regression coefficients and **X** is independent variables (reflectance values)

- Multiple Regression: multiple linear regression is a linear regression model with one dependent variable and more than one independent variables. The general form of the multiple linear regression model is as follows:

$$Y_i = A + B_1X_1 + B_2X_2 + \ldots + B_nX_n \ldots\ldots i = 1, 2, 3\ldots N \quad (3.6)$$

Where **Yi** is dependent variable, **A,B1,B2 ,….., Bn** are regression coefficients, and **X1 ,X2 ,….,Xn** are independent variables in the model(reflectance values).

- **Accuracy assessment**

To calculate the accuracy of the developed models, Root mean square error (*RMSE*) and coefficient of determination (R^2) were used to compare between in-situ measurements and derived values. These notations were defined as follow:

$$RMSE = \sqrt{\frac{\sum_{i=1}^{N}(xderiv,i - xinsitu,i)^2}{N}} \quad (3.7)$$

$$R^2 = \frac{1}{N}\sum_{i=1}^{N}(xderiv,i - xinsitu,i)^2 \quad (3.8)$$

Where *x in-situ,i* and *x derived,i* are the actual and derived values, respectively, and *N* is the number of samples. The RMSE gives the absolute scattering of the retrieved remote sensing reflectance as well as water quality parameter concentration/depth. Whereas, R^2 indicts the strength of relationship between in-situ values and derived values. The resultant regression function of the best model was applied to Landsat 8 OLI image to obtain the spatial distribution of the parameter of interest.

Chapter (4)

Seawater Quality Prediction Model

The study employed the potential of Remote Sensing in evaluating and monitoring the coastal zone of the Gaza city. The study included water quality and bathymetric maps. However, not all seawater quality parameters were investigated in this study due to either lack of measuring apparatus or complicity of relating some quality parameters to remote sensing imagery, accordingly, Fecal coliform, COD, TSS, Phosphorus, and SDD have been investigated.

4.1 Biological Water Quality

4.1.1 Fecal Count (FC)

Wastewater disposal into the Mediterranean coast of the Gaza Strip has many negative effects, whether on the environment or on human health, therefore, microbiological contamination of seawater samples has been investigated by considering the fecal coliform as a contamination proxy. The results showed that the bacterial count of fecal coliform ranges from 8 CFU to 252 CFU per 100 mL with mean value of 70 CFU per 100mL. Such high levels of FC in the study area, that supposed to be zero in bathing water, indicates a direct discharge of wastewater containing human excrement that causes fecal contamination, therefore the seawater is not suitable for swimming and bathing.

 The maximum value of 252 CFU per 100 mL was found at sample point 9, which is located close to the sewage outfalls of Al-Shata'a Camp, whereas, the lowest value of fecal coliform, less than 30 CFU per 100mL, were recorded at points (28, 29, 30, and 31) and were located far enough from shoreline and sewage outfalls in the southern part of Gaza port.

The result cloud be classified in to three ranges; FC less than 100, between 100 -200, and greater than 200. Based on these classification, the area surrounding sample point was considered to be lowly contaminated, moderately contaminated and highly contaminated respectively. In all cases, even small amount of FC makes the area unsuitable for human activities.

It was noticed that microbiological contamination increased highly near the beach and at shallow seawater areas, but decreased as going far offshore. This could be attributed to dilution process of pollutants discharging from sewage outfalls with increasing distance and also due to surface water circulation. Fig (4.1) illustrates that the concentration values of FC sampling points at Gaza fishing port basin and its northern part were higher than those to the south (Sample No.9

, sample No.41, sample No.1, sample No.8, sample No.33, and sample No.11), this could probably because of prevalent wave direction in the study area carrying pollutants from south to north.
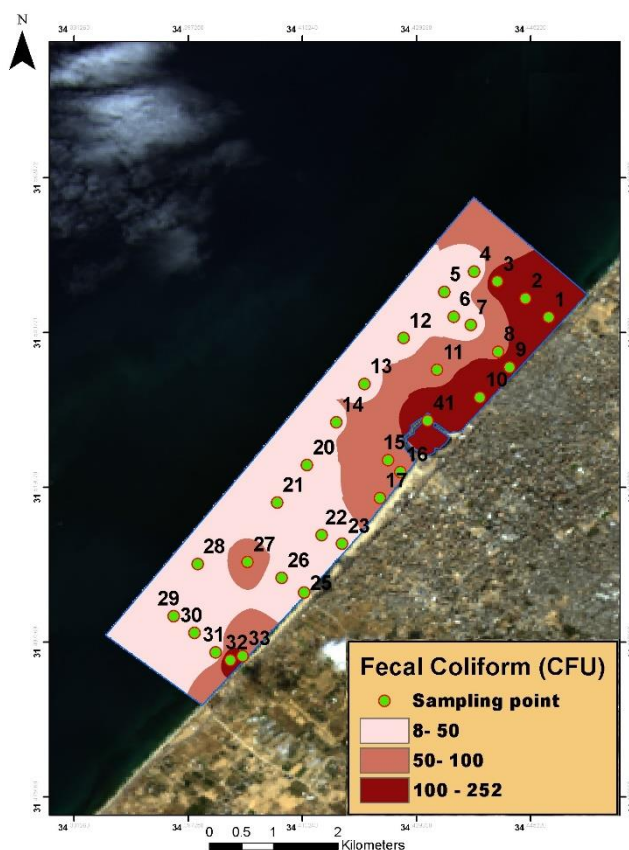
Fig (4.1): Fecal coliform distribution along the study area

4.2 Chemical Parameters for Water Quality

Two water quality parameters were used to evaluate the chemical contamination in the coastal zone of the study area namely, COD and Phosphorus.

4.2.1 Chemical Oxygen Demand (COD)

The coastal study area receives a daily considerable amount of wastewater from 4 major outfalls, (1, 3, 6, and 4), in addition to other minor sewage outfalls (2 and 5) as illustrated in Fig (3.1). High concentration of organic matter in seawater causes detrimental effects on human health and marine life. Levels of organic matter could be measured in laboratory using COD values.

Laboratory analysis showed that COD concentrations of 31 collected samples ranged between 32 mg/L- 288 mg/L. According to Palestine standard for treated wastewater reuse, the permissible limit of COD meant to be discharge to seawater should not exceed 250 mg/l. Fig (4.2) shows that southern part of the study area had higher levels of COD compared to the northern part of the study area that was different to the FC pattern. These elevated concentrations could be explained by more number of sewage outfalls in the southern part.

It was noticed that the highest concentrations of COD were found in regions that exists far from the beach compared with other points along the beach, this might be caused due to water circulation.
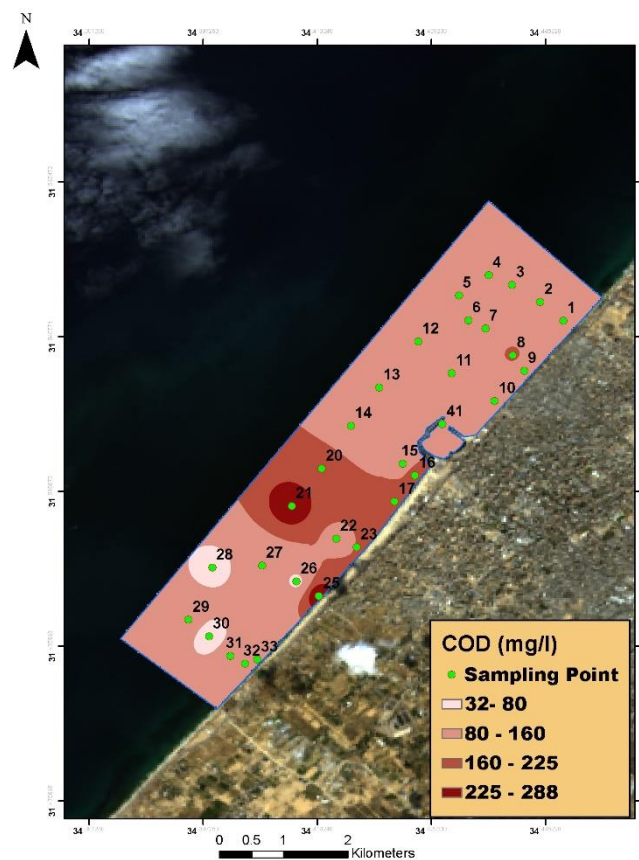
Fig (4. 2): COD distribution of along the study area

4.2.1.1 COD Model Development (Calibration)

Statistical approach was utilized to establish the relation between the measured COD concentration and spectral reflectance of Landsat8/OLI image for predicating COD in the entire coastal region. Single-band models and band-ratio models were used to relate in-situ COD concentrations and Landsat8/OLI reflectance values.

- **Single-Band Model**

Primarily, the correlation coefficient (R) between OLI reflectance values Rrs (λ) of single-bands (visible /IR) and COD concentrations was calculated. Table (4.1) illustrates that single-band models has not reflected any strong correlation that could be used for COD prediction (R <0.5). However, B3, B4 and B5 showed a slight correlation coefficient (R) of 0.3 compared with the remaining bands (B1 and B2). B3 show P-value less than 0.05 which give an indication that it could be used for further development of strong model.

Table (4.1): Regression statistics of single-band model between OLI reflectance (IR/ visible bands) and COD

Regression Statistics	B1	B2	B3	B4	B5
R	0.100	0.232	0.399	0.340	0.332
R2	0.010	0.054	0.159	0.116	0.110
P-value	0.596	0.215	0.028	0.065	0.072
Observation	30	30	30	30	30

- **Band-Ratio Model**

In terms of band-ratio model, their correlation coefficients (R) were relatively similar to that of single-band models with values less than 0.5 as shown in Table (4.2), where other bands-ratio ((B1/ B3), (B2/ B3)) showed a correlation coefficients of 0.37 which is still very weak relationship.

In general, no significant relation, (R> 0.5) and P-value < 0.05, were found between OLI reflectance values (visible and IR) and COD in study area. According to some similar studies, no certain OLI wavelength could be used with high confidence to perform an appropriate model

to estimate COD from water reflectance that might be referred to the weak optical characteristic of COD leading to the low accurate estimation of COD using remote sensing technology.

Meanwhile, other studies show that remote sensing is feasible approach to measure COD using different satellite or different approach. For instance, Wang et al. (2004) found high correlation coefficient of 0.626 between COD concentration and reflectance values of band 1-3 of the Landsat 7 using multiple linear regression approaches in comparison with linear, exponential and log transformations. Also, Phuong et al, (2013) proved that artificial neural network approach provided better COD estimation than traditional regression model.

Table (4.2): Regression statistics of band-ratio models between OLI reflectance (IR/ visible bands) and COD

Regression Statistics	B1/B2	B1/B3	B1/B4	B2/B3	B2/B4
R	0.301	0.372	0.303	0.370	0.279
R2	0.090	0.138	0.092	0.137	0.078
P-value	0.105	0.042	0.102	0.043	0.135
Observation	30	30	30	30	30
Regression Statistics	B2/B5	B4/B5	B3/B4	B3/B5	B1/B5
R	0.253	0.118	0.069	0.151	0.291
R2	0.064	0.014	0.004	0.023	0.084
P-value	0.177	0.535	0.715	0.423	0.118
Observation	30	30	30	30	30

4.2.2 Phosphorus

Marine productivity is limited by the amount of phosphorus present in seawater which in turn affect the marine organisms. It is usually delivered to coastal area via natural weathering or due to human intervention. Therefore, P measurements is considered as one of the essential water quality parameters in coastal waters. In the study area, concentrations of phosphorus were analyzed at three different depths: P1 at the surface, P2 at 2-m depth and P3 at 3-m depth. A total of 67 samples was divided as followed:

- 29 for P1: ranges between 0.1836 mg/L-1.1 mg/L with an average value of 1.69 mg/L.

- 10 for P2: ranges between 0.0306 mg/L -0.5202 mg/L with an average value of 1.165 mg/L.
- 28 for P3: ranges between 0.2142 mg/L – 0.7956 mg/L with an average value of 1.52 mg/L.

Analysis results of phosphorus exhibited high levels in the study area, which exceeded the recommended seawater quality limit, $P < 0.1$ mg/L, set by EPA for marine and estuarine waters. The presence of fish farming outfall and sewage outfalls in study area, discharging huge amount of wastewater, was the main cause of these elevated phosphorus concentrations.

As shown in the Fig (4.3), samples of high average phosphorus concentration were noticeably located in the northern part of study area where the densely populated residential area, Al-Shata'a camp, is located. Coastal water of Al-Shata'a camp is generally much polluted due to the huge amount of sewage discharged into the sea compared to other regions as well as the prevalent currents direction in study area which carries the pollutants northward to Al-shata'a camp. In addition, it was obvious that Gaza fishing port basin had high levels of phosphorus as semi enclosed area of stagnant seawater, receiving direct discharge of wastewater from sewage outfall (4) inside the port basin, Fig (3.1).

Serious environmental and health risk could be emerged because of high P concentration, threating human and aquatic life, through inducing blooms of harmful algae which hinders sunlight penetration and reduces the amount of dissolved oxygen in water.
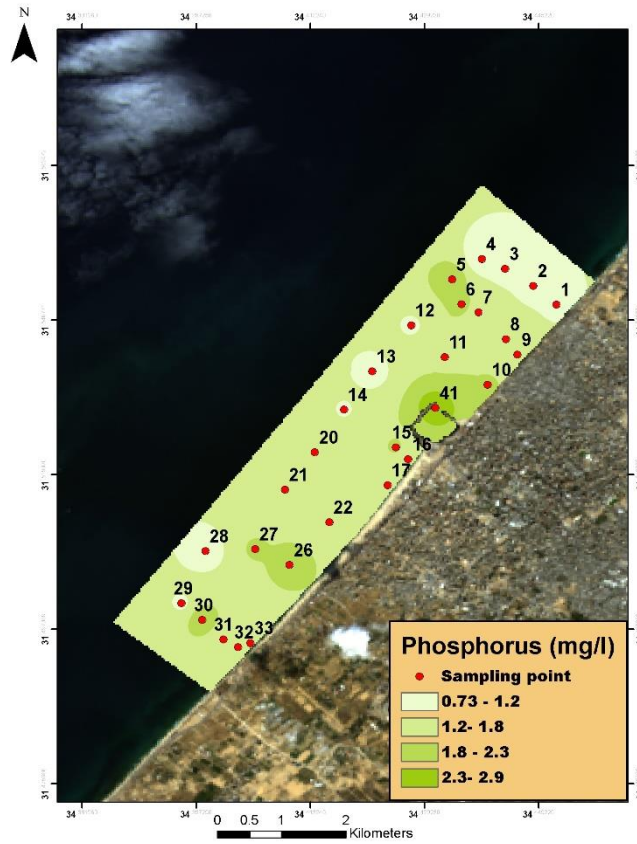
Fig (4.3): Average P distribution along the study area

4.2.2.1 Phosphorus Model Development (Calibration)

Statistical approach was applied to build the Phosphorus retrieval models at different depths P1 (surface), P2 (2m), and P3 (3m) using processed Landsat8/OLI reflectance values $Rrs(\lambda)$. Single-band models and band-ratio models of Visible bands/infrared band were tested to determine the relations between Phosphorus concentrations and OLI reflectance values $Rrs(\lambda)$. Considering model type, single or ratio, the results could be divided in two sets at different depths.

- **Single-Band Model (P1, P2, And P3)**

Generally, results of single-band models revealed that the correlation coefficients (R) between Phosphorus concentrations at surface (P1) and Landsat 8 reflectance values varied between weak and moderate (R ≥ 0.5). B1 and B2 showed an acceptable correlation coefficients (R) of 0.49 and 0.55 respectively and coefficient of determination (R^2) of 0.246 and 0.311 respectively that were higher compared with other bands B3, B4 and B5, Table (4.3).

Regarding (P3), weak correlation coefficients were obtained with Phosphorus concentration at 3-meter depth (P3) and OLI reflectance values of single bands. However, B1 and B5 bands showed a slight correlation coefficient (R) of 0.3 and coefficient of determination (R^2) of 0.1 that was better compared with other bands (B2, B3 and B4),Table(4.3).

On the contrary, the correlation coefficient values (R) of P at 2-meter depth (P2) were relatively higher compared to that of (P1) at surface and (P3) at 3 m. The strongest correlation coefficient of 0.85 was calculated between B5 and P2, with high coefficient of determination R^2 of 0.73, Fig (4.5). Also, it was observed that B3 has strong R and high R^2 with P2 that are 0.76 and 0.0.5861 respectively, as illustrated in Fig (4.4).

Table (4.3). Regression statistics of single-band model between OLI reflectance (IR/visible bands) and P

	Regression Statistics	B1	B2	B3	B4	B5
Phosphorus at surface	R	0.496	0.558	0.364	0.319	0.022
	R2	0.246	0.311	0.133	0.102	0.0005
	P-value	0.036	0.016	0.136	0.195	0.928
	Observation	9	9	9	9	9
Phosphorus at 2m-depth	Regression Statistics	B1	B2	B3	B4	B5
	R	0.569	0.625	0.765	0.673	0.858
	R2	0.323	0.391	0.586	0.452	0.736
	P-value	0.086	0.052	0.131	0.032	0.062
	Observation	5	5	5	5	5
Phosphorus at 3m-depth	Regression Statistics	B1	B2	B3	B4	B5
	R	0.369	0.218	0.186	0.287	0.364
	R2	0.136	0.047	0.034	0.082	0.132
	P-value	0.143	0.398	0.473	0.263	0.150
	Observation	8	8	8	8	8
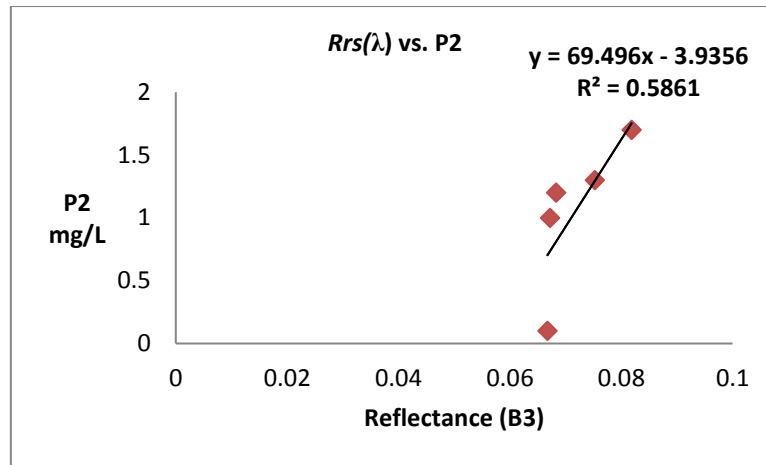
Fig (4.4): Regression analysis plot between B3 and P2
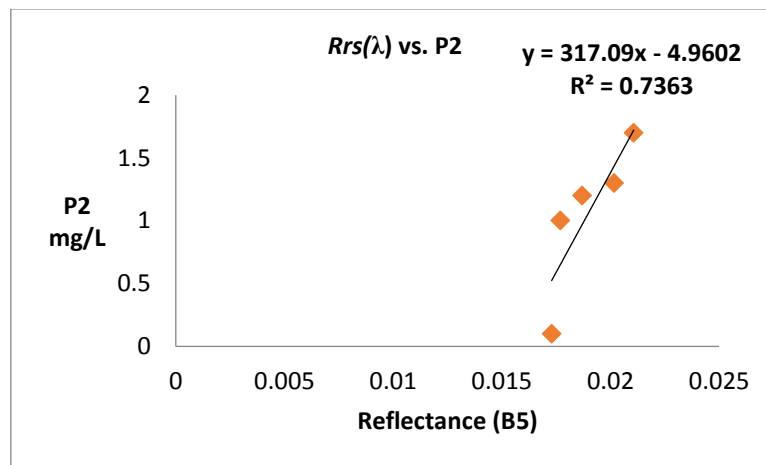
Fig (4.5): Regression analysis plot between B5 and P2

- **Band-Ratio Model**

Band-ratio model of visible bands/inferred band was used to explore the relationship between P levels and OLI reflectance values at different depths. At surface, it was found that band-ratio model of B3/B5 and B4/B5 had strong correlation coefficients values (R) of 0.89 and 0.75 respectively, Fig (4.6) and Fig (4.7), and high coefficient of determination (R^2) > 0.5 with (P-value) less than 0.05, compared with other band-ratio models that had weak correlation coefficients (R^2) less than 0.5.

At 3-meter depth, Table (4.4) illustrates that no strong correlation coefficient (R) was noticed between Phosphorus concentrations and band-ratio reflectance values. However, B2/B5 had a moderate correlation coefficient (R) of 0.47 compared with other bands.

On the other hand, Fig (4.8) reveals that P at 2-m depth had strong correlation coefficient (R) of 0.835 with band ratio B1/B5.Additionlly,the results show that other band-ratio models, for instance (B1/B3, B1/B4, B2/B3, and B2/B4), had relatively the same moderate value of correlation coefficient (R= 0.6).

The lack of strong relationship between P3 and OLI reflectance values might be interpreted by the depth at which the samples were collected where light penetration is quickly attenuated compared to samples collected at shallower depths.

Meanwhile, P2 had a larger number of models correlated to P in spite of its small number of samples. It is Probable that spatial heterogeneity of seawater quality in the study area and irregular distribution of sewage outfalls weakened the correlation between P concentration and reflectance values. Further possible reasons were that samples collected at 2-meter depth was more efficient to develop retrieval model compared with samples collected at surface or at 3-m depth. Therefore, the depth at which sample is collected is questionable and needed to be reconsidered.

In general, band-ratio models yielded better correlation compared to single-band models at the development phase. A combinations of Green or blue with red band had significant relation with P concentration. These results come with agreement with different studies reported in the literature.

Table (4.4): Regression statistics of band-ratio model between OLI bands reflectance (IR/visible) and P

|	Regression Statistics	B1/B2	B1/B3	B1/B4	B1/B5	B2/B3
Phosphorus at surface	R	0.505	0.296	0.211	0.104	0.237
	R2	0.255	0.088	0.044	0.011	0.056
	P-value	0.032	0.231	0.398	0.678	0.342
	Observations	9	9	9	9	9
	Regression Statistics	B2/B4	B2/B5	B3/B4	B3/B5	B4/B5
	R	0.157	0.199	0.006	0.899	0.754
	R2	0.0249	0.039	4.2E-05	0.809	0.569
	P-value	0.518	0.411	0.978	0.0009	0.018
	Observations	9	9	9	9	9
Phosphorus at 2m-depth	Regression Statistics	B1/B2	B1/B3	B1/B4	B1/B5	B2/B3
	R	0.390	0.659	0.672	0.835	0.670
	R2	0.152	0.434	0.452	0.698	0.449
	P-value	0.264	0.038	0.032	0.078	0.033
	Observations	5	5	5	5	5
	Regression Statistics	B2/B4	B2/B5	B3/B4	B3/B5	B4/B5
	R	0.670	0.380	0.274	0.216	0.312
	R2	0.450	0.144	0.075	0.046	0.097
	P-value	0.033	0.278	0.442	0.547	0.378
		5	5	5	5	5
Phosphorus at 3m-depth	Regression Statistics	B1/B2	B1/B3	B1/B4	B1/B5	B2/B3
	R	0.047	0.276	0.380	0.446	0.322
	R2	0.002	0.076	0.144	0.199	0.103
	P-value	0.856	0.281	0.132	0.072	0.207
	Observations	8	8	8	8	8
	Regression Statistics	B2/B4	B2/B5	B3/B4	B3/B5	B4/B5
	R	0.413	0.472	0.418	0.280	0.023
	R2	0.171	0.223	0.175	0.078	0.0005
	P-value	0.098	0.055	0.094	0.275	0.930
	Observations	8	8	8	8	8
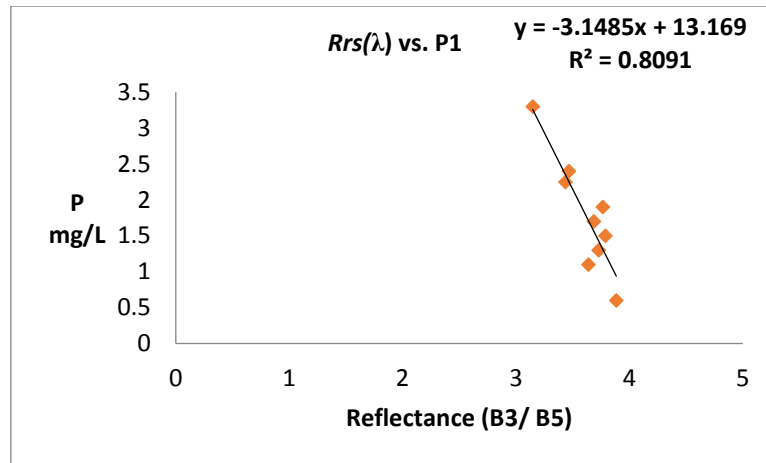
Fig (4.6): Regression analysis plot between B3/B5 and P1
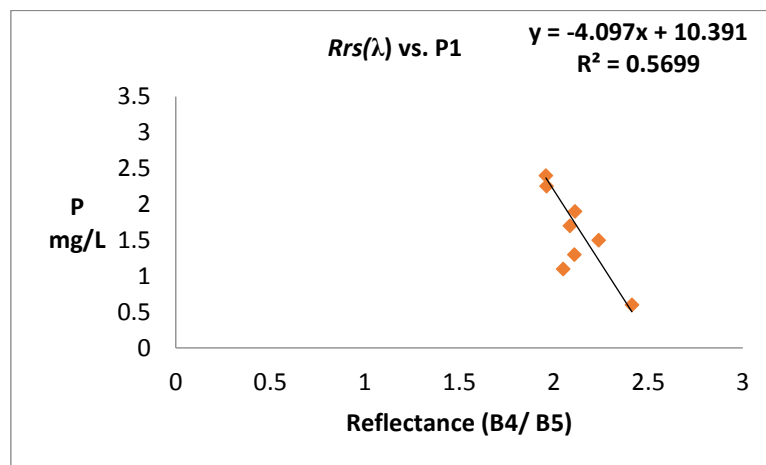
Fig (4.7): Regression analysis plot between B4/B5 and P1
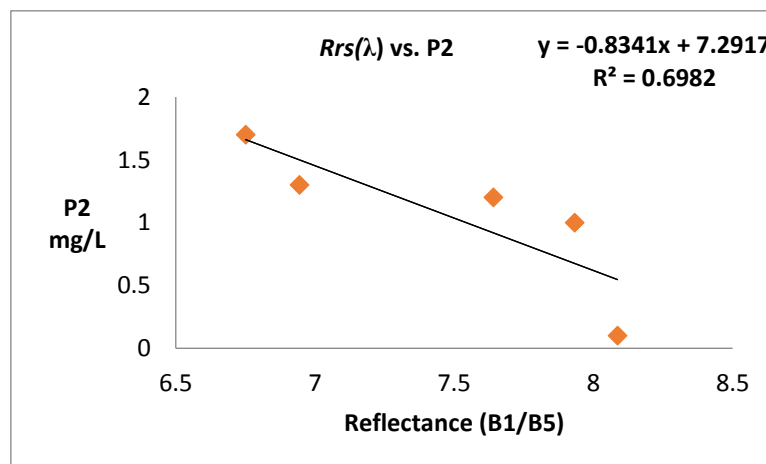
Fig (4.8): Regression analysis plot between B1/B5 and P2

4.2.2.2 Accuracy Assessment of P Model

All models with coefficient of determination (R^2) > 0.5 and (P-value) less than 0.05 were tested with in-situ measurements using the two statistical indices; coefficient of determination (R^2) and root mean square error (RMSE), as illustrated in Table (4.5). As for P1, the results showed that B3/B5 (model1) demonstrated an acceptable accuracy, $R^2_{accuracy}$=0.5139 and RMSE=0.33, compared with (model 2) of B4/B5, $R^2_{accuracy}$ = 0.4 and RMSE=0.4.As result, (moded1) could be used to predict the spatial distribution of surface Phosphorus (P1), Fig (4.9).

Meanwhile, Fig (4.10) demonstrated that B1/B5 exhibited a considerable accuracy for (P2), $R^2_{accuracy}$ = 0.7129 and RMSE=0.38919. It is obvious that band-ratio outperformed the single-band model in estimating P level in the study area.

Table (4.5): Statistical parameters for accuracy testing of Phosphorus prediction model

Model No.	Band/Band ratio	Regression equation	R^2 calibration	R^2 accuracy	RMSE
P1 at surface					
Model1	**B3/B5**	**3.15*(b3/b5)+13.169**	**0.8091**	**0.5139**	**0.331457**
Model2	B4/B5	4.09*(b4/b5)+10.391	0.5699	0.4358	0.4682
P2 at 2-m depth					
Model3	B3	69.496*b5-3.9356	0.5861	0.2143	0.3116
Model5	B5	317.09*b5-4.9602	0.7363	0.7129	0.38919
Model 6	**B1/B5**	**0.831*b1/b5+7.2917**	**0.6982**	**0.7177**	**0.377607**
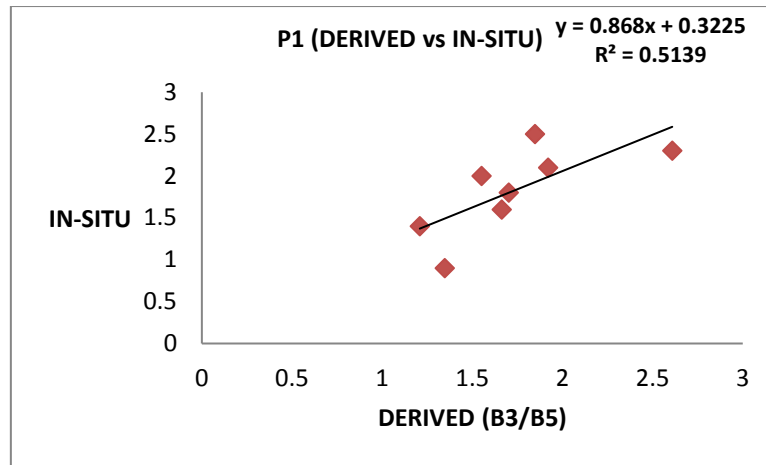
Fig (4.9): Plot of accuracy assessment of P1 derived values by B3/B5 model and in-situ data
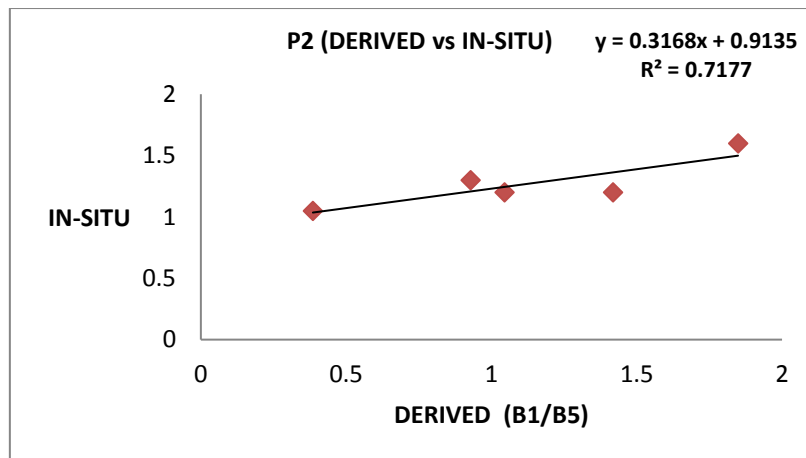
Fig (4.10): Plot of accuracy assessment of P2 derived values by B1/B5 model and in-situ data

4.3 Physical Parameters for Water Quality

The study included the parameters of SDD and TSS to examine the physical water quality.

4.3.1 Secchi Disk Depth (SDD)

Secchi disc depth is used to assess the depth of light penetration and seawater transparency. The surveying trip was conducted and synchronized with the passage of landsat8/OLI to form the best retrieval model. According to the in-situ bathymetry survey, 19.6 m was the maximum depth measured in the study area. The SDD measurements of 40 points exhibited the overall range from 0.54-8 m with average value of 4.88 m. The distribution of the SDD values was depicted in Fig (4.11). As seen in the figure, SDD values were shallow along beach compared

50

with its depth due to sediment suspension and turbidity related to wastewater discharge. According to UNEP-WHO (1982), the hotspots along coastal stretch, where water Secchi depths fall below the critical values of 2 to 3 m. Also, Fig (4.11) illustrates that the SDD became deeper as moving far off the beach.
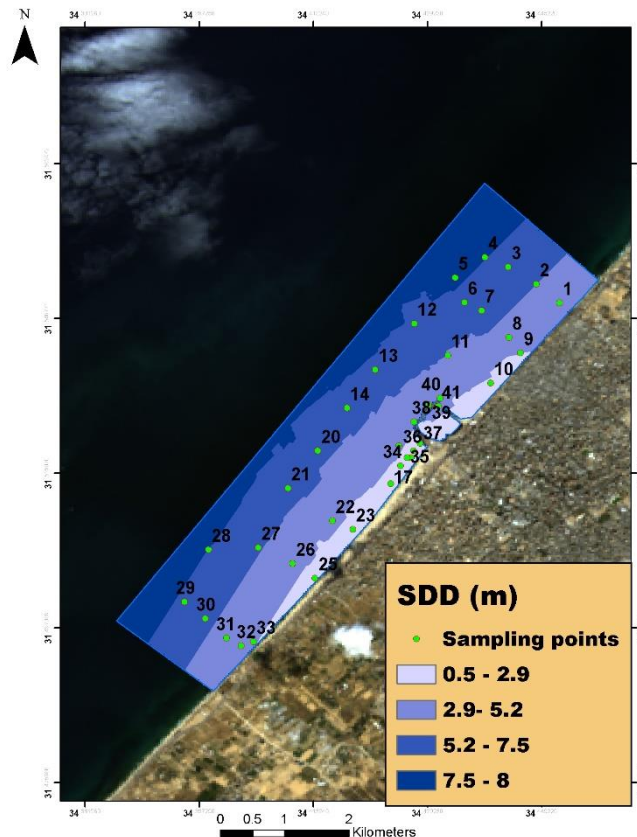
Fig (4.11): SDD distribution along the study area

4.3.1.1 SDD Model Development (Calibration

SDD measurements are commonly used to infer water body turbidity. Turbidity is measured using several methods, but the easiest and least expensive method is through utilization of a Secchi disk.

The two main steps were carried out to develop SDD retrieval model: calibration using empirical model for the determination of SDD values and accuracy assessment by comparing the field measurements with derived SDD values.

The sampling points were divided into two part: 24 points used for model development, the remaining 16 points were used for accuracy test. Landsat 8 OLI reflectance values Rrs (λ) were extracted after the necessary atmospheric and radiometric correction were performed.

In the first step, statistical approach of SDD to relate in-situ data and their corresponding Landsat8/ OLI reflectance values of (visible and infrared bands) was applied using regression analysis. The attempts to obtain the optimal retrieval algorithm for SDD estimation values included two model types: single-band model and band-ratio model. The correlation coefficient (R), coefficient of determination (R^2) and P-value of all 15 developed models were calculated to find the best SDD Algorithm. The results were summarized as follows:

- **Single-Band Model**

The results showed that correlation coefficients (R) between SDD field measurements and reflectance values of B1 and B2 single-band models were weak (R) < 0.5, Table (4.6). Meanwhile, a strong correlation coefficients were found between the SDD values and reflectance values of both B4 model and B5 model; which were R=0.81 and R=0.86 respectively with (P-value) < 0.05, Fig (4.13) and Fig (4.14).

Then, Fig (4.12) illustrates that B3 also showed a moderate coefficient of determination R^2=0.62, as B4 and B5, with correlation coefficient value (R) of .078. It is possible that single bands of red and inferred yield better correlation with SDD values due to elevated level of turbidity in the study area. These results are in accordance with many studies mentioned in the literature including the results of Hellweger et al., (2004) to estimate turbidity in relevance to the Secchi disk depth measurements, the results show that the use of ratios that include red reflectance are widely used and for multispectral sensors like Landsat 8, there are promising results for Secchi disk depth correlation even with the red band itself.

Table (4.6): Regression statistics of single-band model between OLI reflectance (IR/visible bands) and SDD

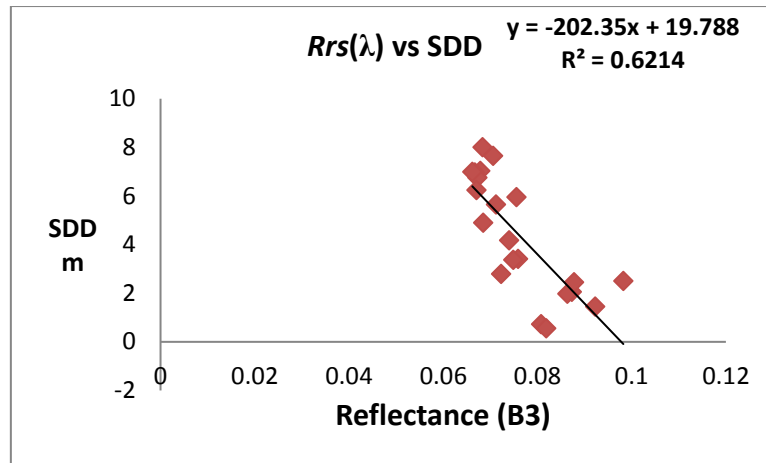| Regression Statistics	B1	B2	B3	B4	B5
R	0.068	0.274	0.788	0.869	0.811
R2	0.004	0.075	0.621	0.755	0.65862
P-value	0.690	0.104	2.2E-05	3.1E-07	8E-06
Observations	24	24	24	24	24

Fig (4.12): Regression analysis plot between B3 and SDD
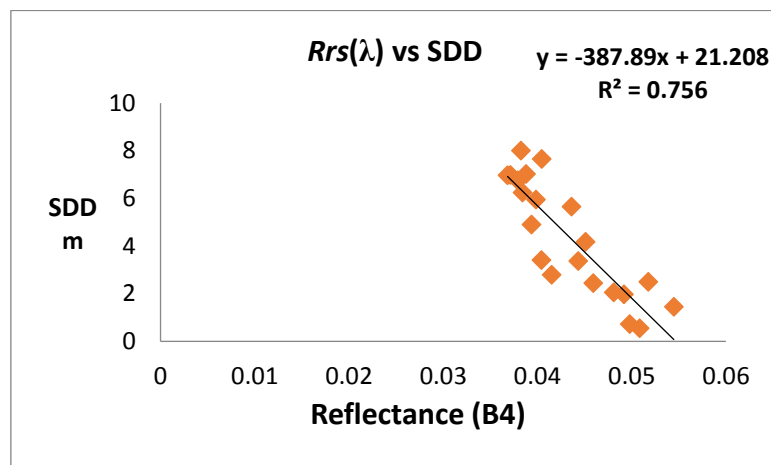

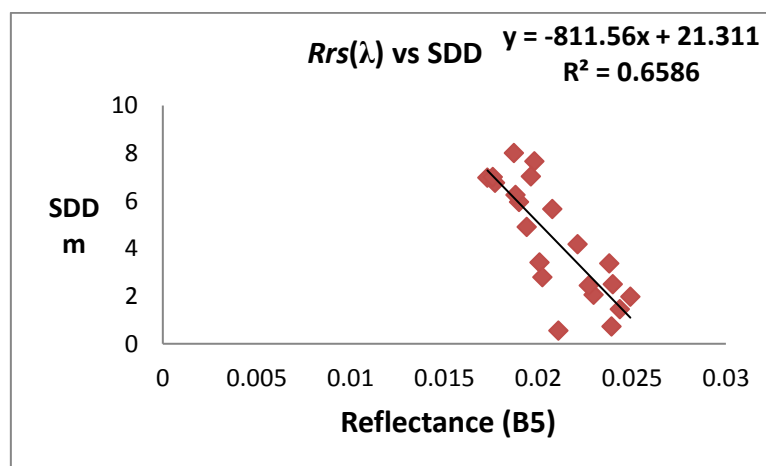**Fig (4.13): Regression analysis plot between B4 and SDD**

Fig (4.14): Regression analysis plot between B5 and SDD

53

- **Band-Ratio Model**

Thereafter, the SDD retrieval algorithm was built using regression analysis models to examine the relation between SDD and Landsat8/OLI reflectance values of band-ratio models. Table (4.7) illustrates that six tested band-ratio models out of ten models were found to have high correlation coefficients(R)>0.5.

The highest correlation coefficient (R=0.87) was yielded by B1/B4 model with coefficient of determination ($R^2 = 0.771$) as shown in Fig (4.15). This was then followed by band-ratio models of B2/B4, B2/B3 and B1/B3 which had relatively the same coefficient of determination, (R^2=0.7). Thereafter, band-ratio model of B1/B5 and B2/B5 came next with coefficient of determination (R^2 =0.6).

Generally, band-ratio correlation coefficient yields higher values than that of single-bands transformation with SDD. The same results found in many relevant literature, (Kabbara et al., 2008; Kratzer et al., 2008; Zhang, 2005; Hellweger et al., 2004), which showed that models with the highest correlation value used indices which included the blue and red spectral bands and sometimes bands from the infrared spectral region and green band. Additionally, Olmanson et al., (2011); Nelson et al., (2003), (2005); Sass et al., (2007) indicated that algorithms that made use of the Blue/Red ratio were selected as they have shown to be effective in describing SDD.

Table (4.7). Regression statistics of band-ratio model between OLI reflectance (IR/visible bands) and SDD

Regression Statistics	B1/B3	B1/B2	B1/B4	B1/B5	B2/B3
R	0.843	0.411	0.878	0.813	0.866
R2	0.711	0.169	0.771	0.661	0.750
P-value	1.5E-06	0.012	1.6E-07	7.4E-06	3.89E-07
Observations	24	24	24	24	24
Regression Statistics	B2/B4	B2/B5	B3/B4	B3/B5	B4/B5
R	0.865	0.782	0.252	0.022	0.238
R2	0.749	0.611	0.063	0.0005	0.057
P-value	3.9E-07	2.8E-05	0.137757	0.89624	0.160509
Observations	24	24	24	24	24
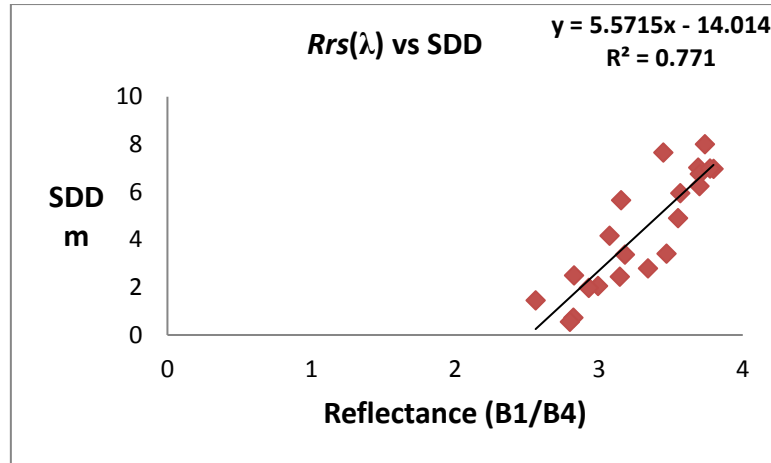
Fig (4.15): Regression analysis plot between B1/B4 and SDD

4.3.1.2 Accuracy Assessment for SDD Model

In order to assess the performance of the developed algorithms, the accuracy between in-situ data and derived SDD were tested using (RMSE) and (R^2). Table (4.8) shows that only calibrated models with strong correlation coefficient (R) and significant (P-value) were tested for accuracy.

A total of 16 test points out of 40 were selected randomly to examine the model accuracy. Band-ratio model of B2/B4 gave the highest accuracy of $R^2_{accuarcy}$ =0.783 and RMSE=1.051m, Fig (4.16), despite the fact that B1/B4 had the highest correlation coefficient during the development phase. Therefore, the regression algorithm equation shown in Fig (4.17) with independent variable of band-ratio of B2/B4, SDD=7.365(B2/B4)-15.367, could be used to model SDD in the study area.

Table (4.8): Statistical parameters for accuracy testing of SDD prediction model

Option N0	Band/band ratio	R^2 calibration	Regression equation	R^2 accuracy	RMSE (m)
Single -Band model					
Model 1	**B3**	0.6214	-202.35X+19.788	0.3813	1.679185
Model 2	**B4**	0.756	-387.89X+21.208	0.5861	1.396491
Model 3	**B5**	0.6586	-811.56X+21.311	0.5845	1.368399
Band-Ratio model					
Model 4	**B1/B3**	0.7119	10.086x-14.569	0.5245	1.47274
Model 5	**B1/B4**	0.771	5.5715X-14.014	0.7646	1.097929
Model 6	**B1/B5**	0.661	2.5861X-13.348	0.6542	1.251762
Model 7	**B2/B3**	0.7502	14.602x-17.89	0.6307	1.306266
Model 8	**B2/B4**	**0.7496**	**7.365x-15.367**	**0.783**	**1.051532**
Model 9	**B2/B5**	0.6116	3.3042X-14.02	0.6156	1.319558
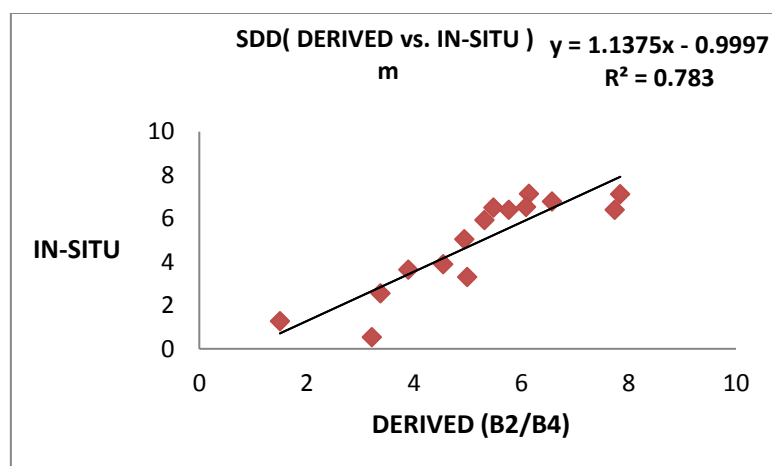
Fig (4.16): Accuracy assessment of SDD-derived data by B2/B4 model and in-situ data
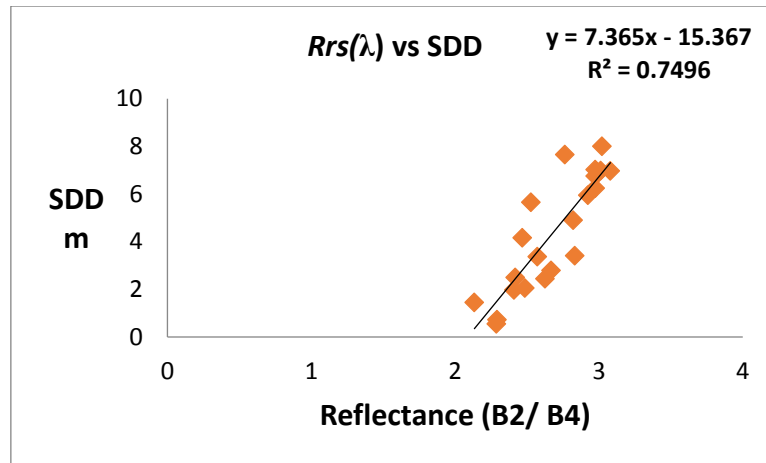
Fig (4.17): Regression analysis plot between B2/B4 and SDD

4.3.2 Total Suspended Solids (TSS)

TSS is one of water constituent which can be used as indicators for water quality. TSS in the coastal waters influences not only the rates and types of biological and chemical processing, but also geomorphic processes constructing the landforms. TSS samples were divided to three sets according to the field campaign:

- TSS1: represents TSS samples collected at the surface of seawater. TSS1 results ranged between 0.45 and 90.5, the highest concentration found at point 11 that was located relatively close to the sea beach at the northern direction. Sample points of high concentration were at different distances off the beach .e.g. the concentration of 20.6 found at point 5, far from the beach. Meanwhile, the sample point of 33, 30 and 23 were somehow close to the shoreline and high in concentration. The lowest concentration of 0.45 was found very close to the shoreline. Similarly, the point 16 and point 10 have low concentration and are close to the sea beach. In general, the TSS at sea surface showed a fluctuating pattern in terms of its location and compared to COD and FC.

- TSS2: stands for TSS samples collected at 2-m depth. Number of samples were small including 10 samples and its concentrations ranged between 0.18 and 9.06 found at point 355 and 350 respectively.

- TSS3: symbolizes TSS collected at 3-m depth. It had high concentration of 34.85 and low concentration of 0.12.

Results showed that the closer the sample to seabed was, the higher the TSS concentration became, and this could be demonstrated by the results of TSS3.

Fluctuating pattern of TSS were probably due to Irregular sewage influx discharging from outfalls along the study area. Also, sea currents direction from SWW to NNE along the Gaza Sea plays an important role in dilution and circulation processes of TSS. Fig (4.18) shows the distribution of average TSS.
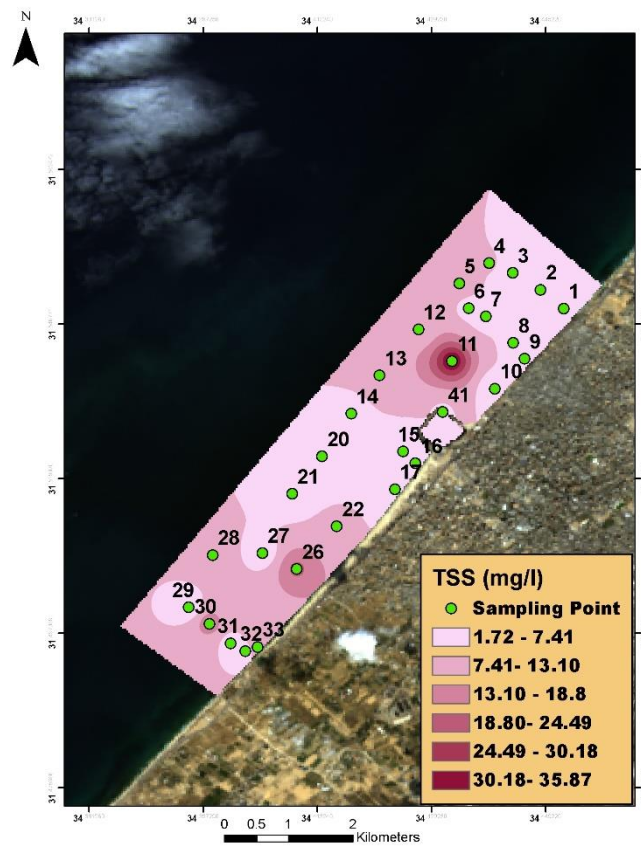
Fig (4.18): Average TSS distribution along the study area

4.3.2.1 TSS Model Development

Single-band and band-ratio models were examined using statistical analysis in attempts to find strong correlation between TSS and OLI reflectance Rrs (λ) and to develop TSS retrieval model.

In study area, results show that no correlation reported between both variables (TSS and OLI reflectance) either in single-band model case or band-ratio case. However, TSS at the depth 2-

m demonstrated a slight correlation, Fig (4.19), but the results still not enough to generate prediction model.
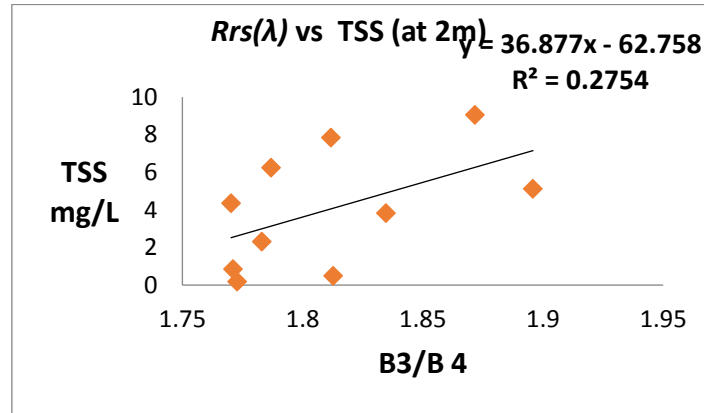
Fig (4.19): Regression analysis plot between B3/B4 and TSS at 2m

The low correlation between in-situ data and OLI reflectance values could be attributed to many reasons:

- Atmospheric correction algorithm performed by USGS has proved by many studies to have limitation. This phenomenon was reported by Setiawan, using a set of high quality in situ reflectance data collected over Lake Kasumigaura, Japan and also was reported by Jelani, examining the performance of USGS atmospheric correction and indicted that low correlation between measured and estimated TSS concentrations were caused not only by the performance of developed TSS estimation retrieval algorithms but also the accuracy of atmospherically corrected reflectance of Landsat product.

- Wastewater discharge: Wastewater discharge might have their negative contribution in TSS estimation as organic pollutants from sewage outlets discharging in water column influences the light path which will reflect off the water surface. So consequently, reflectance values will be affected in the satellite images. Moreover, uneven flow and spatial distribution of sewage outlets in the study area might weaken the correlation between reflectance and TSS concentration. The wastewater flow characteristics varies from one outlet to another, thereof, the optical characteristics of seawater would be spatially different. In return, the relationships between the reflectance values and TSS becomes more complicated and yields low correlation coefficient. These correlation could be improved if further data of seawater constituents that impact reflectance values in water column are considered.

Chapter (5)

Bathymetry Prediction Model

A total of 40 depth points were collected from the study area using depth electronic sounder, Fig (5.1). This in situ measurements are very necessary to run the regression analysis and calibrates the model. In order to obtain satellite derived bathymetry (SDB), the obtained OLI image was preprocessed starting from performing radiometric correction by converting digital numbers into reflectance values. Then, atmospheric correction was performed to remove the effect of clouds and aerosols. The following steps included water separation, spatial filtering, glint correction and bathymetry extraction as shown in Fig (3.2).
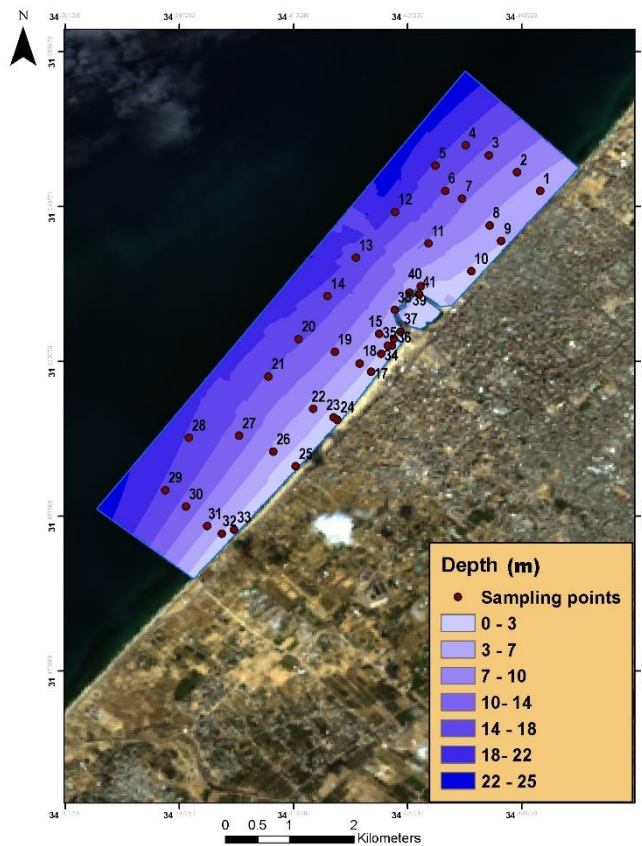
Fig (5.1): A bathymetric map showing the sampling depth points in the study area

Consequently, model development (calibration) and accuracy tests are necessary steps to develop the optimal retrieval bathymetry model. The strength of relationship between Landsat OLI/8 reflectance values and in-situ depth values was analyzed using linear regression statistics including correlation coefficient (R), coefficient of determination (R^2) and (P-value) in order to develop well-established model.

61

Thereafter, the actual depth was statistically compared to satellite derived bathymetry (SDB) values to assess accuracy of the developed model using different statistical indictors (R^2) and (RMSE).

5.1 Model Development

Empirical approach was used to establish the bathymetry retrieval model between in-situ depth values and Landsat8 reflectance values. The calibration results were divided based on model type (single-band, band-ratio) and depth range (shallow, deep and entire measured depth range).

5.1.1 Model Type

Over the study area, two model types were used to develop depth retrieval model over the entire field-measured depth range (0 m-20 m): Single-band and band-ratio.

- **Single-Band Model**

Firstly, regression statistics were calculated between the visible single-bands reflectance values (B1, B2, B3 and B4) and in-situ depth as illustrated in Table (5.1). The results showed that B3 and B4 had strong correlation coefficient (R) of 0.7320 and 0.7732, Fig (5.2) and Fig (5.3), respectively with (P-value) < 0.05 in comparison with B1 and B2 that demonstrated weak correlation coefficient (R) of 0.15 and 0.19 respectively. These findings could a good indication that Landsat OLI/8 bands might be used to build the incoming relationship between depth and reflectance values Rrs (λ).

Table (5.1): Regression statistics of single-band model between OLI reflectance (visible Bands) and depth (0-20) m

Regression Statistics	B1	B2	B3	B4
R	0.1503	0.193	0.732	0.773
R^2	0.022	0.037	0.535	0.597
P-value	0.453	0.334	1.42E-05	2.26E-06
Observation	27	27	27	27

Fig (5.2): Regression analysis plot between B3 and depth (0-20) m
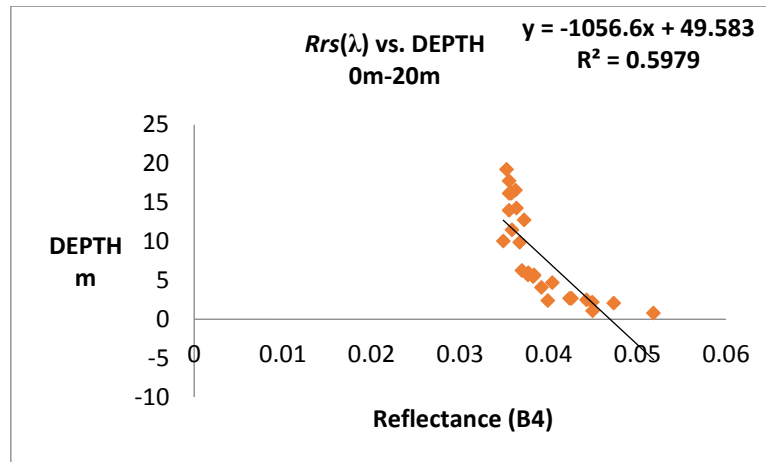
Fig (5. 3): Regression analysis plot between B4 and depth (0-20) m

- **Band-Ratio Model**

Secondly, a combination of band-ratio models based on pretested single-band models was statistically examined as shown in Table (5.2). Fig (5.4) shows that the highest correlation value (R) of 0.87 was achieved by the band-ratio model of B2/B3 with (P-value) less than 0.05 and (R^2 =0.76) followed by a correlation coefficient (R) of 0.84 of both B1/B3 model and B1/B4 model, Fig (5.5) and Fig (5.6), respectively. Also, band-ratio model of B2/B4 model gave a good correlation coefficient (R) of 0.82, Fig (5.7). According to the obtained results, it was concluded that band-ratio model could be more effective in extracting bathymetry over wide

range of depths and particularly band-ratio model making use of green and blue bands had the higher correlation coefficients (R) compared with other band-ratio models.

Table (5.2): Regression statistics of band-ratio model between OLI reflectance (visible bands) and depth (0-20) m

Regression Statistics	B1/B2	B1/B3	B1/B4
R	0.481737213	0.843845063	0.84494058
R^2	0.232070742	0.71207449	0.713924584
P-value	0.010948493	0.010948493	2.9619E-08
Observation	27	27	27
Regression Statistics	B2/B3	B2/B4	B3/B4
R	0.874506573	0.828657169	0.049386934
R^2	0.764761746	0.686672703	0.002439069
P-value	2.48823E-09	9.40064E-08	0.806744435
Observation	27	27	27

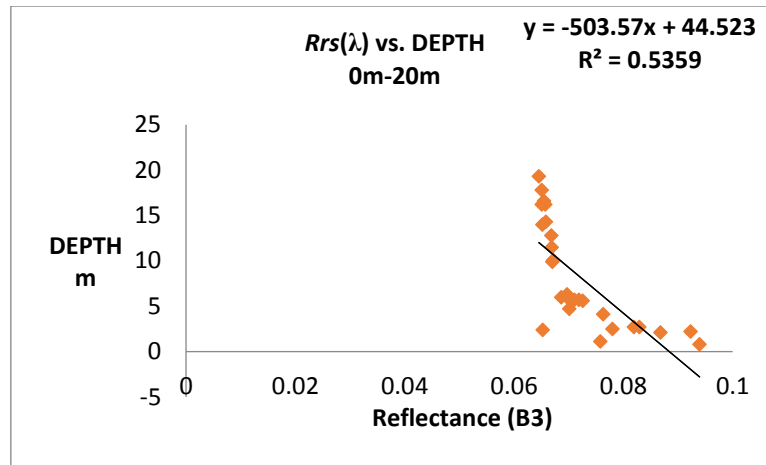**Fig (5.4): Regression analysis plot between B2/B3 and depth (0-20) m**

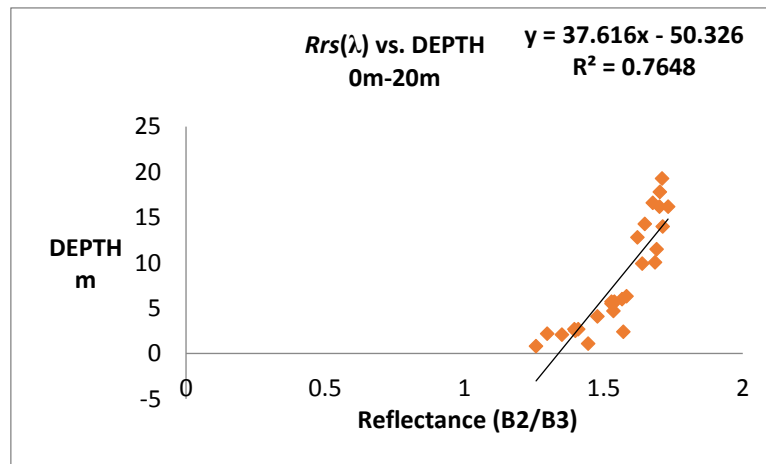**Fig (5. 5): Regression analysis plot between B1/B3 and depth (0-20) m**

Fig (5. 6): Regression analysis plot between B1/B4 and depth (0-20) m
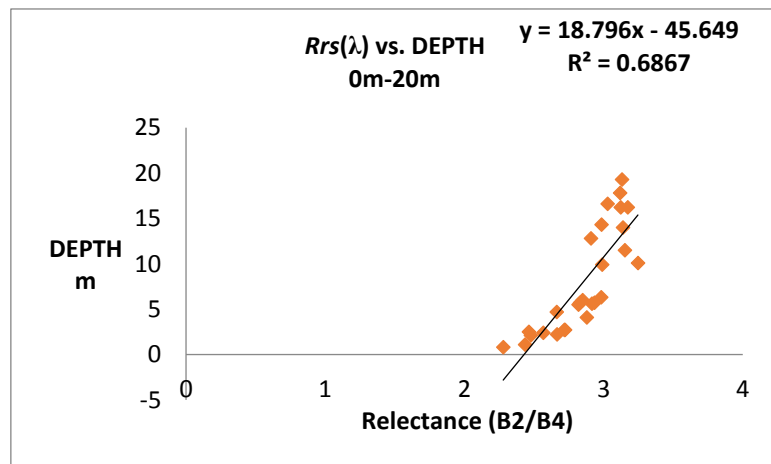
Fig (5. 7): Regression analysis plot between B2/B4 and depth (0-20) m

5.1.2 Depth Range

Considering the data distribution in the previous scatter plots of model type section (5.1.1), it was noticed that there were two distinctive depth ranges. Therefore, as a kind of model improvement, in-situ depth points were divided in two ranges (0 m to 8 m) and (9 m to 20 m). Subsequently, the regression statistical indictors including (R, R^2 and P-value) of both model types (single, ratio) were retested over the divided two depth ranges to find the best relationship. Accordingly, the results could be divided in four groups:

1. Single-band model over the range of 0 m to 8 m
2. Single-band model over the range of 9 m to 20 m
3. Band-ratio model over the range of 0 m to 8 m
4. Band-ratio model over the range of 9 m to 20 m

- **Single-band model over the range of 0 m to 8 m**

Single-band models were examined over the shallow depth range (0m-8m), the outcomes showed that single-band models of B3 and B4 had strong correlation coefficient (R)>0.5, Fig (5.8) and Fig (5.9) respectively. Particularly, B3 model shows the highest correlation coefficient (R) of 0.88. While B1 model has the weakest correlation coefficient (R) of 0.38, Table (5.3).

Table (5.3). Regression statistics of single-band model between OLI reflectance (visible bands) and depth (0-8) m

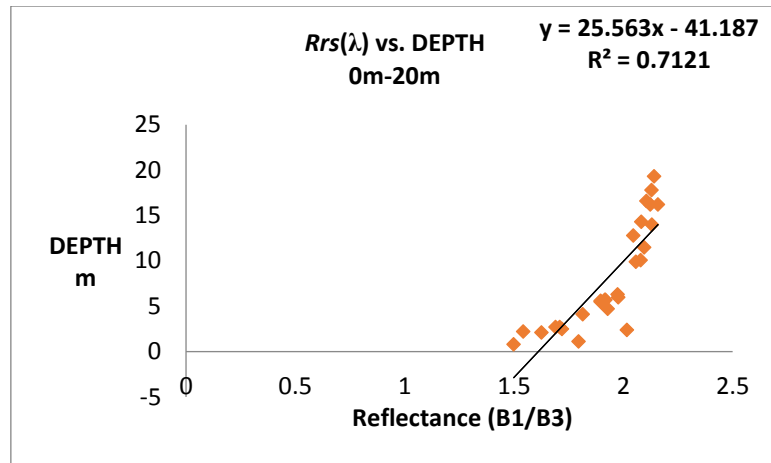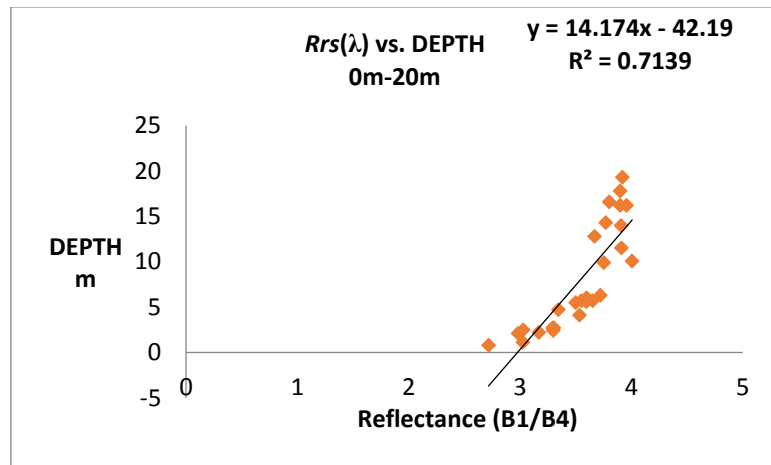| Depth range (0m-8m)				
Regression Statistics	B1	B2	B3	B4
R	0.384	0.607	0.885	0.878
R^2	0.147	0.368	0.784	0.771
P-value	0.141	0.012	4.94E-06	7.531E-06
Observation	16	16	16	16
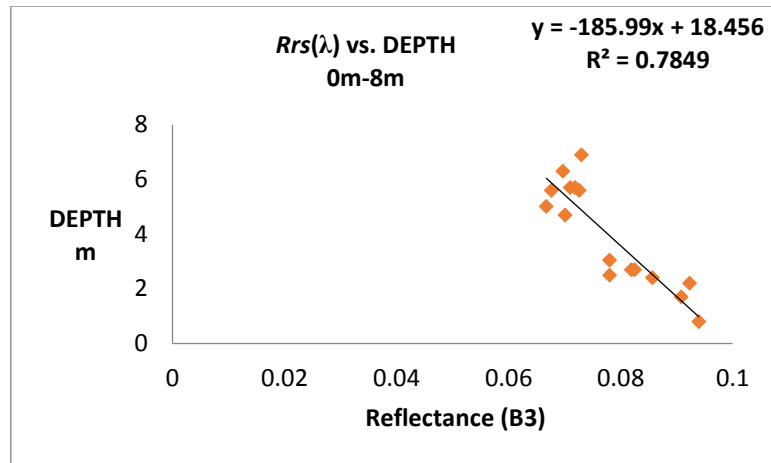
Fig (5.8): Regression analysis plot between B3 and depth (0-8) m
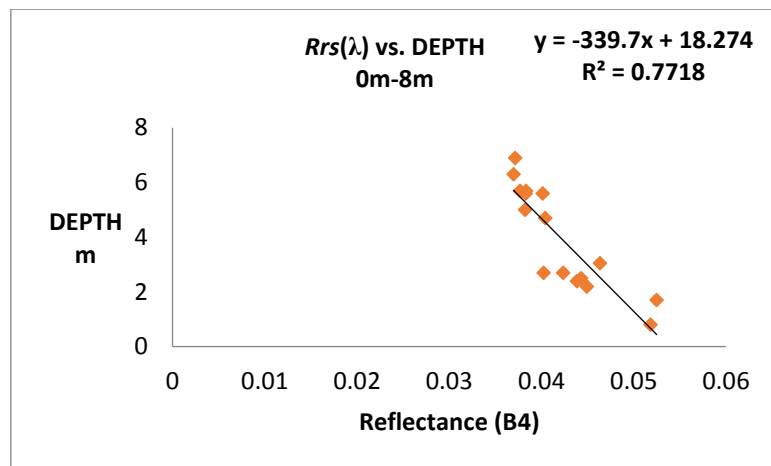
Fig (5.9): Regression analysis plot between B4 and depth (0-8) m

- **Single-band model over the range of 9 m to 20 m**

Results demonstrated that points of deep range (9m-20m) had low correlation coefficients with single-band models of B1, B2, and B4 as shown in Table (5.4). However, B3 model strongly correlated, R=0.85, with points in deeper range with (P-value) < 0.05, Fig (5.9).

Table (5.4): Regression statistics of single-band model between OLI reflectance (visible bands) and depth (9-20) m

Depth range (9m-20m)				
Regression Statistics	B1	B2	B3	B4
R	0.296	0.369	0.849	0.231
R^2	0.088	0.136	0.721	0.053
P-value	0.375	0.263	0.0009	0.493
Observation	11	11	11	11
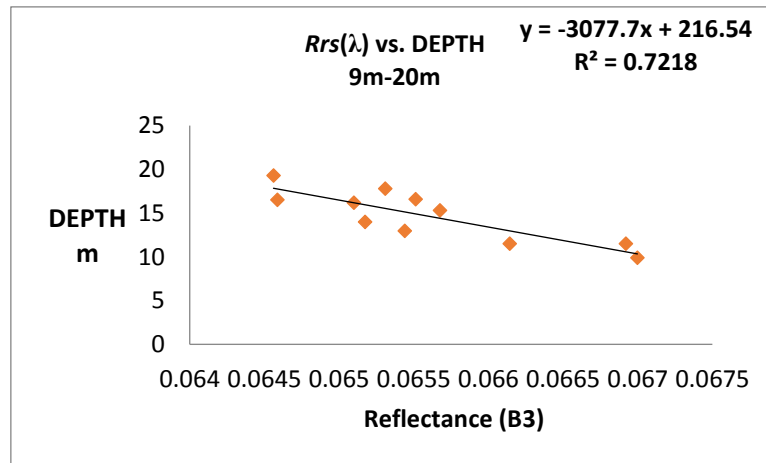
Fig (5.10): Regression analysis plot between B3 and depth (9-20) m

Afterward, the significance of Landsat8/OLI band-ratio models over the two distinct ranges was investigated.

- **Band-ratio model over the range of 0 m to 8 m**

The strongest correlation coefficient (R) of 0.95 was found between the band-ratio model of B2/B3 and OLI reflectance values over the range (0m-8m), Fig(5.11). Also, Table (5.5) illustrates that B1/B2, B1/B3, B1/B4 and B2/B4 also had a high correlation coefficient (R)> 0.5 with shallow depths.

Table (5.5). Regression statistics of band-ratio model between OLI reflectance (visible bands) and depth (0-8) m

Depth rang (0m-8m)			
Regression Statistics	B1/B2	B1/B3	B1/B4
R	0.790	0.935	0.867
R^2	0.625	0.875	0.752
P-value	0.0002	1.03E-07	1.330E-05
Observation	16	16	16
Regression Statistics	B2/B3	B2/B4	B3/B4
R	0.950	0.795	0.022
R^2	0.902	0.633	0.0004
P-value	1.78E-08	0.0002	0.0002
Observation	16	16	16
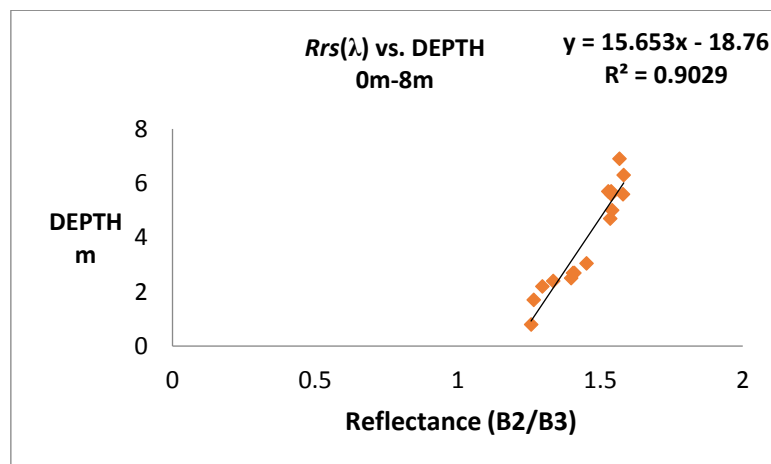
Fig (5. 11): Regression analysis plot between B2/B3 and depth (0-8) m

- **Band-ratio model over the range of 9 m to 20 m**

Whereas, low correlation coefficient valves, (R) < 0.5, were obtained over deep range (9m-20m) as shown in Table (5.6). In general, over shallow depths, band-ratio models were more effective than single-band models yielding better statistical indictor as opposed to deeper points which were in good terms with single-band model.

Table (5.6). Regression statistics of band-ratio model between OLI reflectance (visible bands) and depth (9-20) m

Depth range (9m-20m)			
Regression Statistics	**B1/B2**	**B1/B3**	**B1/B4**
R	0.417302113	0.598533692	0.075238515
R^2	0.174141053	0.35824258	0.005660834
P-value	0.201616993	0.051722652	0.825980958
Observation	11	11	11
Regression Statistics	**B2/B3**	**B2/B4**	**B3/B4**
R	0.328833426	0.038329226	0.482454888
R^2	0.108131422	0.00146913	0.232762719
P-value	0.323455629	0.910914319	0.132846588
Observation	11	11	11

5.1.3 Accuracy Assessment

In order to select the optimal depth retrieval model, the relationship between the satellite derived bathymetry (SDB) and in-situ depth data was checked to assess model accuracy using different statistical indictors: coefficients of determination (R^2) and root mean square error (RMSE). Only depth models that yielded ($R^2_{Calibration}$)> 0.5 and (P-value) less than 0.05 were tested for accuracy. The suitable prediction model was selected based on the highest coefficients of determination (R^2) and the acceptable root mean square error (RMSE) to obtain the spatial distribution of data. Results of accuracy assessment were divided into three parts: entire depth range (0-20) m, shallow depth range (0-8) m, and deep depth range (9-20) m.

- **Entire in-situ depth range (0m-20m)**

The accuracy results for the entire depth range are shown in Table (5.7). The results revealed that both band-ratio models of (B2/B3) and (B1/B3) achieved the highest ($R^2_{accuracy}$) of 0.78 between the SDB values versus in-situ measurements. However, band-ratio model of B2/B3, Fig (5.12), was adopted to predict depth in the study area since model.5 (B2/B3) achieved RMSE = 2.81m that is lesser than the value of RMSE=2.9 of model.3 (B1/B3), Table (5.7).

Table (5.7): Statistical parameters for accuracy testing of Bathymetry prediction model (0-20) m

Depth range (0-20) m					
Model No.	**Band/band ratio**	**R^2** calibration	**Regression equation**	**R^2** accuracy assessment	**RMSE (m)**
Single-band models					
Model.1	**B3**	0.5359	-503.57B3+44.523	0.5577	3.966049
Model.2	**B4**	0.5979	-1056.6B4+49.583	0.5427	4.182621
Band-ratio models					
Model.3	**B1/B3**	0.7121	25.563*b1/b3-41.187	0.7819	2.911399
Model.4	**B1/B4**	0.7139	14.174B1/B4-42.19	0.6831	3.522471
Model.5	**B2/B3**	**0.7648**	**37.616b2/b3-50.326**	**0.78**	**2.813227**
Model.6	**B2/B4**	0.6867	18.796b2/b4-45.649	0.6283	3.835946
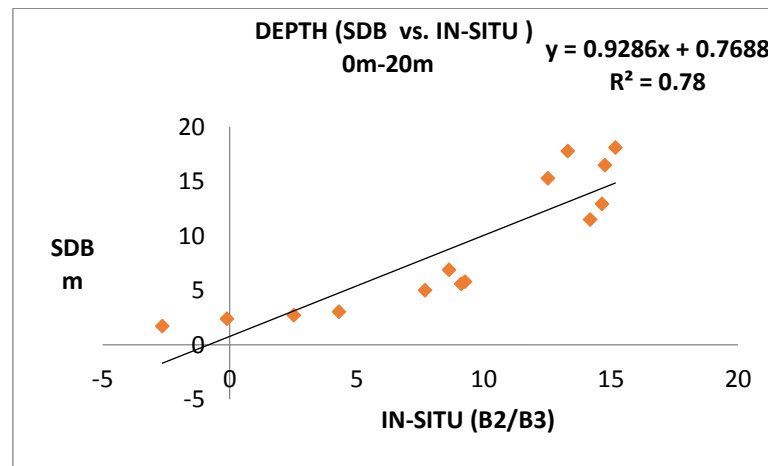
Fig (5. 12): Accuracy assessment between SDB using B2/B3 model and in-situ data

- **Depth range (0-8) m**

Each model with ($R^2_{calibration}$)>0.5 and significant (P-value) less than 0.05 was examined in accuracy assessment step as illustrated in Table (5.8). Although B2/B3 model, model.9, yielded the highest coefficient of determination ($R^2_{calibration}$) and correlation coefficient (R) during calibration step, results demonstrated that B1/B4 model had the highest ($R^2_{accuarcey}$) of 0.76 and acceptable RMSE =1.07m, Fig (5.13). The values of these indices showed that the band-ratio model was more effective than the single-band model in accurately estimating the depth of

shallow area (0m -8m). Generally, all band-ratio models that include B4 are proven to be effective in shallow depth as reported by Jupp. Model.7, Fig (5.14), could be used to determine shallow depths over the study area.

Table (5.8): Statistical parameters for accuracy testing of Bathymetry prediction model (0-8) m

Depth range (0-8) m					
Model No.	**Band/Band ratio**	**R^2** calibration	**Regression equation**	**R^2** accuracy assessment	**RMSE m**
Single-band model					
Model 1	B3	0.7849	-185.99B3+18.456	0.3103	1.82342
Model 2	B4	0.7718	-339.7B4+18.274	0.7214	1.192664
Band-ratio model					
Model 5	B1/B2	0.6256	63.4B1/B2-73.891	0.0962	2.266597
Model 6	B1/B3	0.8754	10.34B1/B3-14.492	0.3328	1.764805
Model 7	**B1/B4**	**0.7529**	**4.8698B1/B4-12.122**	**0.7647**	**1.071674**
Model 8	B2/B4	0.6335	6.027B2/B4-12.236	0.7038	1.120166
Model 9	B2/B3	0.9029	15.653B2/B3-18.76	0.4408	1.575946
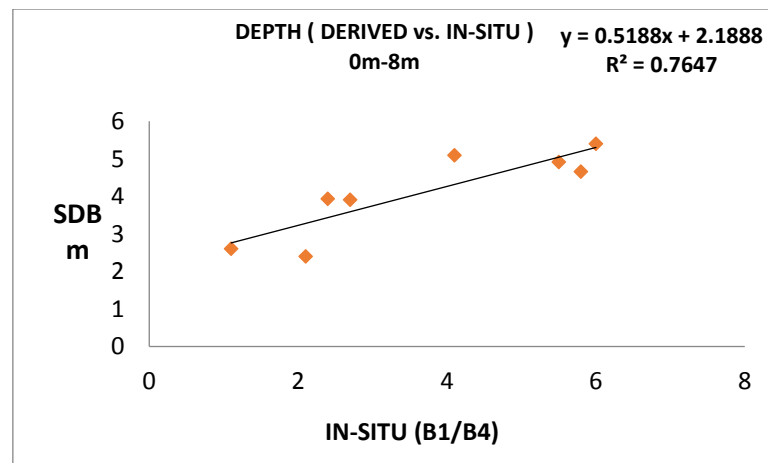
Fig (5.13): Plot of accuracy assessment between SDB using B1/B4 model and in-situ data
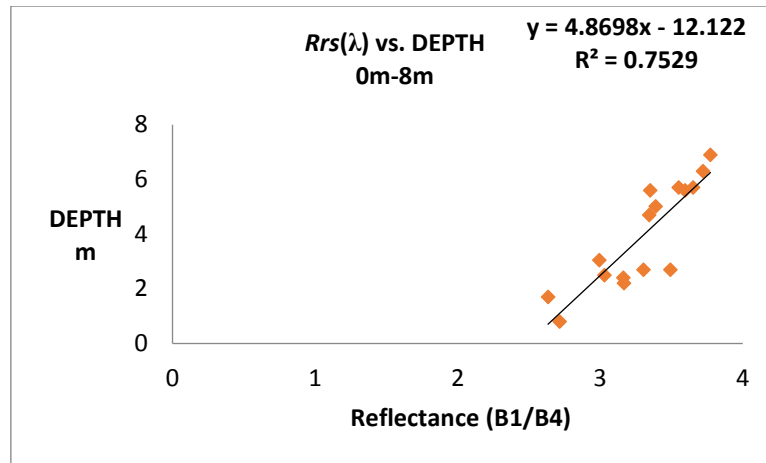
Fig (5.14): Regression analysis plot between B1/B4 and depth (0-8) m

- **Deep rang (9-20) m**

Only single-band model of B3 showed the highest correlation coefficient during calibration ($R^2_{Calibration}$=0.82) and accuracy assessment ($R^2_{accuracey}$= 0.87) over deep range as shown in Table (5.9) and Fig (5.15). This indicted that single-band transform model was more effective in deeper range of the study area and despite that band-ratio models minimize the bottom variation but it doesn't necessary improve the statistical relationship over all depth ranges

Table (5. 9): Statistical parameters for accuracy testing of Bathymetry prediction model (9-20) m

Model No.	Band/band ratio	R^2 calibration	Regression equation	R^2 accuracy assessment	RMSE m
Depth range (9-20) m					
Single-band model					
Model 1	B3	0.7218	-3077.7b3+216.54	0.901	1.324408

73
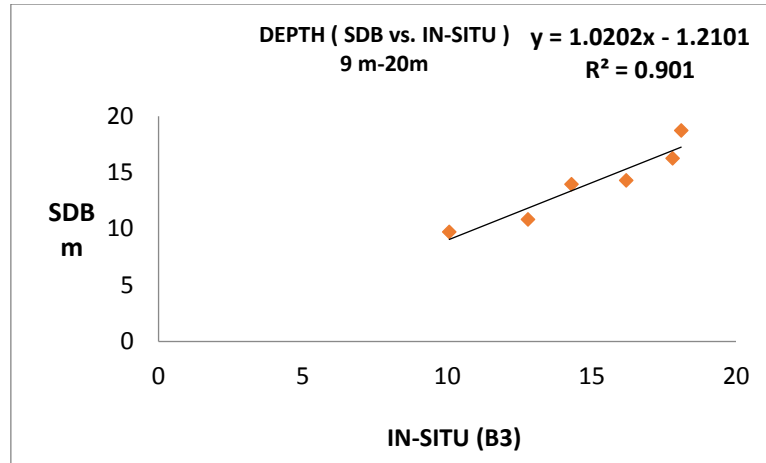
Fig (5.15): Plot of accuracy assessment between SDB using B3 model and in-situ data

5.2 Combined Model

As advanced step to improve accuracy of the derived depth values, a combined model of single-band, band ratio was developed. As with the single and ratio models, the unknown parameters were determined by applying multiple linear regression on the 3 chosen combined models over the 3 depth ranges. These models were built based on the statistical results obtained from previous analysis of each model type separately, (single-band, band-ratio), by combining highly correlated single-band models and band-ratio models in one model with depth values. The three statistical indices (R, R^2 and P-value) were determined for three different combined models. The results (SDB) obtained from combined models were compared with the SDB extracted by single-band or band-ratio models performed separately. Models were divided into three groups based on depth range:

- **The entire measured depth range**

Over the range (0-20)m, accuracy test showed that SDB obtained separately by the band-ratio model of B2/B3 and single-band model of B3 correlated very well with the in-situ depth measurements that was $R^2 = 0.76$ and $R^2 = 0.53$ respectively. Using method of combined model of both (B3 and B2/B3) with Landsat8/OLI reflectance values showed that relationship was improved at the development step and the accuracy test step, Table (5.10). Accurate results were demonstrated by model.3 in Fig (5.16), through the statistics indices (RMSE=2.5 m, $R^2 = 0.84$) compared with the B2/B3 model that had RMSE of 2.8 m.

Table (5. 10): Summary of optimal statistics parameters for accuracy testing over the depth range (0-20) m

Model No.	Band	R	R^2 calibration	P-value	Equation	RMSE (m)	R^2 accuracy assessment
Model.1	B2/B3	0.8745	0.764762	2.49E-09	37.616X-50.326	2.813	0.78
Model.2	B3	0.732	0.5359	1.42E-05	-503.57X+44.523	3.9660	0.5577
Model.3	B2/B3,B3	0.91	0.83	3.791E-10	159.7+665.32B3+77.074B2/B3	2.55	0.84
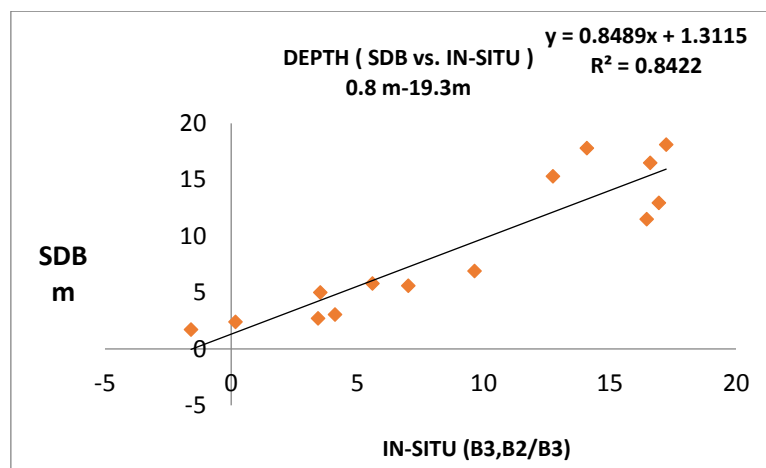
Fig (5. 16): Plot of accuracy assessment between SDB using combined model of (B3, B2/B3) and in-situ data

- **Shallow depth range**

While improvement was shown over the entire range depth (0-20) m, the method of combination had no improvement over the range (0-8) m using combined model of B4, B1/B4. The statistical indicators of (model.1 and model. 3), Table (5.11), were relatively similar, ($R^2_{accuracy}$ =0.7and RMSE=1.1), so the simpler one (Model.1) was selected as the optimum model.

Table (5. 11): Summary of optimal statistics parameters for accuracy testing over the depth range (0-8) m

Model No.	Band	R	R^2 calibration	P-value	Equation	RMSE(m)	R^2 accuracy assessment
Model.1	**B1/B4**	**0.867719**	**0.752935**	**1.33E-05**	**4.8698X-12.122**	**1.07167**	**0.7647**
Model.2	B4	0.8785	0.7718	7.53E-06	-339.7X+18.274	1.19266	0.7214
Model.3	B1/B4,B4	0.88	0.77	5.995E-05	**9.259219-241.23B4+1.47B1/B4**	1.113	0.74

- **Deep depth range**

It was noticed that reflectance values, over the deeper range of (9-20) m, only correlated with B3 models of all single-band and band-ratio models. In order to perform combined transform model, B1/B3 model was chosen to represent band-ratio term in the combined model as it displayed moderate correlation coefficient (R) of 0.59. Multivarite regression analysis of B3, B1/B3, used to develop the combined retrieval model, showed a nearly close results. However, combined model gave a more acceptable RMSE of 1.1 compared with B3 model individually, Table (5.12), Fig (5.17).

Table (5.12): Summary of optimal statistics parameters for accuracy testing over the depth range (9-20) m

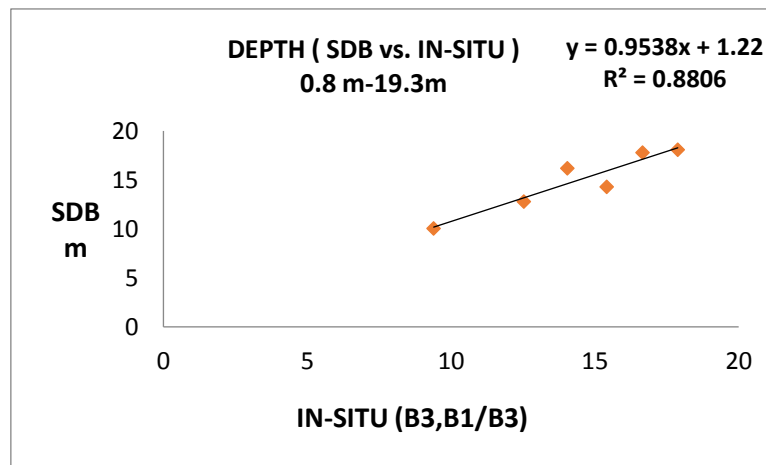| Model No.	Band	R	R^2 calibration	P-value	Equation	RMSE(m)	R^2 accuracy assessment
Model1	B3	0.849615	0.721846	0.00093	-3077.7X+216.54	1.324	0.901
Model2	B1/B3	0.5985	0.358	0.0517	60.19X-113	-	-
Model3	B1/B3,B3	0.88	0.77	0.002462508	402.25-4455.03*B3-B1/B3*44.96	1.136	0.88

Fig (5. 17): Accuracy assessment between SDB using combined model of (B3, B1/B3) and in-situ data

Chapter (6)

Implementation of Prediction Models

6.1 Seawater Quality Prediction Model

Following the selection of optimal retrieval model, some preprocessed Landsat8 Imageries were selected based on certain criteria which includes a relatively similar atmospheric and meteorological conditions. Therefore, the models were applied on images acquired one or two-month prior and following the sampling trip date in order to estimate the value of both SDD and P concentrations. A specified criteria were set because empirical models are limited in their application to the condition for which the data are collected. A general view of derived water quality parameters (P and SDD) were represented using color-coded maps for the study area.

Many factors play an important role in the SDD and P spatial patterns in the study area including oceanographic factors e.g. current direction, wave and wind direction, sewage nature, sewage volume and sewage discharge frequency.

6.1.1 Phosphorus Prediction Model

Spatial distribution of P levels on sampling trip day (4 November 2017) is shown in Fig (6.1), with an average value of 1.25 mg/l. The highest P concentration, ranges from 1.5 to 2.5 mg/l, is observed in the Gaza port basin since it is a semi-enclosed area of stagnant seawater that receives sewage effluent from outfall No.6. In addition, the southern part of the port basin exhibits high P levels at several spots that represents sewage outfalls (1, 2 and 3), given that sewage outfall 2 is owned by fish farm disposing nutrient-rich sewage. Meanwhile, the northern part of the study area shows a moderate concentration of P compared with the southern part. The difference in sewage outfall numbers and the nature of sewage from place to place might be the reason of P variation between north and south. As result of the prevailing northward current direction, a moderate P levels drifted a considerable distance far from the beach.
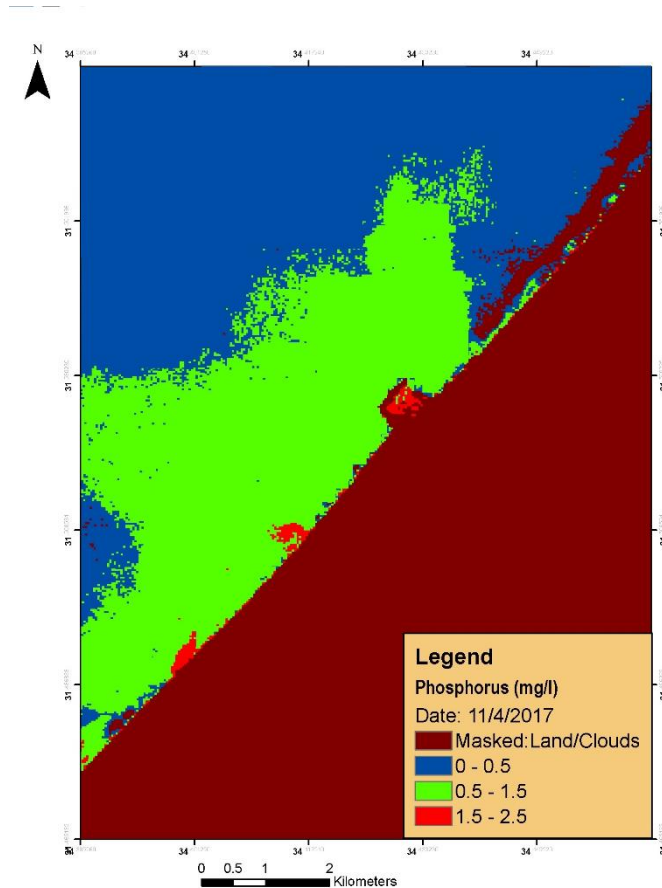
Fig (6.1) P distribution using prediction model on 4, November 2017

The spatial distribution of predicted P values along the study area on 1, September 2017 is shown in Fig (6.2.A) respectively. It is noticed that the area adjacent to the beach is heavily polluted (red-covered) with phosphorus in both direction (north, south) including Gaza port basin, it is possible that all sewage outfalls spotted in the study area was working on full capacities on that day or the sewage discharge volume was huge enough to disseminate close to the beach. While levels of P in the south starts to decrease going offshore, the concentration of P increases moving far from the beach in the southern part of Gaza fishing port. It is possible that the prevailing northward currents is pushing the pollution from north to south.

With regards to the image 27, October 2017, the P concentration appears to be low compared to other images, however, the Gaza port basin still exhibits the highest concentration. It is possible that all sewage outfalls were not working on that day, Fig (6.2.B).

80

Whereas, Fig (6.2.C) shows that 11, November 2017 image has comparatively the same spatial distribution of sampling image (4, November 2017) in which Gaza fishing port and the southern part have the highest concentration of P compared with the moderate concentration of P in the northern parts as well as that the pollution spreads far from the beach. However, there is one difference that green area(moderate transparency) on 11, November 2017 is smaller compared with 4, November 2017, the reason might be the outfall NO.2, No.3 is not working in that day.
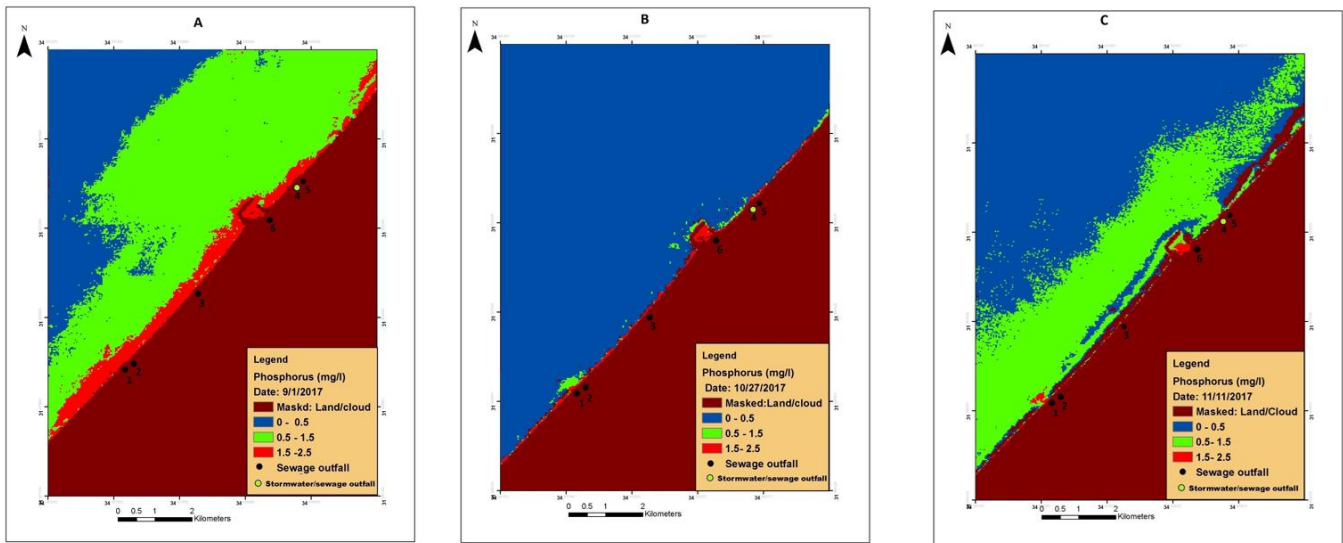
Fig (6. 2): P distribution using Prediction model on: A) 1, September 2017, B) 27, October 2017, C) 11, November 2017

6.1.2 Secchi Disc Depth Prediction Model

Spatial patterns of SDD derived on sampling day (4, November 2017), using Landsat8, along Gaza coastal area are shown in Figure (6.3). The predicted SDD values have an average value of 5 m. Due to sediment suspension and sewage outfalls, the shallower SDD values (red color) is found adjacent to the beach and in shallower waters. Meanwhile the green color, representing moderate SDD values, covers considerable distance in the southern part of the Gaza fishing port. Fig (6.4) illustrates that the spatial distribution of P in that day is to some extent close to SDD, in which the northern part of Gaza fishing port has deeper SDD and lower P levels compared to the south of the Gaza port basin, which might be reflected by sewage outfalls numbers and nature of sewage discharge. Another common aspect between SDD image and P image that green color (moderate P and moderate SDD) reaches considerable distances far from the beach.
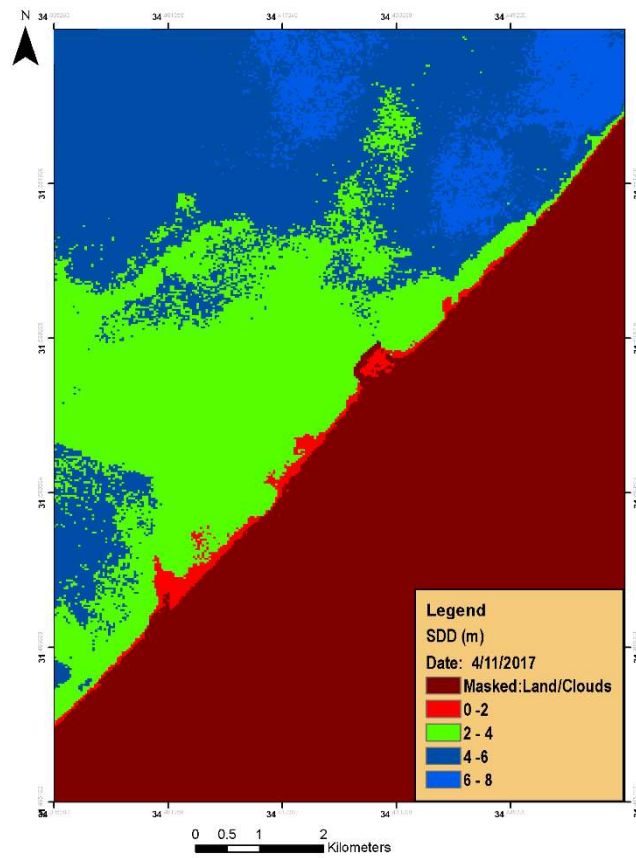
Fig (6.3): SDD distribution using prediction model on 4, November 2017
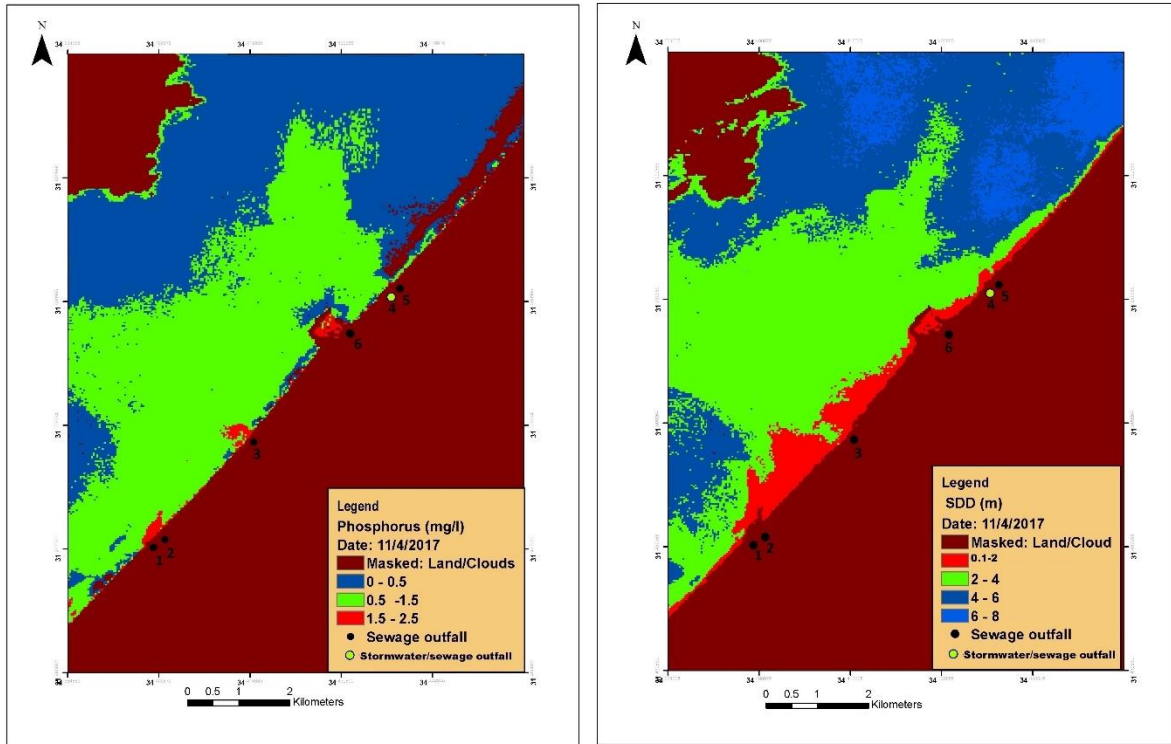
Fig (6.4): P and SDD distribution using prediction model on 4, November 2017

On 1, September 2017, SDD value ranges between 0-8 with mean value of 4 m. Fig (6.5.A) demonstrates that the red color, covering a near-shore area, indicates low transparency. This high levels of turbidity are possibly caused by sewage outfalls and northward current direction. The SDD and P distribution show that the pollution in September image is more prevalent, particularly in the northern part.

It is also observed that area covered with the shallower SDD in September image are wider compared with the near-shore area in November and October, Fig (6.5). There are two possible interpretations for the P and SDD variation between September and November, first due to differences of season (summer/fall) or due to currents direction which help carry pollution to the northern parts or sewage outfall.

Meanwhile, in October, 2017, Fig (6.5.B) shows that SDD increases normally as the depth increases. SDD is shallower when close to the beach and at the fishing port due to sediment suspension and sewage outfalls. This normal distribution gives indication that the turbidity levels are in its allowable ranges.

Regarding the image of 11, November 2017, after a week of sampling, Fig (6.5.c) shows that the area close to beach has shallow SDD values (low transparency). Also, it is observed that that SDD is shallower in the southern area where P levels is high, whereas northern part has deeper SDD values .It is noticed that offshore southern part has moderate to shallow SDD values. The light blue color barely appears which might give indication that pollution drifts away from the beach.
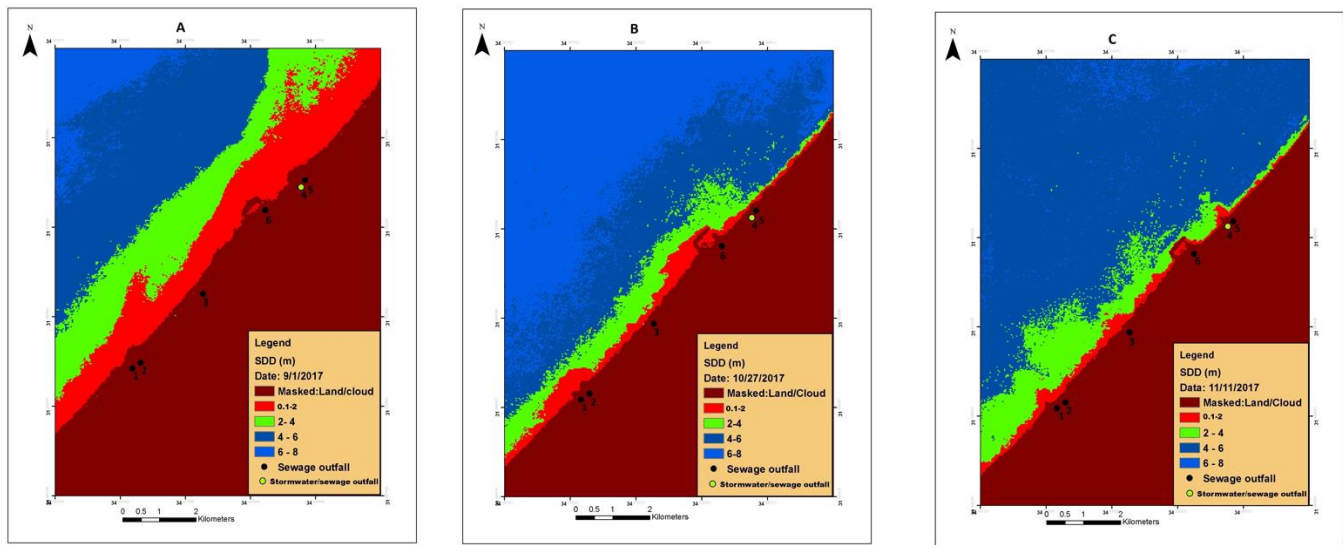
Fig (6.5): SDD distribution using prediction model on: A) 1 September, B) 27 October 2017, C) 11, November 2017

In general, Red areas, where SDD is low and Phosphorus is relatively high, can be observed at several hotspots adjacent to the shoreline, in particular along the southern coastal stretch and Gaza fishing port basin. The turbid water plumes along the coastal stretch, where water SDD fall below the critical values of 2 to 3 m according to UNEP-WHO, (1982), display P concentrations up to and above 1 mg/. Sewage outfalls, at various locations, indicated in the maps, might be at least partly responsible for such conditions, due to their abundant release of organic matter and nutrients. The spatial patterns of predicted SDD and P concentrations are reflecting a spatial compatibility along the study area.

6.2 Bathymetry Prediction Model

This section demonstrates and compares the various SDB maps produced from the Landsat8 images over different years (2014, 2017 and 2018). Model3, Table (6.10), was applied to obtain bathymetrical data over the study area.

2014

The analysis results of Image 2014 shows that the southern near-shore shallow area of Gaza fishing port have greater quantity of sediments compared with northern part that could be inferred from depth ranges. Northern area of Gaza fishing port is known of continuous erosion due to construction of Gaza fishing port which causes the prevention of sediment movement. Meanwhile, the Southern near-shores shallow area of Gaza Fishing port works as sediment traps causing deposition of blocked sediment transportation by the southern groin of Gaza fishing port, Fig (6.6).
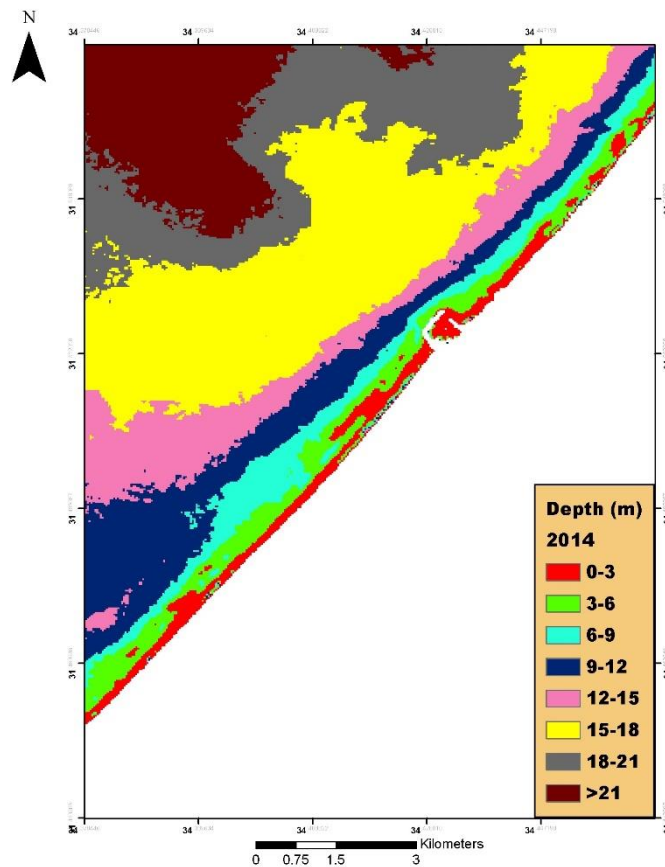
Fig (6. 6): Bathymetry survey of the study area using prediction model on 2014

2017

The results shows that sediment quantity increases directly behind the southern breakwater of the fishing port and in the area surrounding the fishing port. On the contrary to 2014, Fig (6.7) show that sediments starts to accumulate in the area behind the Northern breakwater of Gaza fishing port and the area becomes more obvious as going far in the northern direction. Such

change might occur due to the protection units (rocks) placed near the shoreline to prevent the erosion in the northern area particularly in opposite of Al-shata'a camp. Additionally, the groins built in Al-Sudaniya area "Blue Beach Resort" might have a role in decreasing the erosion rate in the northern side.
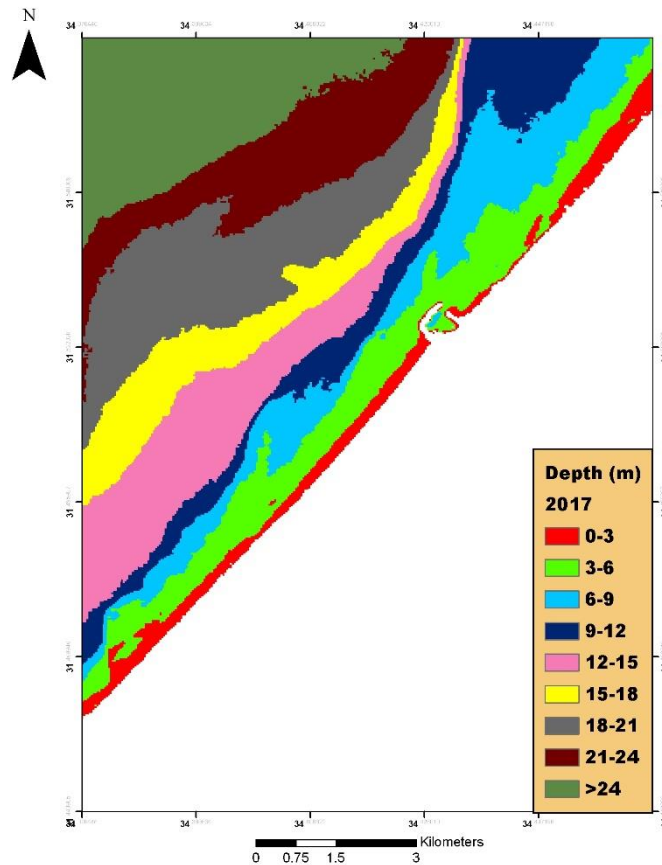
Fig (6. 7): Bathymetry survey of the study area using prediction model on 2017

2018

Fig (6.8) shows that image 2018 is relatively the same to image 2017 in which sediments accretion becomes more clearly in the northern part, in particular behind the northern groin of Gaza fishing port. However, sediments in southern part appears to retreat, possibly due to predominate Northern ward current direction which carries sediments to the northern parts of fishing port or due to the construction of Khanyounis port in 2016 that hinders the transportation of sediments coming from the Nile river.
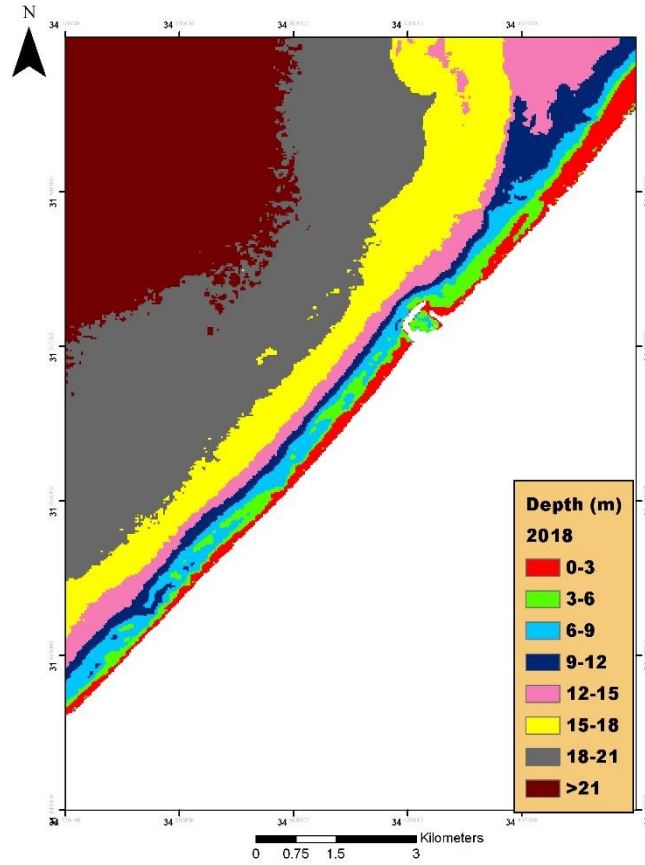
Fig (6. 8): Bathymetry survey of the study area using prediction model on 2018

6.3 Bathymetry Change Assessment (2014-2018)

6.3.1 Average Depth

In order to estimate the change in bathymetry, three regions were selected in different parts of the study area including southern near-shore shallow area of Gaza fishing port, northern near-shore shallow area of Gaza fishing port and deep offshore area, Fig(6.9). The selected regions were identical for each image (2014, 2018). The average depth value of each segment were calculated. Five trials for each image were made to obtain more accurate average depth value for each year (2014, 2018).
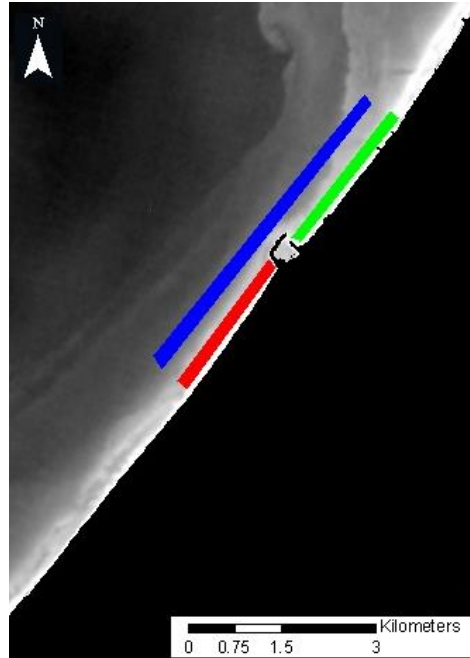
Fig (6.9): Selected regions for estimating bathymetry change

Regarding 2014 image, the results showed that average depth for the southern part was 5.8m while the northern part had an average depth of 7.1 m that was deeper than southern part which could be interpreted by the erosion caused by Gaza fishing port in these years. An average depth value of 9.67 m was obtained in the deep offshore area.

4 years later, the results of 2018 image showed that a considerable change occurred in which average depth in the northern part and the southern part were 2.27 m and 3.75 m respectively. Meanwhile, the deep offshore area had an average depth of 10 m.

6.3.2 Seabed profile:

Seabed profiles were created from the derived bathymetric maps to depict the seabed topography. Fig (6.10) shows the profile difference between year 2014 and year 2018, both profiles of year 2014 (north (A), south (B)) appears to be have sharp curvature (erosion) compared to year 2018 profiles (north (A), south (B)) which have a smoother curvature (accretion).
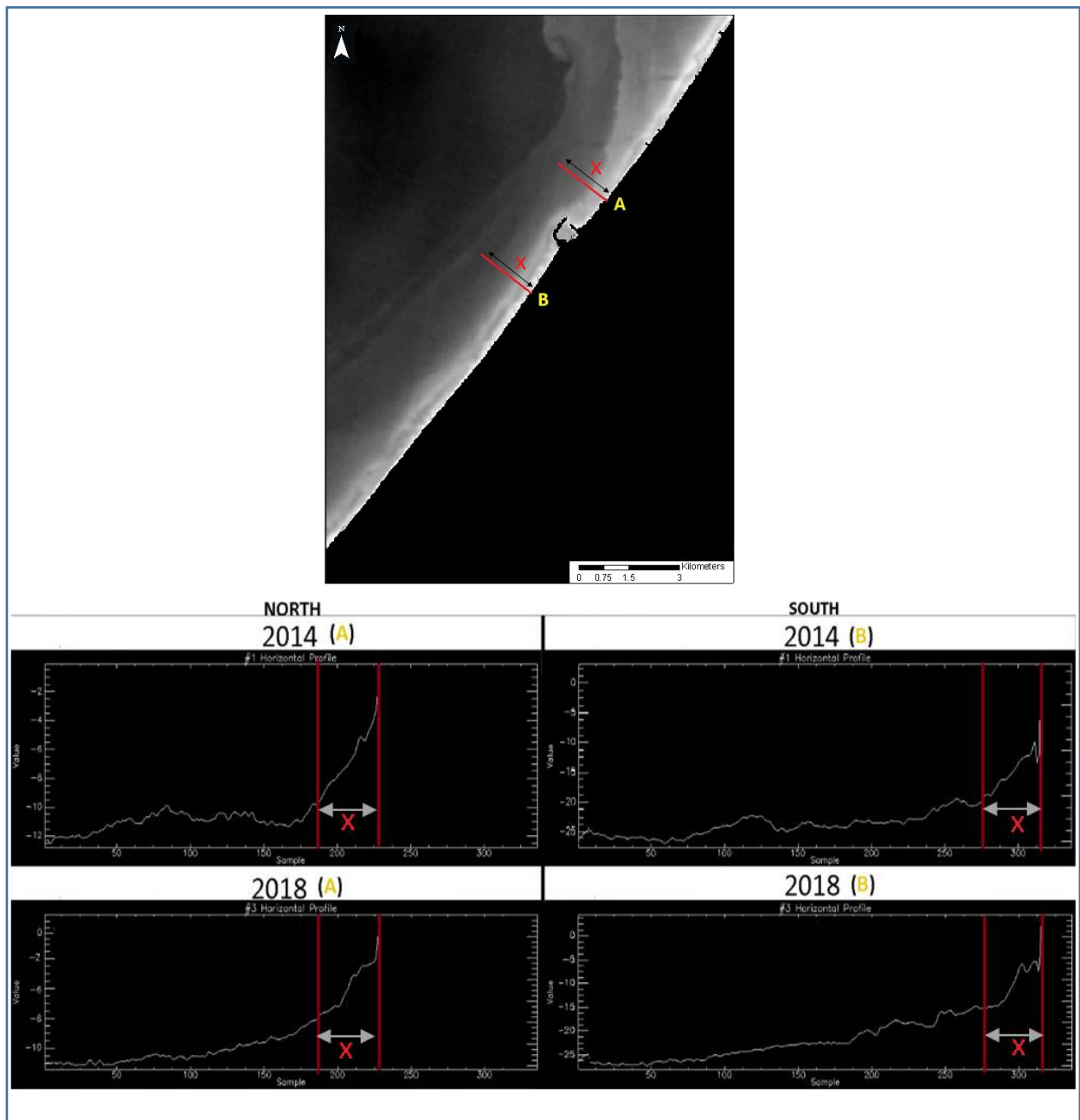
Fig (6. 10): Seabed profile north and south Gaza fishing port on (2014 and 2018)

6.3.3 Changes of seabed profile:

The results showed that the period 2014 to 2018 witnessed increase in seabed sediments of about 4.75 m/yr. in the northern part of the Gaza fishing port that was equivalent to 1.19 m/yr. Also, the southern part had a seabed sediment increase of about 2.05 m, equivalent to 0.5 m/yr. Such pattern gave indication that accretion was the dominant status. Whereas, the deep offshore area had relatively no change in seabed profile. It was worth noted that the increase of sediments in

the southern parts was lesser than that of the northern parts, contrary to what used to be in the previous years.

Table (6.1): Summary of seabed change assessment over the study area based on combined model of B2/B3 and B3

Average depth for each segment in (m)			
Year	North Up to 800 m (From the shoreline)	South Up to 800 m (From the shoreline)	Deep (off-shore) Up to 1600 m (From the shoreline)
2014	7.1m	5.8m	9.67m
2018	3.75m	2.27m	10 m
Depth change			
2014-2018	4.75m	2.05m	-0.33m
Depth change rate/year			
2014-2018	1.9 m/yr.	0.5 m/yr.	-0.08 m/yr.
Dominant Sediments process			
2014-2018	High sedimentation region	Low sedimentation region	No change

6.4 Importance of derived prediction models for desalination intake system

As desalination becomes a solution for water scarcity in the Gaza strip, regular seawater quality monitoring is required to ensure optimal performance of desalination processes. SDD retrieval models shows that turbid water plums, demonstrated by low SDD values, are obvious close to the beach when sewage outfalls in the study area are in operation. High turbidity in seawater adversely impacts the desalination processes, so intake water system should be placed at considerable distance from the beach to avoid turbid waters and reduce fouling of desalination membrane. Also, high phosphorus level is demonstrated by the P retrieval model as result of sewage outfalls. Sewage discharge contains huge amounts of organic matters and nutrients that promote problem of fouling as well as scaling such as phosphate that cannot be easily avoided by use of anti- scalants. Thus, the design and installation of the intake system should take into consideration seawater quality parameters.

In terms of satellite derived bathymetry, it is concluded that Landsat8/OLI satellite image could effectively use to evaluate the change in seafloor and gives an indication of sediment budget

status in the study area. Such bathymetrical studies are fundamental in the selection of the proper location for the desalination intake system. Based on the obtained results in the study area, intake system should be located at the southern side of the Gaza fishing harbor at the distance between 800m-1600m offshore where sediments quantity decrease (less turbidity).

Based on the generated maps (SDD, P and bathymetry) by prediction models, the concerned institutions and decision makers will be able to determine the seawater quality range and extensions.

Chapter (7)

Conclusion, limitations and Recommendations

7.1 Conclusion

Seawater quality plays a fundamental role in sustainable development of coastal cities in different aspects of life e.g. a potential source of desalinated water, recreational use and fishing as a source of living. However, due to anthropogenic activities and industrial development, seawater quality has dramatically degraded. Thus, continuous monitoring are required to make sure that global standards and criteria are met. A combination of remote sensing technology and traditional in-situ sampling can lead to perform a better monitoring program for seawater quality parameters and bathymetry mapping at a regional scale in various water bodies, replacing traditional field-based approaches.

The principal objective was to investigate the relationship between spectral reflectance value of the Landsat 8 and in-situ measurement of the four water quality parameters (SDD, P, COD, and TSS) and to monitor and derive spatial changes of seawater quality parameter in coastal water of the study area. The research also examined the potential use of OLI sensors for bathymetry mapping in a polluted coastal water and monitoring the changes in seafloor morphology.

Optical remote sensing data and in-situ data are necessary to build a robust retrieval algorithm to assess changes. The remotely sensed data from the Landsat OLI 8 sensor was collected on 4 November 2017 in conjunction with the field trip. Seawater sampling at different water depths was carried out in dry season to reduce adverse effects from the weather conditions, such as heavy rain or cloud. Thereafter, seawater samples were stored at a reasonable temperature to avoid changes of samples characteristics before laboratory work was conducted to analyze samples.

The optical bands in the region from blue to near infrared and all the possible band-ratios were used to explore the relation between the reflectance of water body and observed data. Various pre-processing steps of optical data were carried out to establish the relationship between spectral reflectance values and in-situ data including radiometric calibration and atmospheric correction, separating water/land and masking land related pixel, extracting reflectance values, and developing the model for estimating spatial distribution of the unknown concentration/depth.

In this study, statistical analysis of in-situ measurements (water quality and bathymetry) and their corresponding Landsat 8 OLI reflectance values were analyzed to obtain the optimal retrieval algorithm.

In other words, the correlation analysis was utilized to determine the linear relationship between the variables, in order to find the significant relationships between various OLI bands and each of the water quality parameters and water bathymetry as well.

Regression analysis was conducted for all seawater quality parameters and bathymetry on all the visible bands and their combinations. The Reflectance of visible bands and their ratio constructed the independent variables, while seawater quality parameter/depth is the dependent variable and represents measured (or known) water quality parameters/depth at sampling point.

Only developed models with efficient significance were selected to be validated. The best model to monitor the coastal area was chosen based on the highest coefficient of determination (R^2) and acceptable RMSE achieved between in-situ data and predicted.

Based on the objective of the research, the results was divided into two parts: water quality and bathymetry.

Seawater quality

Different combinations of single-band and band-ratio were investigated to determine the defined seawater quality parameters (SDD, TSS, COD, and P). The results of different models were evaluated by statistical indices of R^2 and RMSE.

- **Secchi disc depth**

SDD of 40 points were measured, 24 points were used to develop SDD model and 16 points for accuracy test. A set of 15 models (single-band and band-ratio) were statistically examined in the development step. Nine models, showed correlation coefficient above 0.5, were tested for accuracy using R^2 and RMSE within different SDD values. The study emphasized that band-ratio correlation coefficients gave higher values than that of single-bands especially (red and coastal blue). The same result has been concluded by many researches, showing that models with the highest correlation rates includes band-ratio of blue and red spectral bands and sometimes bands from the infrared spectral region and green band.

Based on a high accuracy developed B2/B4 model, the SDD map was generated for the study area. The deeper SDD value points, represents less turbid water which is located far from beach, while the shallowest SDD values are more turbid.

- **Chemical Oxygen Demand**

In general, no significant relation, (R> 0.5) and P-value < 0.05, was found between OLI reflectance values (visible and IR) and COD in study area. According to some similar studies, no certain OLI wavelength could be used with high confidence to perform an appropriate model to estimate COD from water reflectance that might be referred to the weak optical characteristic of COD leading to the low accurate estimation of COD using remote sensing technology.

- **Total dissolved solids**

The results of TSS showed insignificant correlation at different depths. For water samples at depth of 2 meter, a slight correlation was noticed. This results could be attributed to several reasons including limited number of samples. Also, it might be referred to low performance of atmospheric correction algorithm in polluted coastal water.

Furthermore, seawater Pollution and wastewater discharge might have their negative contribution in TSS estimation. Pollutants from wastewater discharge in water column influences the light path that will reflect off the water surface. Moreover, uneven spatial distribution of sewage outlets weaken the correlation between reflectance and TSS concentration.

- **Phosphorus**

As for Phosphorus in seawater, a strong correlation coefficient R of 0.89 was found between B3/B5 model and phosphorus concentrations at the surface generating an acceptable accuracy, $R^2_{accuracy}$=0.5139 and RMSE=0.33 .Also, B1/B5 model showed a good correlation coefficient R of 0.835 with Phosphorus concentration at 2-m depth. It was obvious that band-ratio outperformed the single-band model in estimating P level in the study area.

However, Phosphorus at 3-meter depth (P3) demonstrated low coefficient correlation with OLI reflectance values compared to the P0 (at water surface) and P2 (at 2 m).

- **Bathymetry**

Different combinations of band-ratio and single-band model were tested for generating bathymetry model over depth range (0m-20m). Some Landsat8 band models, either band-ratio or single-band, proved to be effective over different depth ranges in the study area.

For instance, results demonstrated that band-ratio model of B1/B4, ($R^2_{accuracy}$) of 0.76 and RMSE of 1.07m, was more effective than the single-band model in accurately estimating shallower depths in the study area (0m-8m), whereas, over deep range, only single-band model of B3 showed the highest correlation coefficient during calibration step (R=0.84) and accuracy assessment step ($R^2 = 0.9$). This indicted that single-band model was more effective in deeper range of the study area and despite that band-ratio models minimize the bottom variation but it doesn't necessary improve the statistical relationship between reflectance values and deeper depths.

While regarding the entire measured depth range, (0m-20m), band-ratio model of B2/B3 was adopted to predict depth, achieving RMSE of 2.81m. It is concluded that band-ratio model could be more effective in extracting bathymetry over wide range of depths and particularly band-ratio model that makes use of green and blue bands yielding better statistical results compared with other band-ratio models.

Consequently, as type of modification, the combination between two model types (single-band and band ratio) was utilized in attempt to obtain improved accuracy, where the combination between bands could minimizes the destructive effects of variations in depth and water clarity. Over the range (0m-20m), the combination between single-band model B3 and band-ratio model B2/B3 exhibited improvement in retrieving depth in which the calculated RMSE of combined models was more acceptable and equals 2.5 m, compared with the band-ratio model B2/B3 itself that has higher RMSE of 2.8 m.

While relative improvement was shown over the entire range depth (0m-20m) m, the method of combination has no improvement in retrieving shallow depths (0m-8m), relatively similar statistical indictors were obtained using combined model of B4, B1/B4. Therefore, the simpler one (B1/B4) was selected as the optimal model to retrieve shallower depths in the study area. Over the deeper range of (9m-20m), combining between B3 model and B1/B3 model showed a nearly close statistical results. However, combined model gave a more acceptable RMSE of 1.1m compared with B3 model individually.

- **Model Application and GCDP Intake System**:

Both bathymetry and seawater quality retrieval models have the potential of providing regular and cost-effective monitoring of coastal water conditions which are necessary to ensure optimal performance of desalination processes. Through the application of seawater quality models (SDD and P) that visualize the spatial patterns of water quality parameters, it is concluded that distance between sewage outfalls and desalination intake system should be taken in account when design and installing process starts. Also, bathymetry models helps infer the change in sediments volume by studying the topographical change in seafloor. Sediment budget status is perquisite for determining the proper location of desalination intake system. Based on the obtained results in the study area, intake system should be located at the southern side of the Gaza fishing harbor at the distance between 800 -1600m offshore where sediments rate becomes more constant and seawater is less turbid.

Overall, the research indicts that multispectral satellite Landsat 8 prove its effectiveness in coastal water bathymetry mapping. Also, it can be operationally employed for to detect some water quality parameters in the study area under the right conditions that involves sufficient water clarity, bottom type homogeneity, and good atmospheric conditions.

7.2 Limitations

Many challenges are identified in this study as follows

- Lack of required sampling devices and laboratory instruments in Gaza city e.g. TSS fiber glass filter
- Dealing with insufficient in-situ data or reference data set to cover larger study area and obtain more accurate results as field surveying is cost-consuming and labor-intensive.
- Implementation of the study in highly-polluted study area due to excessive wastewater discharge was one of major limitation since high turbidity in seawater has a negative contribution in preventing light penetration. Thus, inaccurate seawater quality parameters estimation are obtained.
- The spatial resolution of Landsat8 image and sampling point; one Landsat 8 OLI image pixel covers a $30 \cdot 30$ m square or $15 \cdot 15$ m area, while its corresponding sampling points value is generally obtained from a water sample collected at a certain location and it is generally assumed that parameter values within a pixel are homogeneous when

developing the retrieval model. However, such an assumption is not always valid for the study area because of spatial and temporal variability nature of the coastal area or localized water pollution.

7.3 Recommendations

–Regular monitoring programs for seawater quality must be carried out by the local authorities and related agencies.

–Bathymetric mapping should be implemented on regular basis to maintain a historical record for future studies and projects as well to quantify seabed and morphologic changes in coastal zone.

–Further researches are needed in the remote sensing field and developing reliable qualitative and quantities retrieval model

–Mitigation measures must be taken to protect the Gaza Strip beach of the current deterioration due to wastewater discharge and erosion problem.

-bathymetry and seawater quality data should be taken in consideration for all anticipated coastal and developmental project components including the intake system of central desalination plants.

References

1. Abu-Alhin, K., & Niemeye, I. (2009). Calculation of erosion and accretion rates along the Gaza coastal zone using remote sensing and geoinformation systems. In *The 4th EARSeL Workshop Remote Sensing of the Coastal Zone, Chania, Greece.*

2. Abu-Alhin, K. S. (2011). Assessment of the Gaza Strip Coastal Zone Using Remote Sensing and Geoinformation Techniques *.Doctoral dissertation, Verlag nicht ermittelbar.*

3. Abualhin, K. (2016). Mapping of Underwater Seabed Morphology of the Gaza Strip Coastal Zone Using Remote sensing technique. *Earth Sciences Research Journal*, 20(2), 1-7.

4. Abualhin, K., & Niemeyer, I. (2018). Deriving Bathymetric Maps of the Shallow Coastal Water of the Gaza Strip Coastal Zone Using Passive Remotely Sensed Imagery. *Journal of the Indian Society of Remote Sensing*, 46(9), 1341-1351.

5. Abualtayef, M., Ghabayen, S., Foul, A. A., Seif, A., Kuroiwa, M., Matsubara, Y., & Matar, O. (2012). The impact of Gaza fishing harbour on the Mediterranean coast of Gaza. *Journal of Coastal Development,* 16(1), 1-10.

6. Ali, M. (2002, March). The coastal zone of Gaza strip-Palestine management and problems. *In Presentation for MAMA first kick-off meeting.*

7. Alparslan, E., Aydöner, C., Tüfekçi, V., Tüfekçi H. (2007). Water quality assesment at Ömerli Dam using remote sensing techniques. *Environmental Monitoring Assessment*, 2007, 135(1-3): 391-398.

8. Brezonik, P., Menken, K. D.,Bauer, M. (2005). Landsat-based remote sensing of lake water quality characteristics, including chlorophyll and colored dissolved organic matter (CDOM). *Lake and Reservoir Management*, *21*(4), 373-382.

9. Bukata, P.; Bruton, E.; Jerome, H. (1985). Application of direct measurements to the estimation of lake water quality indicators. *Environment Canada Inland Waters Directorate.*

10. Canh, B. D. (2016). Application of Remote Sensing for Qualifying Total Suspended Solid Concentrations in Coastal Waters: The Case Study of Ba Lat Estuary *.Doctoral Dissertation, Vietnam National University.*

11. Carder, L.; Steward, G.; Harvey, G.; Ortner. P. (1989). Marine humic and fulvic acids: their effects on remote sensing of ocean chlorophyll. *Journal of Limnology and Oceanography*, 34(1), 68-81.

12. Carlson, R. E. (1977). A trophic state index for lakes 1. *Limnology and oceanography*, 22(2), 361-369.

13. Cavalli, R. M., Laneve, G., Fusilli, L., Pignatti, S., & Santini, F. (2009). Remote sensing water observation for supporting Lake Victoria weed management. *Journal of Environmental Management*, 90(7), 2199-2211.

14. Chebud, Y., Naja, G. M., Rivero, R. G., & Melesse, A. M. (2012). Water quality monitoring using remote sensing and an artificial neural network. *Water, Air, & Soil Pollution*, 223(8), 4875-4887.

15. Chen X., Y. S. Li, Z. Liu, K. Yin, Z. Li, O. W. H. Wai, and B. King. (2004). Integration of multi-source data for water quality classification in the Pearl River estuary and its adjacent coastal waters of Hong Kong, *Continental Shelf Research,* 24(16),1827–1843.

16. Deutsch, E., Almandine, I., El-Fadel, M. (2014). Developing Landsat Based Algorithms to Augment in Situ Monitoring of Freshwater Lakes and Reservoirs.

17. Domagalski, J., Lin, C., Luo, Y., Kang, J., Brown, L., & Munn, M. (2006). Eutrophication study at the Panjiakou-Daheiting Reservoir system, northern Hebei Province, People's Republic of China: Chlorophyll-α model and external and internal sources of phosphorus and nitrogen. *Chinese Journal of Geochemistry*, *25*, 136-137.

18. Eugenio, F., Marcello, J. and Martin, J. (2015) High-resolution maps of bathymetry and benthic habitats in shallow-water environments using multispectral remote sensing imagery. *IEEE Transactions on Geoscience and Remote Sensing* 53(7): 3539–3549.

19. Fauzi, M., & Wicaksono, P. (2016, November). Total Suspended Solid (TSS) Mapping of Wadaslintang Reservoir Using Landsat 8 OLI. *In IOP Conference Series: Earth and Environmental Science,* 47(1), 012029.

20. Gholizadeh, M., Melesse, A., & Reddi, L. (2016). A comprehensive review on water quality parameters estimation using remote sensing techniques. *Sensors*, 16(8), 1298.

21. Hadjimitsis, D. G., Clayton, C., & Toulios, L. (2010). Retrieving visibility values using satellite remote sensing data. *Physics and Chemistry of the Earth, Parts A/B/C*, 35(1-2), 121-124.

22. Hastie, W. J. (1983). Sediment transport in the near shore marine environment, Timaru, New Zealand.

23. He, W., Chen, S., Liu, X., & Chen, J. (2008). Water quality monitoring in a slightly-polluted inland water body through remote sensing—Case study of the Guanting Reservoir in Beijing, China. *Frontiers of Environmental Science & Engineering in China*, 2(2), 163-171.

24. Hellweger, F.L., Schlosser, P., Lall, U., issel J.K. (2004). Use of satellite imagery for water qualities in New York Harbor, Estuarine Coastal and Shelf Science, 61(3): 437-448.

25. https://oceanservice.noaa.gov/facts/bathymetry.html

26. Isaac, J., & Rishmawi, K. (2015). Status of the Environment in the State of Palestine 2015. ARIJ, Bethlehem.

27. Jaelani, L. M., Limehuwey, R., Kurniadin, N., Pamungkas, A., Koenhardono, E. S., & Sulisetyono, A. (2016). Estimation of Total Suspended Sediment and Chlorophyll-A Concentration from Landsat 8-Oli: The Effect of Atmosphere and Retrieval Algorithm. *IPTEK the Journal for Technology and Science*, 27(1).

28. Jerlov N (1976) Preface to the second edition. *In: Jerlov N (ed.) Marine Optics, Elsevier Oceanography Series*, 14(2). 7–10.

29. JUPP, D. L. (1988). Background and extensions to depth of penetration (DOP) mapping in shallow coastal waters. *In Proceeding of the Symposium on Remote Sensing of the Coastal Zone Queensland*.

30. Kabbara, N., Benkhelil, J., Awad, M., & Barale, V. (2008). Monitoring water quality in the coastal area of Tripoli (Lebanon) using high-resolution satellite data. *ISPRS Journal of Photogrammetry and Remote Sensing*, 63(5), 488-495.

31. Kabiri, K. (2017). Accuracy assessment of near-shore bathymetry information retrieved from Landsat-8 imagery. *Earth Science Informatics*, 10(2), 235-245.

32. Kabiri, K., & Moradi, M. (2016). Landsat-8 imagery to estimate clarity in near-shore coastal waters: Feasibility study-Chabahar Bay, Iran. *Continental Shelf Research*, 125, 44-53.

33. Kallio, K. (2000). Remote sensing as a tool for monitoring lake water quality. *Hydrological and Limnological Aspects of Lake Monitoring; John Wiley & Sons: New York, NY, USA*, p. 237.

34. Kirk, J. T. (1994) Light and photosynthesis in aquatic ecosystems. *University Press*, Cambridge.

35. Kloiber, S. M., Brezonik, P. L., Olmanson, L. G., & Bauer, M. E. (2002). A procedure for regional lake water clarity assessment using Landsat multispectral data. *Remote Sensing of Environment*, 38-47.

36. Jaelani, L. M., Setiawan, F., & Matsushita, B. (2015). Uji Akurasi Produk Reflektan-Permukaan Landsat Menggunakan Data In situ di Danau Kasumigaura, Jepang. Pertemuan Ilmiah Tahunan Masyarakat Ahli Penginderaan Jauh Indonesia XX, Bogor.

37. Zhang, L., Xia, M., Zhang, L., Wang, C., & Lu, J. (2008). Eutrophication status and control strategy of Taihu Lake. *Frontiers of Environmental Science & Engineering in China*, 2(3), 280-290.

38. Lattemann, S., & Höpner, T. (2008). Environmental impact and impact assessment of seawater desalination. *Desalination*, 220(1-3), 1-15.

39. Lyzenga, D.R., Malinas, N.P. and Tanis, F.J. (2006) Multispectral bathymetry using a simple physically based algorithm. *IEEE Transactions on Geoscience and Remote Sensing,* 44(8): 2251–2259.

40. Ma, R., Dai, J. (2005). Investigation of chlorophyll-a and total suspended matter concentrations using land sat ETM and field spectral measurement in Taihu Lake, Chin. *International Journal of Remote Sensing*, 26(13): 2779–2795.

41. Manoppo, A. K., & Budhiman, S. (2017, January). Estimation on the concentration of total suspended matter in Lombok Coastal using Landsat 8 OLI, Indonesia. *In IOP Conference Series: Earth and Environmental Science,* 54(1), 12073.

42. Miao-fen, H., Xu-feng, X., Xiao-Ping, Q. I., Wu-Yi, Y. U., & Yi-min, Z. (2007). Identification mode of chemical oxygen demand in water based on remotely sensing technique and its application. *IEEE International Geoscience and Remote Sensing Symposium* (1738-1741).

43. Mishra, D.R., Narumalani, S., Rundquist, D., et al. (2007). Enhancing the detection and classification of coral reef and associated benthic habitats: A hyper spectral remote sensing approach. *Journal of Geophysical Research: Oceans*, 112(C8).

44. Mobley, C. D. (1994). Light and water: Radiative transfer in natural waters, *Academic press* San Diego, CA.

45. Morel, A.Y.; Gordon, H.R. (1980)**.** Report of the working group on water color. *Bound Layer Meteorol*, 18, 343–355.

46. Myint, S.; Walker, N. (2002). Quantification of surface suspended sediments along a river dominated coast with NOAA AVHRR and SeaWiFS measurements: Louisiana, USA. *Int. J. Remote Sens*. 23, 3229–3249.

47. Padial, A. A.; Thomaz, S. M. (2008). Prediction of the light attenuation coefficient through the Secchi disk depth: empirical modeling in two large Neotropical ecosystems. *Limnology*, 9(2), 143-151.

48. Phuong, N. T. B., Duy, N. B., & Nghiem, N. C. (2017). Remote sensing for monitoring surface water quality in the vietnamese mekong delta: The application for estimating chemical oxygen demand in river reaches in binh dai, ben tre. Vietnam. *Journal of Earth Sciences*, 39(3), 256-268.

49. Post, J. C., & Lundin, C. G. (Eds.). (1996). Guidelines for integrated coastal zone management.

50. Poppenga, S. K., Palaseanu-Lovejoy, M., Gesch, D. B., Danielson, J. J., & Tyler, D. J. (2018). Evaluating the potential for near-shore bathymetry on the Majuro Atoll, Republic of the Marshall Islands, using Landsat 8 and WorldView-3 imagery.

51. Powell, R., Brooks, C., French, N., & Shuchman, R. (2009). Remote Sensing of Lake Clarity. Ann Arbor: *Michigan Tech Research Institute*.

52. Pushparaj, J., & Hegde, A. V. (2017). Estimation of bathymetry along the coast of Mangaluru using Landsat-8 imagery. *The International Journal of Ocean and Climate Systems*, 8(2), 71-83.

53. Ritchie, J.; Lewis, J. (2003). Qualitative Research Practice: A Guide for Social Science Students and Researchers. *Sage Publications, London*.

54. Ritchie, J.C.; Zimba, P.V.; Everitt, J.H. (2003). Remote sensing techniques to assess water quality. *Photogram. Eng. Remote Sens*. 69, 695–704.

55. Rodrigues, T., Alcântara, E., Watanabe, F., & Imai, N. (2017). Retrieval of Secchi disk depth from a reservoir using a semi-analytical scheme. *Remote Sensing of Environment*, *198*, 213-228.

56. Saputra, A. N., Danoedoro, P., & Kamal, M. (2017, December). Application of Landsat 8 OLI Image and Empirical Model for Water Trophic Status Identification of Riam Kanan Reservoir, Banjar, South Kalimantan. *In IOP Conference Series: Earth and Environmental Science* (98(1), p. 012020).

57. Selamat, M. B., & Nababan, B. (2009). Bathymetric Mapping Using SPOT Satellite of Pandangan Island Waters in The Makassar Strait.

58. Setiawan, K. T., Adawiah, S. W., OSAWA, T., & Nuarsa, I. W. (2017). Application of Van Hengel and Spitzer Algorithm for Information on Bathymetry Extraction Using Landsat Data. *International Journal of Remote Sensing and Earth Sciences (IJReSES)*, 11(1), 73-80.

59. Khondoker, M. S. I., Siddiquee, M. Z. H., & Islam, M. (2016). The challenges of river bathymetry survey using Space borne remote sensing in Bangladesh. *Atmospheric and Oceanic Sciences*, 1(1), 7-13.

60. Song, K., Wang, Z., Blackwell, J., Zhang, B., Li, F., Zhang, Y., & Jiang, G. (2011). Water quality monitoring using Landsat Thematic Mapper data with empirical algorithms in Chagan Lake, China. *Journal of Applied Remote Sensing*, 5(1), 053506.

61. Stumpf RP, Holderied K and Sinclair M. (2003) .Determination of water depth with high-resolution satellite imagery over variable bottom types. *Limnology and Oceanography: Methods*, 48 (1): 547–556.

62. Sudheer, K. P., Chaubey, I., & Garg, V. (2006). Lake water quality assessment from Landsat thematic mapper data using neural network: an approach to optimal band combination selection1. *JAWRA Journal of the American Water Resources Association*, 42(6), 1683-1695.

63. Sutanto, (1992), Penginderaan Jauh Jilid 2. Gadjah Mada Press, Yogyakarta.

64. Tang, K. K. W., & Mahmud, M. R. (2018). Imagery-derived bathymetry in strait of johor's turbid waters using multispectral images. *Int. Arch. Photogramm. Remote Sens. Spatial Inf. Sci*, 139-145.

65. Theologou I.; Kagalou I.; Papadopoulou M.; Karantzalos K. (2016). Multi temporal Mapping of Chlorophyll–α in Lake Karla from High Resolution Multispectral Satellite data. *Environmental Processes*, 3(3): 681-691.

66. Torbick, N., Hession, S., Hagen, S., Wiangwang, N., Becker, B., & Qi, J. (2013). Mapping inland lake water quality across the Lower Peninsula of Michigan using Landsat TM imagery. *International journal of remote sensing*, 34(21), 7607-762.

67. Usali, N.; Ismail, M. H. (2010). Use of remote sensing and GIS in monitoring water quality. J. Sustain. Dev. 2010, 3,228–238.

68. Volpe, V., Silvestri, S., & Marani, M. (2011). Remote sensing retrieval of suspended sediment concentration in shallow waters. *Remote Sensing of Environment*, 115(1), 44-54.

69. Vrieling, A. (2006). Satellite remote sensing for water erosion assessment: A review. *Catena*, 65(1), 2–18.

70. Wang, Y.; Xia, H.; Fu, J.; Sheng, G. (2004). Water quality change in reservoirs of Shenzhen, China: Detection using Landsat/TM data. *Sci. Total Environ,* 328, 195–206.

71. Wetzel, R. G. (2001). Limnology: lake and river ecosystems. *Gulf professional publishing*.

72. Zhang, Y., Pulliainen, J., Koponen, S., & Hallikainen, M. (2003). Empirical algorithms for Secchi disk depth using optical and microwave remote sensing data from the Gulf of Finland and the Archipelago Sea. *Boreal environment research*, 8(3), 251-261.

73. Zheng, P., Deng, Z. and Ye, X. (2014). Retrieval study of lake water depth by using multi-spectral remote sensing in Bangong Co Lake. *Sciences in Cold and Arid Regions* 6(3): 26.

APPENDIX

COD	Regression Statistics	B1	B2	B3	B4	B5
	R	0.100712	0.232723	0.399925	0.340947	0.332462
	R2	0.010143	0.05416	0.15994	0.116245	0.110531
	P-value	0.596437	0.215867	0.028546	0.065216	0.072647
	Observation	30	30	30	30	30

|	Regression Statistics	B1/B2	B1/B3	B1/B4	B1/B5	B2/B3
COD	R	0.301578	0.372679	0.303577	0.370417	0.279309
	R2	0.090949	0.138889	0.092159	0.137209	0.078014
	P-value	0.105322	0.042536	0.102921	0.043908	0.134976
	Observations	30	30	30	30	30
	Regression Statistics	B2/B4	B2/B5	B3/B4	B3/B5	B4/B5
	R	0.253383	0.117754	0.069399	0.151746	0.291393
	R2	0.064203	0.013866	0.004816	0.023027	0.08491
	P-value	0.176685	0.535443	0.715558	0.423433	0.11821
	Observations	30	30	30	30	30

Appendix (3): Regression statistics of single-band model between OLI reflectance (IR/ visible bands) and TSS

	Regression Statistics	B1	B2	B3	B4	B5
TSS at surface	**R**	**0.102294**	**0.140147**	**0.120732**	**0.058686**	**0.051111**
	R2	0.010464	0.019641	0.014576	0.003444	0.002612
	P-value	0.611649	0.485664	0.548599	0.771231	0.800131
	Observation	27	27	27	27	27
TSS at 2m-depth	**Regression Statistics**	**B1**	**B2**	**B3**	**B4**	**B5**
	R	0.317798	0.357104	0.296708	0.135081	0.154524
	R2	0.100996	0.127523	0.088036	0.018247	0.023878
	P-value	0.370875	0.311061	0.405136	0.709843	0.669934
	Observation	10	10	10	10	10
TSS at 3m-depth	**Regression Statistics**	**B1**	**B2**	**B3**	**B4**	**B5**
	R	0.107899	0.131738	0.106195	0.111278	0.067697
	R2	0.011642	0.017355	0.011277	0.012383	0.004583
	P-value	0.615776	0.539472	0.621395	0.604697	0.75329
	Observation	24	24	24	24	24

Appendix (4): Regression statistics of single-band model between OLI reflectance (IR/ visible bands) and TSS

	Regression Statistics	B1/B2	B1/B3	B1/B4	B1/B5	B2/B3
TSS at surface	**R**	0.154296	0.110292	0.051189	0.055333	0.095105
	R2	0.023807	0.012164	0.00262	0.003062	0.009045
	P-value	0.442232	0.583931	0.799832	0.783992	0.637022
	Observations	27	27	27	27	27
	Regression Statistics	**B2/B4**	**B2/B5**	**B3/B4**	**B3/B5**	**B4/B5**
	R	0.028981	0.028653	0.12036	0.108157	0.023481
	R2	0.00084	0.000821	0.014487	0.011698	0.000551
	P-value	0.885901	0.887182	0.549842	0.591278	0.907451
	Observations	27	27	27	27	27
TSS at 2m-depth	**Regression Statistics**	**B1/B2**	**B1/B3**	**B1/B4**	**B1/B5**	**B2/B3**
	R	0.268189	0.245941	0.067933	0.097345	0.231288
	R2	0.071926	0.060487	0.004615	0.009476	0.053494
	P-value	0.453742	0.493382	0.852081	0.789063	0.520265
	Observations	10	10	10	10	10
	Regression Statistics	**B2/B4**	**B2/B5**	**B3/B4**	**B3/B5**	**B4/B5**
	R	0.024696	0.070136	0.524798	0.204858	0.141435
	R2	0.00061	0.004919	0.275413	0.041967	0.020004
	P-value	0.94601	0.847329	0.119357	0.570211	0.696725
		10	10	10	10	10

TSS at 3m-depth	Regression Statistics	B1/B2	B1/B3	B1/B4	B1/B5	B2/B3
	R	0.130349	0.097333	0.094551	0.048529	0.006961
	R2	0.016991	0.009474	0.00894	0.002355	-0.03818
	P-value	0.543794	0.650942	0.660326	0.821837	0.698315
	Observations	24	24	24	24	24
	Regression Statistics	B2/B4	B2/B5	B3/B4	B3/B5	B4/B5
	R	0.07648	0.025188	0.015625	0.076754	0.127544
	R2	0.005849	0.000634	0.000244	0.005891	0.016267
	P-value	0.722444	0.906998	0.942233	0.72149	0.55257
	Observations	24	24	24	24	24
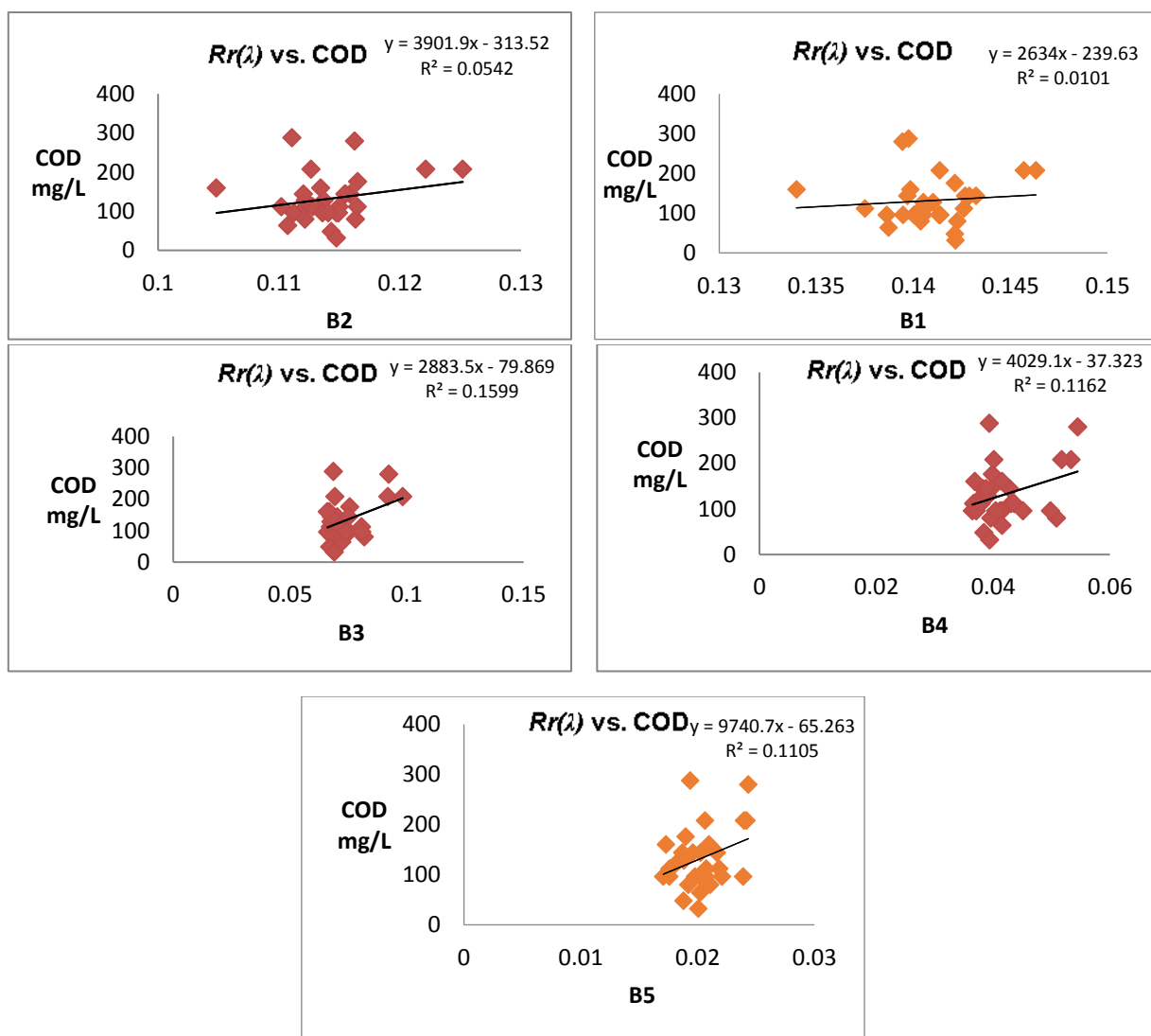
Appendix (5): Regression analysis plot between single-band (visible/IR) and COD
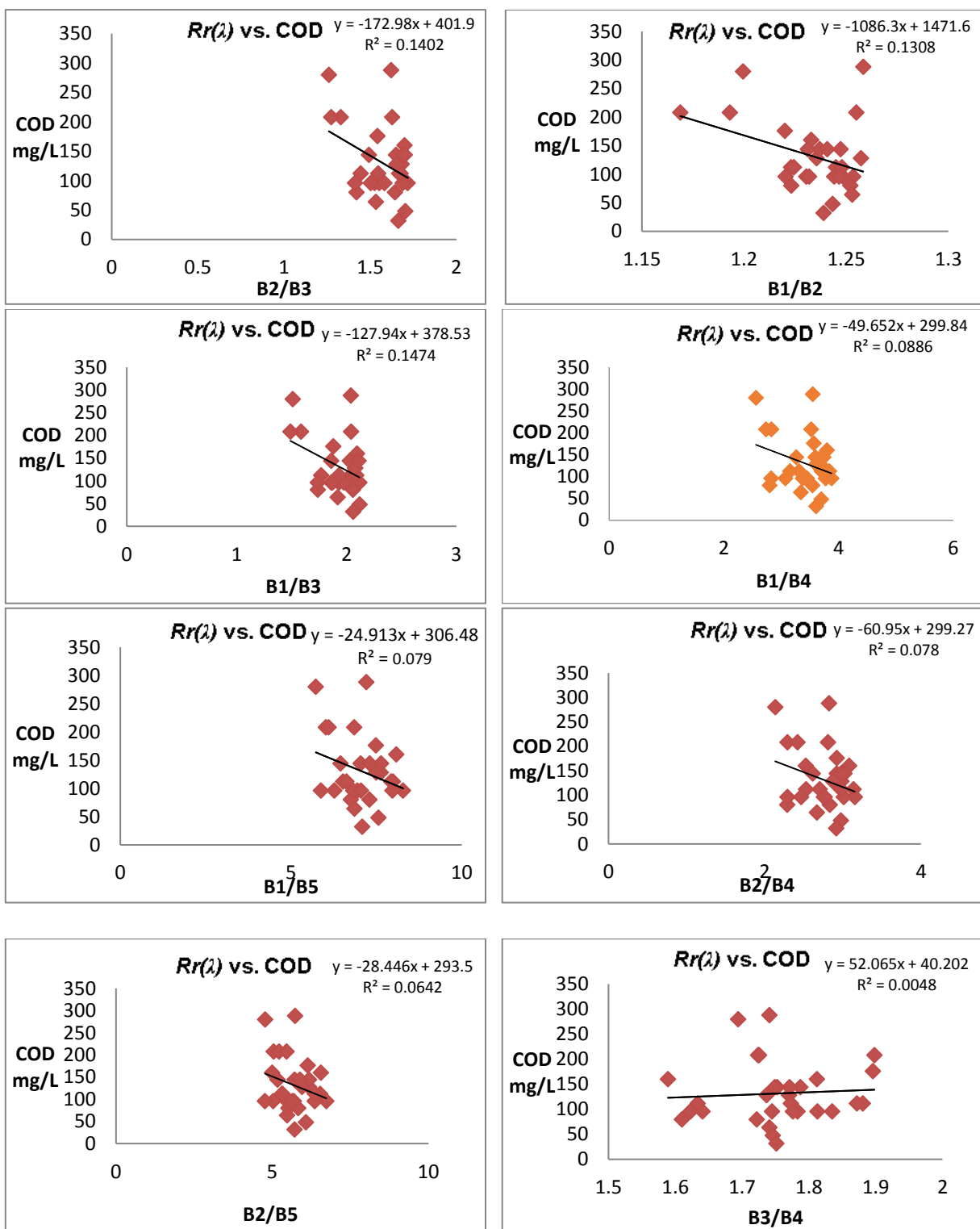
Appendix (6): Regression analysis plot between band-ratio (visible/IR) and COD
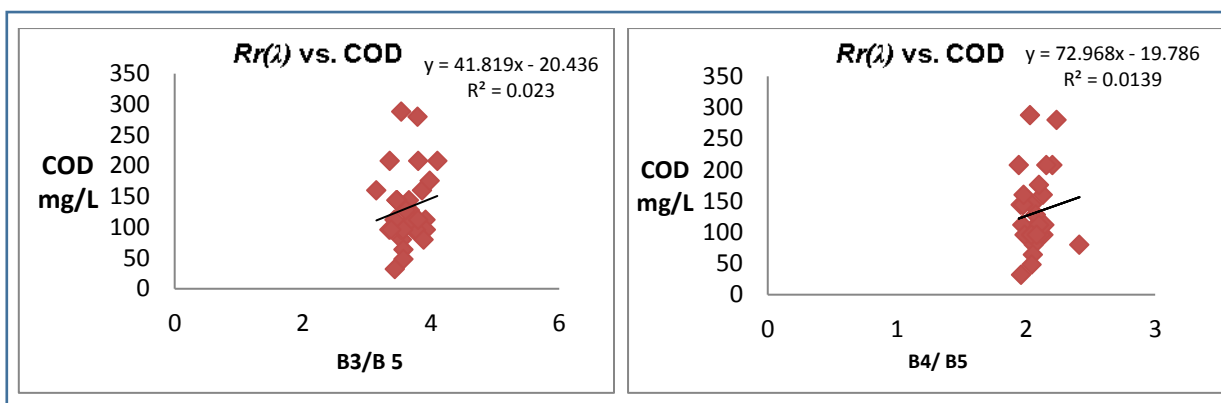
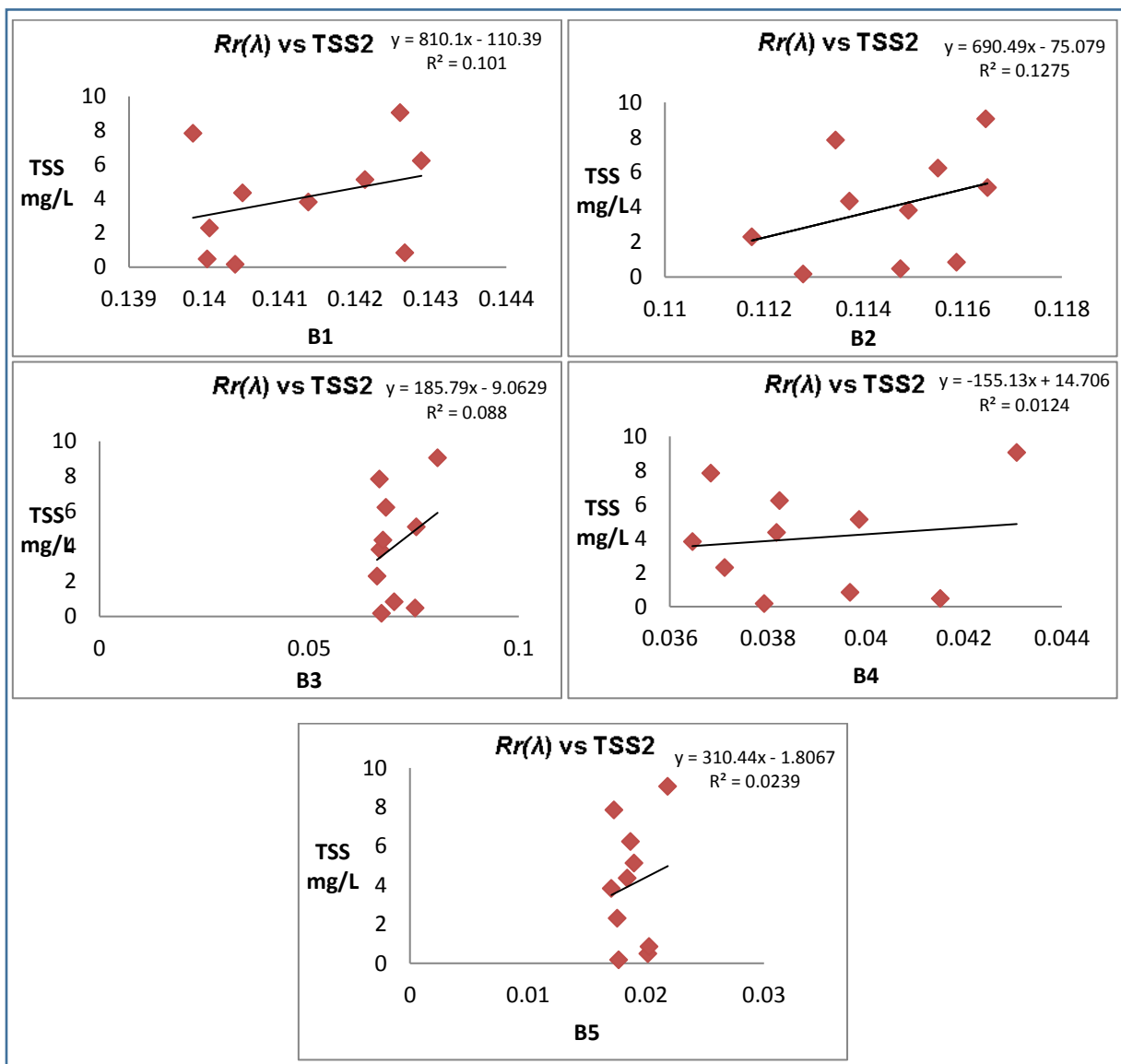**Appendix (6): Regression analysis plot between band-ratio (visible/IR) and COD**
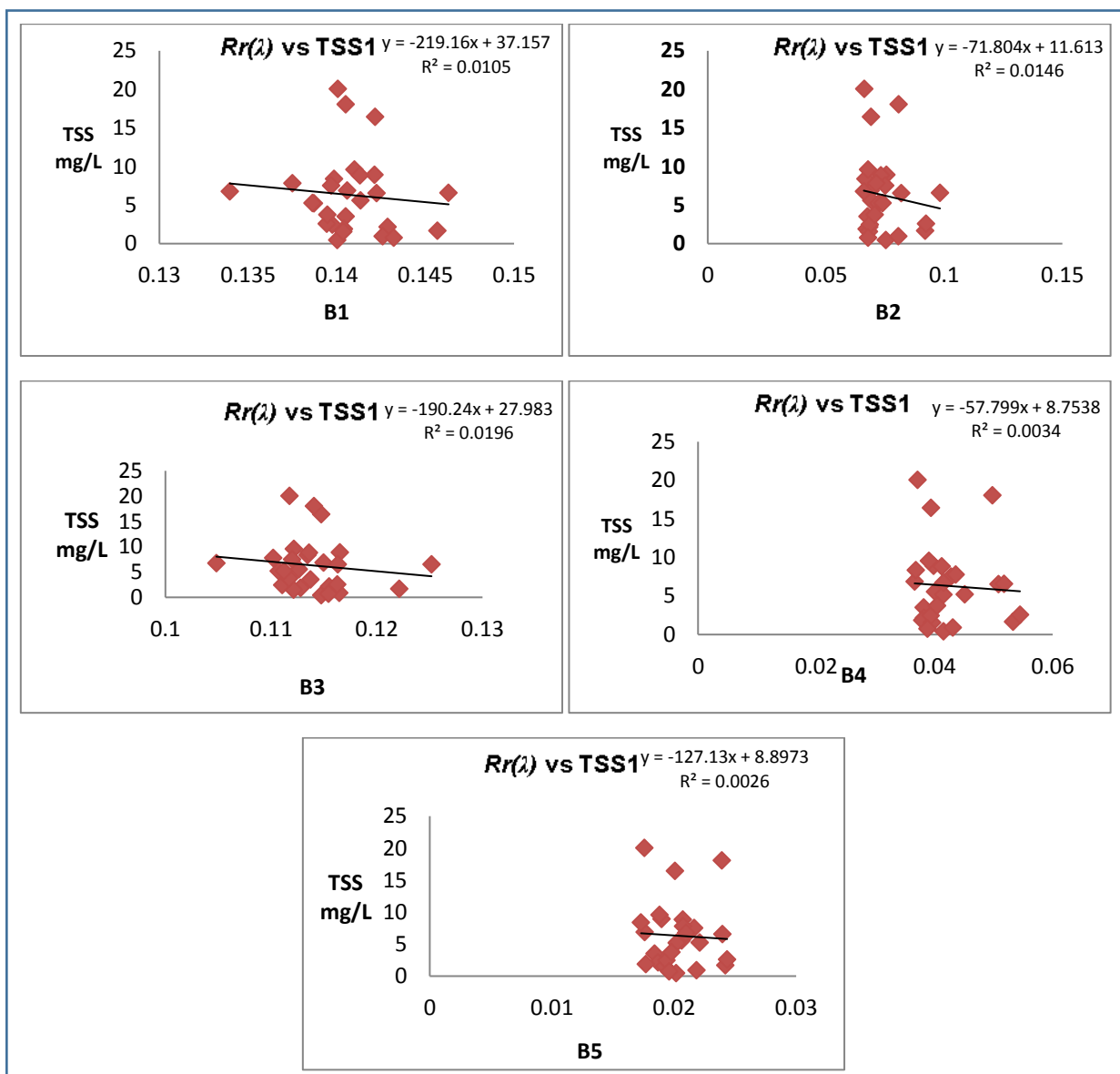
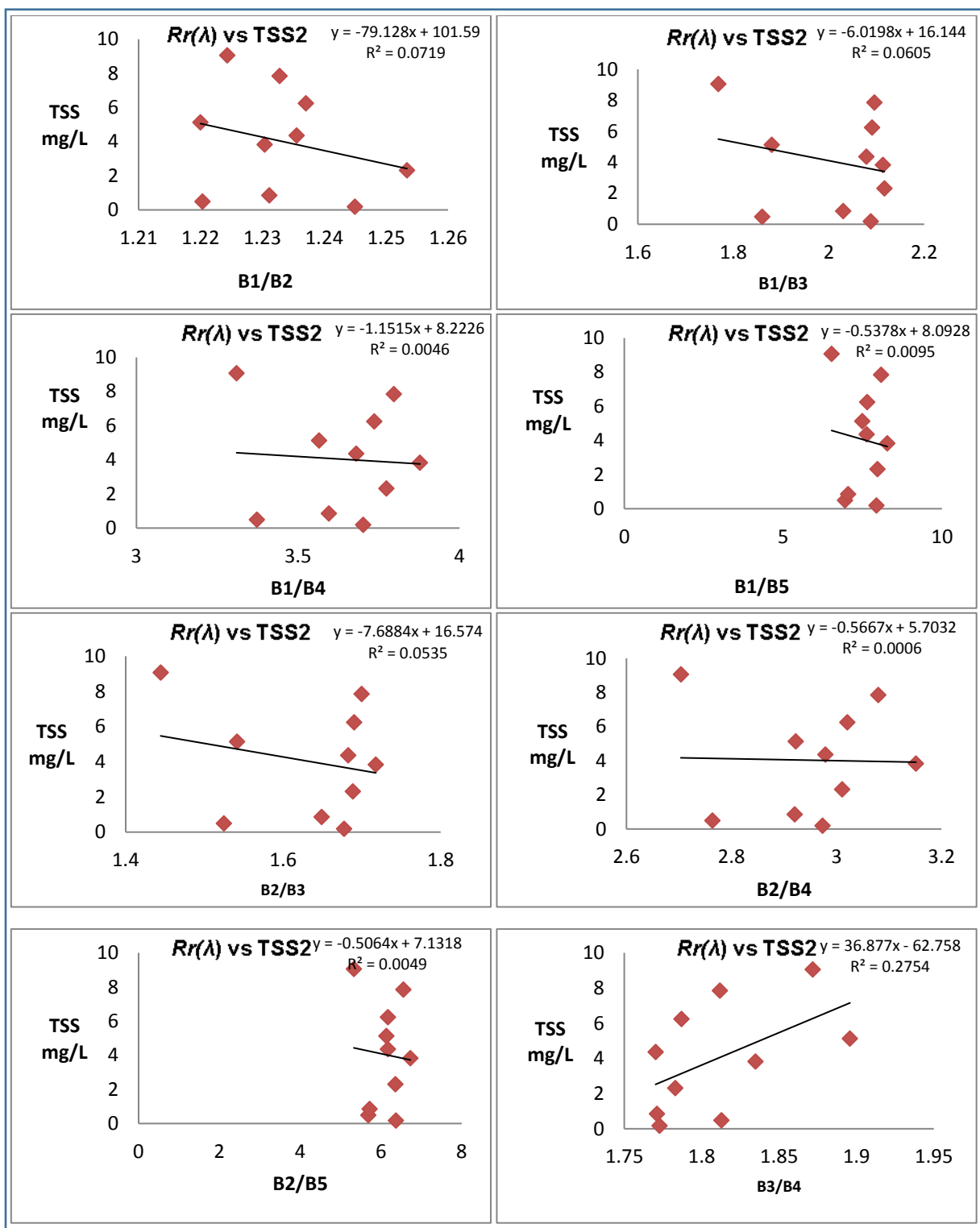**Appendix (7): Regression analysis plot between single-band (visible/IR) and TSS1 (Surface)**
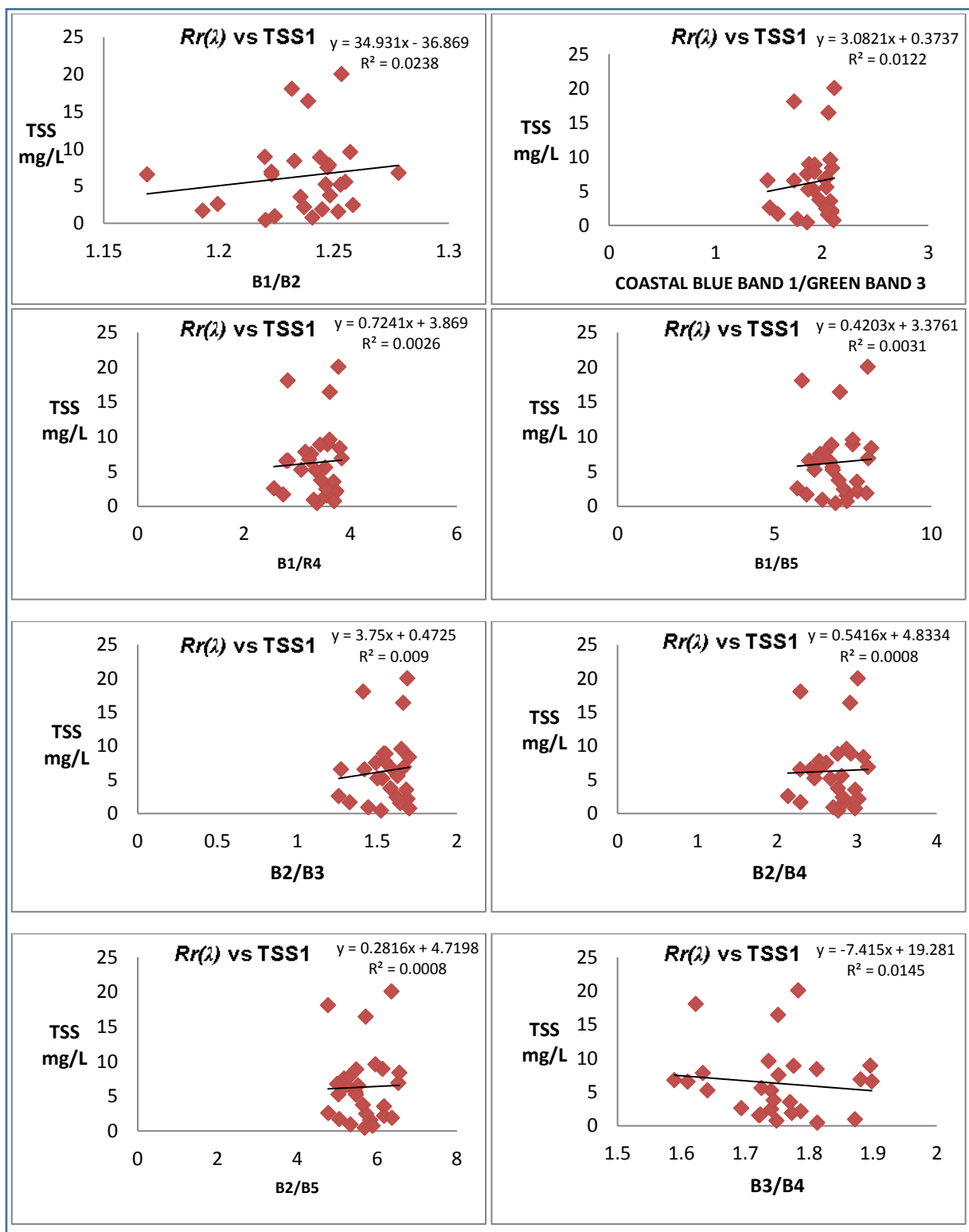
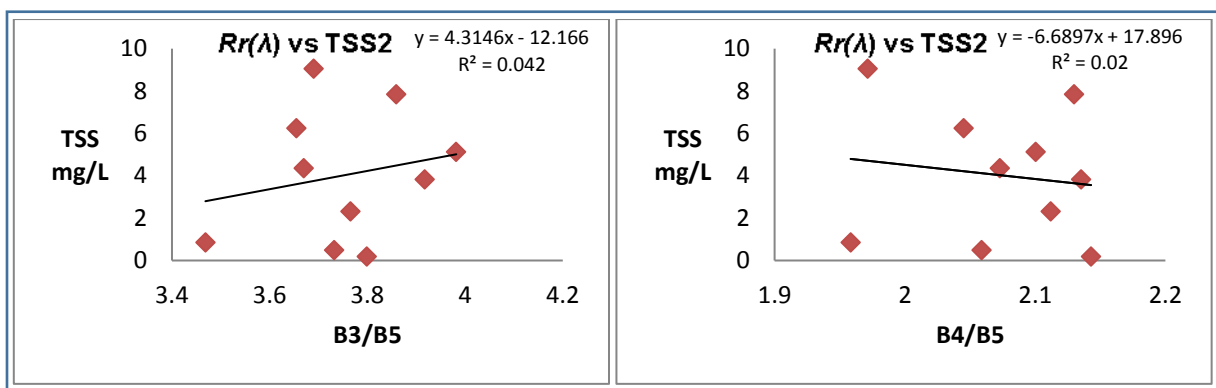**Appendix (8): Regression analysis plot between band-ratio (visible/IR) and TSS1 (Surface)**
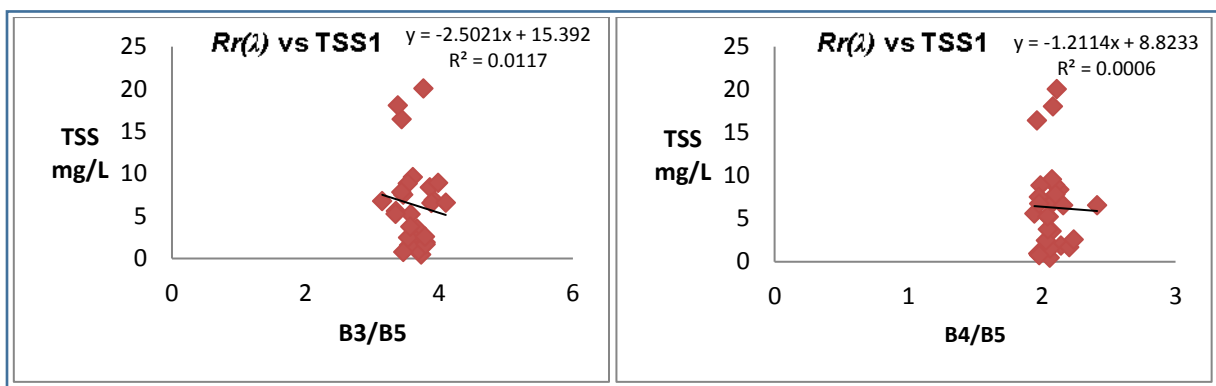
Appendix (8): Regression analysis plot between single-band (visible/IR) and TSS1 (Surface)
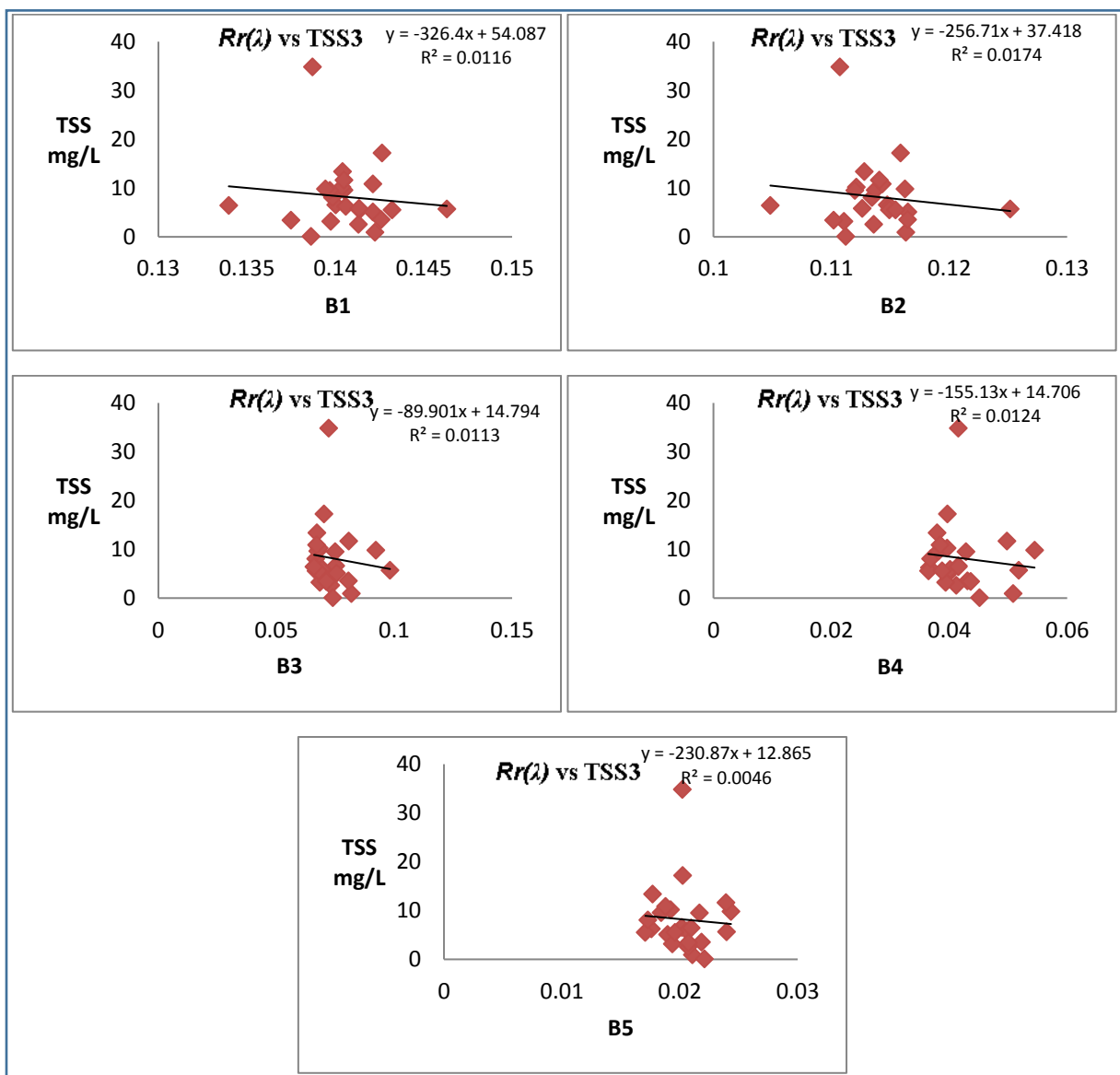

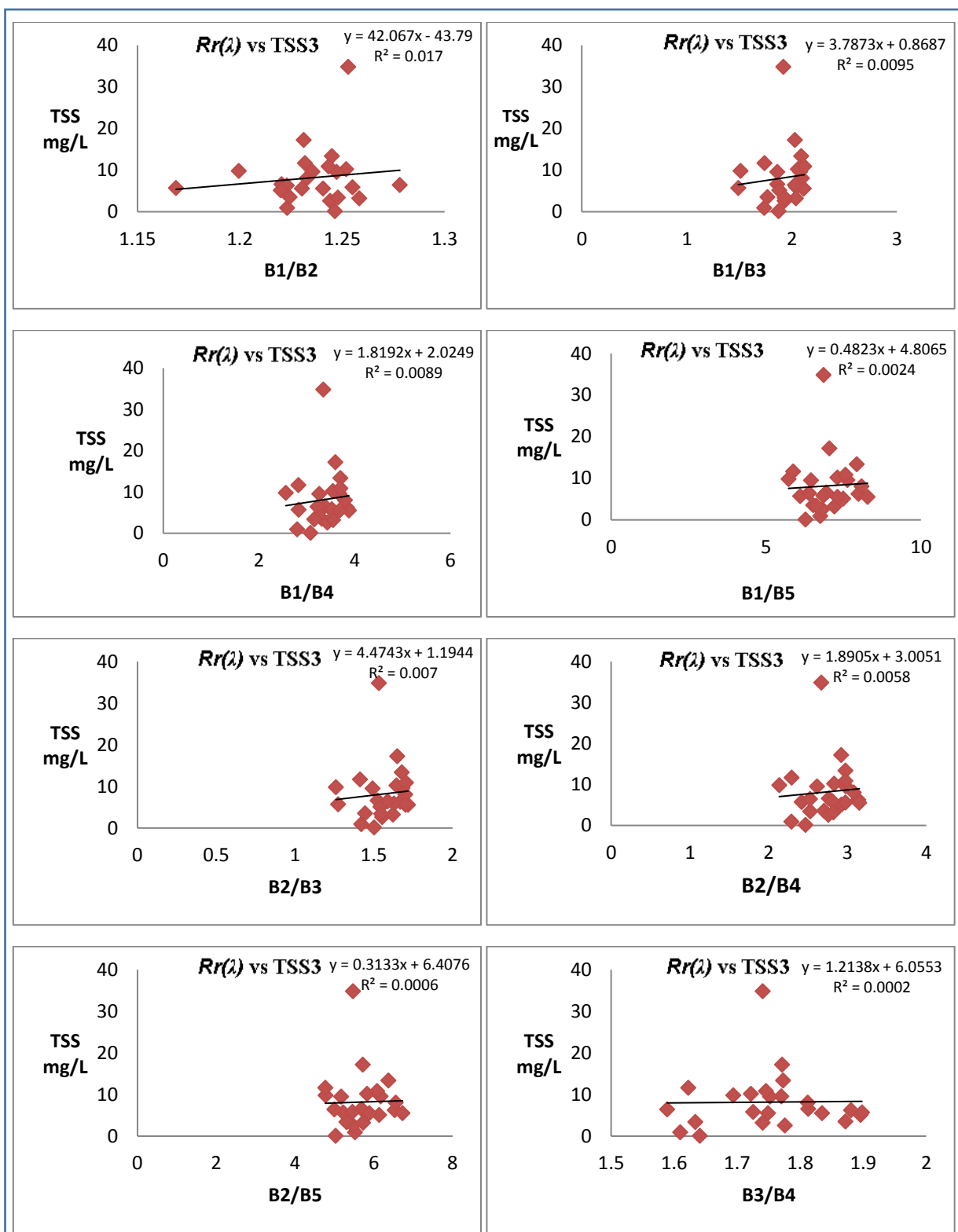**Appendix (9): Regression analysis plot between single-band (visible/IR) and TSS2 (at 2m)**

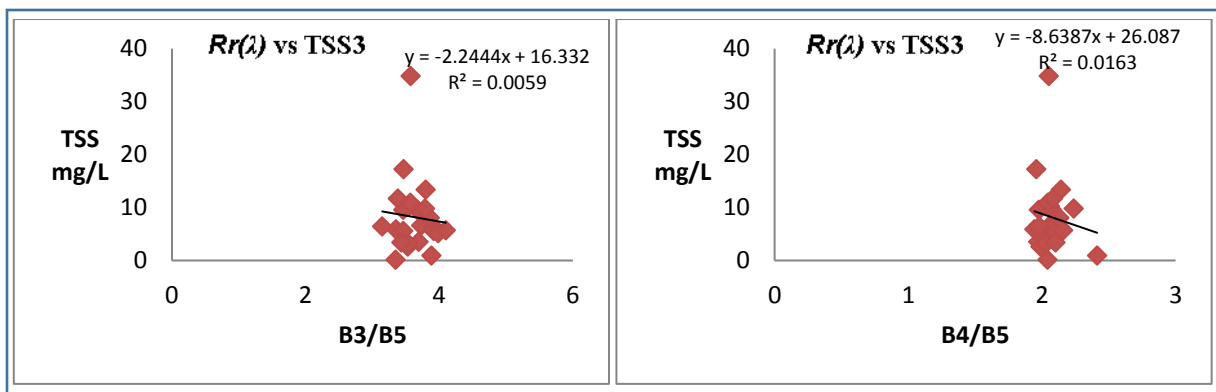**Appendix (10): Regression analysis plot between band-ratio (visible/IR) and TSS2 (at2m)**

Appendix (10): Regression analysis plot between single-band (visible/IR) and TSS2 (at 2m)

Appendix (11): Regression analysis plot between single-band (visible/IR) and TSS3 (at 3m)

Appendix (12): Regression analysis plot between band-ratio (visible/IR) and TSS3 (at 3m)

Appendix (13): Regression analysis plot between single-band (visible/IR) an